J

Jamming of Granular Matter

Bulbul Chakraborty[1], Bob Behringer[2]
[1] Department of Physics, Brandeis University, Waltham, USA
[2] Department of Physics, Duke University, Durham, USA

Article Outline

Glossary
Definition of the Subject
Introduction
Statistical Framework of Jamming
Jamming Phase Diagram
Force Fluctuations, Dynamical Heterogeneities, Length and Time Scales in Granular Flows Approaching Jamming
Force Distributions, Length and Time Scales in Jammed States near the Jamming Transition
Isostaticity and Point J
Future Directions
Bibliography

Glossary

Granular matter Material such as sand or sugar, which is composed of independent, macroscopic particles characterized by short range interactions that do not conserve energy. Energy is lost to excitations of internal degrees of freedom, and is then unavailable for macroscopic flow.

Supercooled liquid A liquid cooled below its freezing point by avoiding crystallization.

Shear deformation Deformation of a material in which internal clusters or layers slide past each other.

Couette flow Flow between two surfaces one of which is moving with respect to the other.

Definition of the Subject

A jammed material is defined as one that is structurally disordered but, unlike a fluid, possesses an yield stress. In the field of traditional condensed matter physics, such a material would be called an amorphous solid. The broader use of "jammed" extends this concept to non-traditional materials such as granular systems, foams and colloids. Jamming is, similarly, the extension of the concept of freezing to the transition from a fluid state to a jammed state. Understanding jamming in granular systems is important from technological, environmental, and basic science perspectives. Jamming of grains in silos causes catastrophic failures. Avalanches are examples of unjamming, which we need to understand prevent and control. The phenomenon of jamming in granular matter poses fundamental challenges in basic science because there is no known framework leading from the microscopic, grain level interactions to the macroscopic properties that reflect collective behavior.

Jamming in granular matter is intimately related to stress propagation, and the nature of jamming will depend on whether the material is under shear or isotropic compression. It will also depend on whether there is sustained motion with the grains having a finite kinetic energy or if the system is at rest and being slowly deformed. In the following sections, we explore different types of jamming in granular matter.

Introduction

Experiments point to many similarities between the jamming transition in granular materials [1,2,3] and other similar non-equilibrium transitions such as that in driven foams, emulsions and gels. The common unifying features are: (a) these are purely non-equilibrium transitions since the flowing state can be maintained only by external driving, (b) the systems exhibit anomalously slow dynamics as the transition is approached and (c) there are no obvious structural signatures of the transition. By structural, we refer to the geometric arrangement of particles. In addition,

we will see that there is increasing evidence for a divergence in correlation functions for forces in the granular case. Features (b) and (c) are, in fact, similar to a transition in a thermal system; that of a supercooled liquid undergoing the glass transition. The origin of the slow dynamics and the relationship between time and length scales has been studied extensively in the context of the glass transition in supercooled liquids, and it has been shown that the dynamics becomes spatially heterogeneous as the glass transition is approached [4,5,6,7]. There is a time scale and a length scale associated with dynamical heterogeneities and these have been measured in experiments [7] and simulations [8]. Inspired by this framework, dynamical heterogeneities have been explored in experiments on granular systems approaching jamming and a length and time scale associated with the jamming transition has been identified [9,10,11].

In granular systems, there is a type of heterogeneity arising from stress transmission which is distinct from the heterogeneity of particle displacements and density fluctuations that are common to both supercooled liquids and granular matter. Stress heterogeneities in flowing granular matter has been studied in experiments on Couette shear flow [12,13,14,15,16,17,18] and in hopper flow [19]. Simulations have a played a seminal role in the developments leading up to the dynamical heterogeneities framework in supercooled liquids. Likewise, simulations of granular flows can play a role in clarifying the relationship between heterogeneity in different dynamical variables. For instance, a simulation of grains flowing through a hopper (a long, vertical tube with a narrow opening at the bottom), has identified/characterized both stress and displacement heterogeneities. However, a clear relationship between the two has not been identified [20]. Indeed, there may be some reason to think that there is anti-correlation between the strong force structures of force chains, and the freedom needed for density fluctuations. Dynamical heterogeneities have been explored in simulations of other types of dense granular flows [21,22,23].

The similarities in dynamics between supercooled liquids and granular systems have raised the intriguing possibility of "universality" in the jamming transition. Universality is a concept associated with continuous phase transitions in thermal systems such as the liquid-gas transition or the Curie point in ferromagnets [24]. In these systems, universality, owes its origin to the presence of a diverging length-scale at the transition. Microscopic properties of the system can be coarse-grained because of the presence of this diverging length scale and universality classes can be specified by properties such as the symmetry of the system and the spatial dimensionality. These concepts are still evolving in the context of granular systems. However, there are an increasing number of studies that have identified a growing, possibly diverging, length scale.

Statistical Framework of Jamming

The ubiquitous presence of force fluctuations, well-defined statistical distributions and similarities to thermal systems observed in granular systems close to jamming, have led researchers to look for a statistical framework that can describe the spatial and temporal fluctuations in static and quasi-static (weakly driven) granular flows.

Experiments and simulations suggest that the phenomenon of jamming has the flavor of a phase transition. Phase transitions can be broadly divided into two classes: (a) Equilibrium and (b) Non-equilibrium. The former encompasses transitions such as the liquid-solid transition, the superfluid and superconducting transitions, and describes transitions between states which are in thermal equilibrium. Non-equilibrium phase transitions are commonly observed in pattern-forming systems such as chemical reactions, a well known example being the Belousov–Zhabotinsky reaction [25], or in fluid flows, such as Raleigh–Bénard convection. The framework of equilibrium statistical mechanics is well established and can be used to analyze and understand equilibrium phase transitions. In contrast, there is no universal framework for nonequilibrium phase transitions even though there are many specific transitions which are well understood [26,27]. In many cases where non-equilibrium transitions occur, the systems are locally close to thermal equilibrium, but not globally so. It is then possible to use hydrodynamic-like descriptions involving gradients in relevant quantities, as well as transport models. Transitions in such systems often involve spatially extended modes which become unstable or stable for different control parameters. In the usual case, it is the most unstable mode which dominates, and thermal fluctuations play a very limited role.

An interesting question is whether a statistical approach can be used to understand jamming and other phenomena in granular matter. In such an approach, one would like to know the ensemble of states that are consistent with the external constraints. In the granular case, there is some evidence to suggest that fluctuations are important, particulary near jamming unlike the typical non-equilibrium transition discussed above.

Granular Packings

A static granular packing is in mechanical equilibrium if every grain satisfies the conditions of force and torque bal-

ance. At the microscopic level, the grains interact via contact forces, which are frictional. For rigid grains, friction leads to a microscopic indeterminacy of the forces since the tangential force magnitude at a contact has to be *less* than the normal force: $|f_t| \leq \mu f_n$, where μ is the friction coefficient.

There is a broader class of indeterminacy which has to do with the fact that there are many packing configurations that are consistent with a set of macroscopic constraints. For example, if one shakes a box of marbles and examines the positions of the marbles after the shaking has stopped, the positions and the contact network will be different each time one stops shaking. This is analogous to the situation of systems in thermal equilibrium: many microscopic configurations of the oxygen molecules in a closed room occur while the temperature and total volume remain fixed. Of course, in the granular case, there is no internal 'shaking' mechanism.

The different configurations of systems in thermal equilibrium (such as the oxygen molecules in a room) have a given probability of occurring at a given temperature. This probability is well known from equilibrium statistical mechanics and is the Boltzmann distribution: $e^{-\beta E}$. Here $\beta = 1/k_B T$ is the inverse of the temperature T multiplied by the Boltzman constant k_B, and E is the energy of the configuration. The probability of finding a configuration is, therefore, completely determined by its energy and does not depend on the particular dynamics or the history. This is the essence of systems in thermal equilibrium and leads to their simplicity.

Edward's Ensemble

The configurations of a box of marbles at the end of a shaking experiment are certainly not in thermal equilibrium. Marbles are large objects, and they dissipate energy as heat when they interact. Ordinary thermal fluctuations are not relevant to a box of marbles; one has to shake them to move them and generate new states. These end states are, however, static. A natural question to ask is whether one can make a priori prediction of the probability of occurrence of a particular configuration, as we can for systems in thermal equilibrium. The first theoretical approach to address this question was that of the Edwards ensemble which asserts that the total volume (V) of a mechanically stable grain packing plays the role of energy, and that there is a temperature-like quantity called the compactivity [28,29,30,31]. The mechanically stable grain packings of infinitely rigid objects have been termed blocked states [31], and are related to strictly jammed states [32]. The basic hypothesis underlying the Edwards ensemble is the microcanonical [24] hypothesis that all blocked states with the same total volume V are equally likely. This hypothesis has been tested in numerical simulations, in experiments, and in some exactly solvable models [33,34,35,36,37,38]. The consensus seems to be that the hypothesis is not universally valid but holds under some conditions. The Edwards hypothesis involves the definition of the Edwards entropy: $S(V) = \ln \Omega(V)$, where $\Omega(V)$ is the density of blocked states, that is, the number of blocked states between V and $V + \delta V$. Evaluating this function has been a challenging problem, although progress has been made recently [39].

Force Ensembles

The Edwards picture was originally based on the assumption of completely rigid particles. However, all physical particles have finite stiffness, and in the usual case, interact via frictional contact forces. The conditions of finite vs. infinite stiffness and frictionless vs. frictional interactions has some important consequences for granular packings. Relaxing the infinite stiffness constraint introduces couplings between the positions of grains and the contact forces. Below we discuss an ensemble for frictionless, spherical particles.

A mechanically stable packing of frictionless, deformable, spherical particles have to satisfy the equations of force balance. In addition, there is force law relating the positions of the particles to the forces [40,41]. For grains interacting through purely repulsive, short-range, forces, there are dN equations of force balance for N grains in a space of dimensionality d:

$$\text{force} - \text{balance} \quad dN \text{ eqs}: \sum_j F_{ij} \frac{\mathbf{r}_{ij}}{|\mathbf{r}_{ij}|} = 0 \tag{1}$$

$$\text{force} - \text{law} \quad \langle z \rangle N/2 \text{ eqs}: \; F_{ij} = f(\mathbf{r}_{ij}) \tag{2}$$

Here $\langle z \rangle$ is the average number of contacts per grain, F_{ij} is the magnitude of the contact force between grains i and j, the angles of the contacts being fixed by the geometry, and $f(\mathbf{r}_{ij})$ is a function specifying the inter-grain force law. For a given geometry, (i. e. fixed $\frac{\mathbf{r}_{ij}}{|\mathbf{r}_{ij}|}$), the equations of force balance involve $\langle z \rangle N/2$ unknowns. The number of force-balance equations cannot be greater than the number of unknowns, otherwise the forces are overdetermined, and, therefore, $\langle z \rangle N/2 \geq dN$.

For rigid, non-deformable grains, the force law becomes a constraint on the positions of the grains [41]. There is one constraint for each contact, which leads to $\langle z \rangle N/2$ equations for the dN positions, the unknowns. Since the number of constraint equations have to be larger

than the number of unknowns, $\langle z \rangle N/2 \leq dN$. The force law and the force balance constraints can, therefore be satisfied only if $\langle z \rangle = z_{\rm iso} = 2d$. This enumeration argument applies only to disordered packings, since for ordered, crystalline packings, angles of the lines connecting the grains are not independent, and therefore, not all the constraint equations are linearly independent. Considering such disordered packings, the enumeration argument leads to the conclusion that packings of rigid, isotropic, frictionless particles have to be *isostatic*; they have to have $\langle z \rangle = z_{\rm iso}$.

For deformable particles, mechanically stable packings can exist for $\langle z \rangle \geq z_{\rm iso}$. If the particles are very stiff, the magnitude of the forces change a lot for small changes in the separation between grains. There is, therefore, an effective separation of scales [40,42] in Eqs. (1) and (2), and one can consider the ensemble of forces which satisfy force-balance for a fixed geometry of the packing, i. e., a packing with fixed grain positions. The properties of such force-ensembles have been studied [40,42,43,44,45,46,47], and it has been shown that $P(F)$, the probability distribution function (PDF) of contact forces, evolves to a exponential form as the particles are made increasingly rigid [40,42]. In addition, work on sheared and isotropically compressed packings have shown that there are more extended spatial correlations of the forces in the force ensembles for sheared packings [48].

The force ensemble approach captures many features of packings near Point J. However, the approach to this point involves coupling between the geometry and forces, as observed in simulations [49]. Below, we discuss a generalized ensemble that allows for the coupling of these two, and applies to spherical and non-spherical grains with and without friction.

Generalized Ensembles

In a more recent development, it has been shown that the "equally likely" hypothesis of Edwards and the Microcanonical ensemble of thermal systems [24] is not essential for the definition of a temperature-like quantity, and a much weaker condition of factorizability of distributions is sufficient [50,51,52]. The necessary conditions for being able to define a temperature-like variable and a statistical ensemble based on this variable are (a) the existence of a physical quantity that is conserved by the natural dynamics of the system (in thermal systems energy is conserved but in dissipative granular media, it is not) and (b) that the frequency of finding different states with the same value of the conserved quantity is factorizable: $\omega_{\nu_1+\nu_2} = \omega_{\nu_1}\,\omega_{\nu_2}$. The latter condition implies that if one creates a configuration by bringing together two configurations $_1$ and $_2$, then the frequency of occurrence of this joint configuration is a product of the frequency ω_ν of the individual configurations.

In the context of mechanically stable packings of grains (soft, deformable or rigid), a conserved quantity that has been identified is the force-moment tensor [53,54,55] which is related to the Cauchy stress tensor:

$$\hat{\sigma} = (1/V) \sum_{ij} \vec{r}_{ij} \vec{F}_{ij} \tag{3}$$

The summation in Eq. (3) is over all contacts $\{ij\}$ in an assembly of grains, occupying a volume V, with contact vectors $\vec{r}_{ij}$ and contact forces $\vec{F}_{ij}$ (for grains with friction $\vec{F}_{ij}$ does not lie along the direction of $\vec{r}_{ij}$).

The microscopic force moment tensor for a grain is given by:

$$\hat{\kappa}_i = \sum_j \vec{r}_{ij} \vec{F}_{ij}\,, \tag{4}$$

where the sum is over all grains j that contact grain i. For grains in mechanical equilibrium, it can be shown, using a generalized Stoke's theorem [28,56,57], that the *total* force moment tensor

$$\hat{\Sigma} = \sum_i \kappa_i$$

becomes a boundary integral for systems with open boundaries and is a topologically conserved quantity for systems with periodic boundary conditions [53]. In two dimensions, this property can be explicitly demonstrated by introducing a set of auxiliary variables [55] which are the analog of the vector potential in electromagnetism. The connection to electromagnetism is natural if one remembers that for mechanically stable packings, the divergence of the stress tensor is zero, just as the divergence of the magnetic field is zero in electromagnetism.

Given the topologically conserved nature and/or the strict boundary sensitivity of $\hat{\Sigma}$, the phase space of all mechanically stable packings can be grouped into sectors characterized by the value of $\hat{\Sigma}$. Thinking of systems with periodic boundary conditions, the topologically conserved nature implies that packings in different sectors are completely disconnected by any natural dynamics, and therefore, $\hat{\Sigma}$ is the type of conserved quantity that meets criterion (a) of the previous paragraph. If we now assume criterion (b), then a statistical ensemble can be constructed to describe the end states of processes such as shaking grains. The role of energy is played by $\hat{\Sigma}$ which is an extensive

quantity (scales with system size) and the analog of temperature is a tensorial quantity, $\hat{\alpha}$ (In the context of infinitely, rigid grains, this intensive variable has been called Angoricity by Edwards [28]). This tensor is defined by:

$$\hat{\alpha}(\hat{\Sigma}) = \frac{\partial Z_0(\hat{\Sigma})}{\partial \hat{\Sigma}} \tag{5}$$

where

$$Z_0(\hat{\Sigma}) = \sum_{\nu} \omega_\nu \delta(\hat{\Sigma}_\nu - \hat{\Sigma})$$

and the sum is over all mechanically stable packings ν.

Tests of the Stress-Based Ensemble

The ability to define an ensemble does not necessarily mean that real granular packings conform to this ensemble. The assumption of factorizabilty could break down or the frequency of occurrence of a packing, ω_ν could be history-dependent making the temperature or the ensemble concept not very useful. It is, therefore, essential to check the predictions of this ensemble against experiments and simulations.

This has been done for simulations of frictionless grain packings in two dimensions [53] and it has been shown to work remarkably well. As a result of this comparison, an equation of state analogous to thermal equations of state, has been derived for frictionless grain packing approaching Point J [53], that is consistent with the field theory constructed for Point J [57].

Two applications of the stress-based ensemble to experiments probing the jamming transition will be discussed below.

Jamming Phase Diagram

About a decade ago, Liu and Nagel proposed that the jamming transitions in all systems, including the glass transition in supercooled liquids can be described by one unified framework through the jamming phase diagram and a special point in this phase diagram referred to as Point J [58]. The proposed phase diagram, shown in Fig. 1, delineates the boundaries of the jammed region in a phase space spanned by a temperature, density, and a *load* axis. The load axis captures the non-equilibrium aspects of these materials. For ideal spherical particles, the transition at Point J is a purely density-driven change, occurring at a critical packing fraction, ϕ_c between an amorphous solid state of dry granular packings and a state where the packings fall apart under any external stress [49]. Recent experiments in granular packings have verified the existence of this, transition [59], as discussed in the section on experiments, and a theoretical description of this specific point is also emerging [56,60,61].

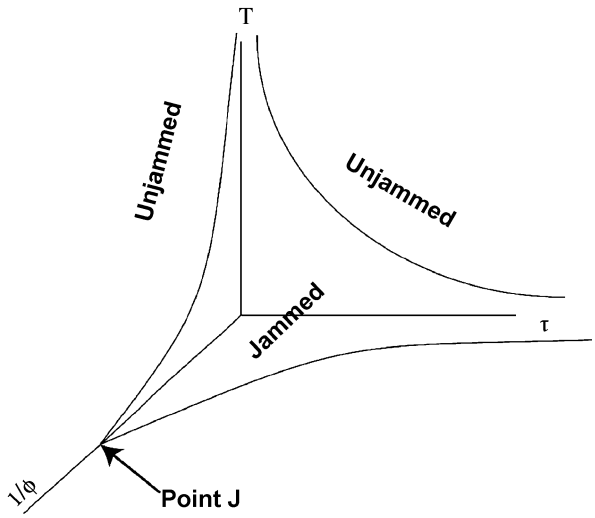

Jamming of Granular Matter, Figure 1
Jamming Phase Diagram proposed by Liu and Nagel. Adapted from [49]

In recent years, a theoretical framework has been developed [62,63,64] that describes the complete phenomenology of the glass transition in supercooled liquids. There are similarities between this framework and the properties of Point J, but whether or not these diverse phenomena can be unified under the umbrella of universality is a subject of intense current research. The stress-based ensemble approach described earlier has been used to construct a coarse-grained field theory of Point J and the jamming transition [56,57]. Since field theories and scaling ideas based on them underlies universality in thermal phase transitions, the extension of this approach to granular materials hold out the promise of identifying different universality classes in the context of jamming.

The special properties of Point J are related to isostaticity [49]. The discussion in Sect. "Statistical Framework of Jamming" analyzes isostaticity for frictionless, spherical grains. In general, isostatic packings are those special ones where the number of contacts is just enough to provide mechanical stability [41]. It has become increasingly evident [65] that isostaticity plays very different roles in spherical vs. non-spherical particles, which raises the question of whether Point J is special to frictionless spheres and disks. Also, it is not clear how generic the properties of this special point are, and whether or not it controls the behavior as one moves away from it in parameter space.

The jamming phase diagram of Liu and Nagel provides a framework for exploring the phenomenon of jamming in granular matter. Since temperature is not a relevant variable in the granular case, the phase space of interest would generically be the loading-density plane. The mechanical failure (or unjamming) of granular packings can occur because of (i) a vanishing bulk modulus (instability with respect to volume fluctuations) or (ii) a vanishing shear modulus (instability with respect to fluctuations of the shear stress). The state at Point J is an especially fragile one since both conditions (i) and (ii) are met. The stress state of the packing at this point is isotropic. In many instances, however, a granular material can be irreversibly deformed through the application of shear, and this process is also frequently referred to as unjamming. Specifically, for large enough shear stresses, a solid-like granular material will dilate, and fail in a process that typically leads to a locally weak and dilated region known as a shear band. This type of process has interesting analogues in the plastic failure of disordered glassy materials, in foams, in colloids and perhaps elsewhere. The tendency of densely packed granular materials to dilate under shear was discovered by Reynolds [66], and the adjustment of the density under shear is incorporated into critical state models of soil mechanics [67]. Although under shear, granular materials yield, and in some sense are 'unjammed', this process typically occurs under non-zero pressure as well as non-zero shear stress. Hence, 'unjamming' due to shear differs from the isotropic-stress state that occurs at Point J. In fact, the vast majority of experiments associated with jamming/unjamming are of this latter shear-induced process. There is compelling reason, discussed below, to think that plastic failure by shearing has a qualitatively different behavior than what occurs at Point J. For instance, jammed states also depend on whether they are isotropic or not, as shown by Majmudar and Behringer [68].

Given the dilatancy effects, and the differences between isotropically and anisotropically stressed states, we organize our discussion of jamming around a phase space spanned by the components of the Cauchy stress tensor (Eq. (3)). This is a symmetric tensor, and in two dimensions we can, therefore, work with the isotropic pressure, P, and the shear stress τ. $P = \sigma_1 + \sigma_2$, and $\tau = \sigma_1 - \sigma_2$, where the σ_i are the principal stresses, i. e. eigenvalues of the stress tensor. Since the principal stresses are positive for granular materials, the physical space is enclosed by the $|\tau| = P$ and $P = 0$ lines. In fact, shear failure typically occurs for $|\tau| < P$. Point J lies at $P = 0\,, \tau = 0$. Along the $\tau = 0$ axis, simulations provide strong evidence of Point J having critical properties with, in particular, at least one diverging length scale [49].

If $\tau \neq 0$ then the jamming behavior could be quite different from that characteristic of Point J. Here, a useful analogy to equilibrium phase transitions may be the difference between a critical point, where a line of first-order phase transitions terminates, such as the ferromagnetic Curie Point which occurs at zero magnetic field and at a characteristic temperature T_c, or a tricritical point, which separates a region of second-order transitions from a region of first-order transitions. This type of a critical point arises in multicomponent, thermodynamic systems and a well-known example is superfluidity in a mixture of He^3 and He^4. For a high enough concentration of He^3, the mixture undergoes a first order transition into two phases, and only one, the He^4-rich phase is superfluid [69]. A characteristic of a tricritical point is the existence of two diverging length scales, and in particular, there is a higher dimensional phase space that describes the various transitions. We present this discussion here purely as an illustrative example of a phase-transition scenario in which the signatures depend on what parameters are varied. We use the phase diagram of Fig. 2 to provide a framework for differentiating between the avenues available for approaching the jamming transition. In much of the literature, no distinction has been made, and we believe that has led to confusion. For each possible path, the transition can also be approached from the jammed side or the unjammed side. If $\tau = 0$, then the unjammed state is fluid-like in the sense that the system cannot respond elastically to any applied stress.

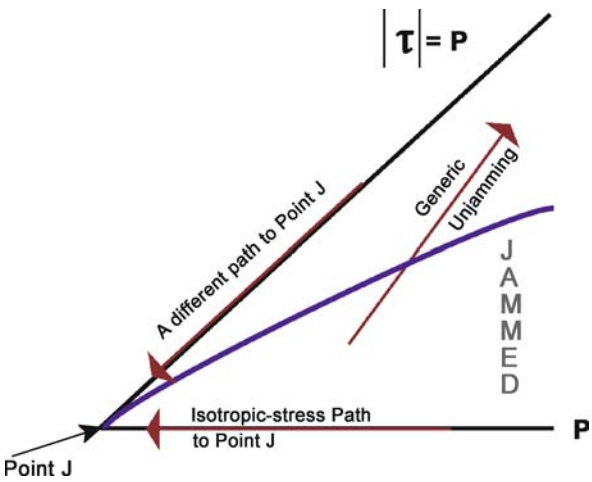

Jamming of Granular Matter, Figure 2
Jamming Phase Diagram in the space of components of the Cauchy stress tensor. The diagram shows a schematic in the $P - |\tau|$ plane, with *arrows* marking possible avenues of unjamming

Below, we first provide an overview of the signatures of jamming observed as the transition is approached from the fluid-like side (Sect. "Force Fluctuations, Dynamical Heterogeneities, Length and Time Scales in Granular Flows Approaching Jamming"), we then discuss the properties of jammed states under both shear and isotropic compression, as the jamming transition is approached from the jammed side (Sect. "Force Distributions, Length and Time Scales in Jammed States near the Jamming Transition"). In Sect. "Isostaticity and Point J", we summarize the experimental and theoretical description of Point J and the associated length and time scales. Related areas of research that we do not include in this article at all, are the phenomenon of aging, non-equilibrium dynamics, and generalized elasticity for granular matter. We refer the interested reader to articles listed in the bibliography.

Force Fluctuations, Dynamical Heterogeneities, Length and Time Scales in Granular Flows Approaching Jamming

In this section, we review a number of physical and numerical experiments which give insight into the nature of the jamming process. Each approach has advantages and disadvantages. Numerics, typically consisting of direct simulations of the equations of motions for a set of particles, has the advantage that it is possible to easily explore parameter space. This approach is referred to as Molecular Dynamics (MD) or as Discrete Element Simulations (DEM), depending on the community. The disadvantage of simulation is that it is difficult to achieve an accurate representation of friction (often friction is neglected), and in addition, simulations are typically done only for spheres in 3D or disks in 2D (which we will refer to as isotropic particles). Experiments do not suffer from issues of accuracy of the interaction law, but it is very difficult to obtain quantitative data except at the boundary of 3D systems. Alternatively, it is possible to obtain information using quasi-2D systems, such as collections of disks, something that is also done frequently for simulations. Two-dimensional systems for both experiments and simulations can yield excellent quantitative information, but may leave open the question of generalizability to higher dimension. With these caveats, we turn to a review of both numerical and physical experiments that probe the jamming transition from the fluid-like side. Granular flows can be broadly divided into two categories, (a) inertial flows dominated by collisions between grains, and (b) quasistatic flows that involve extended contacts and slow evolution from one static, mechanically stable state to another.

Recent results from numerical simulations by Lois et al. [70,71] are of particular interest here. These authors studied shear flow of rigid particles which they modeled using contact dynamics, a version of MD/DEM for rigid particles. A particularly interesting discovery coming from these studies was the existence of a divergent correlation length for forces, associated with the formation of clusters, as the packing fraction approached ϕ_c from below. The presence of a divergent length scale reinforces the idea that jamming is actually a critical transition.

Evidence for critical properties also come from experiments on hopper flow by Longhi et al. [19]. These experiments involved a quasi-2D flow of monodisperse spheres out of a hopper-shaped container. Necessarily, the presence of flow implies that the states studied here were unjammed. As the particles moved by, a small high speed force gauge mounted near the outlet of the hopper yielded the impulse of individual collisions. The collisions could be clearly identified because of a large separation of scales between the duration of contact, and time between contacts. The distributions of these impulses, at large impulses were roughly exponentially distributed, and independent of the flow rate. At small impulses, the distributions evolve with flow rate with a relative increase of small impulse events as the flow rate decreases. A more interesting statistic is the distribution of τ's, the time between successive collisions. As the jamming transition was approached, these distributions approached a powerlaw, $P(\tau) \propto \tau^{-3/2}$.

An MD simulation of hard disks, in a geometry designed to mimic the experiments of Longhi et al. [19], provided an explanation for the evolution of the impulse distribution in terms of increasing velocity correlations [72,73]. These correlations also led to a qualitative explanation of the changes in $P(\tau)$ [72], which occur because the average time between collisions *decreases* as the flow velocity decreases while at the same time the time taken for a particle to fall through its own diameter increases. This leads to a large separation of time scales and a range of times over which the dynamics is scale invariant. The simulations provided strong indications that these physical effects owe their origin to the existence of chains of frequently-colliding particles. In addition, it was shown that these collision chains could be interpreted as stress chains with the stress measured through momentum transfer [20, the counterpart of force chains in this system of flowing hard particles. Fig. 3 is a snapshot of a simulation illustrating the stress chains for two different flow rates, as controlled by the width of the opening at the bottom of the hopper. More recent work on this system of hard disks has provided evidence for the existence of

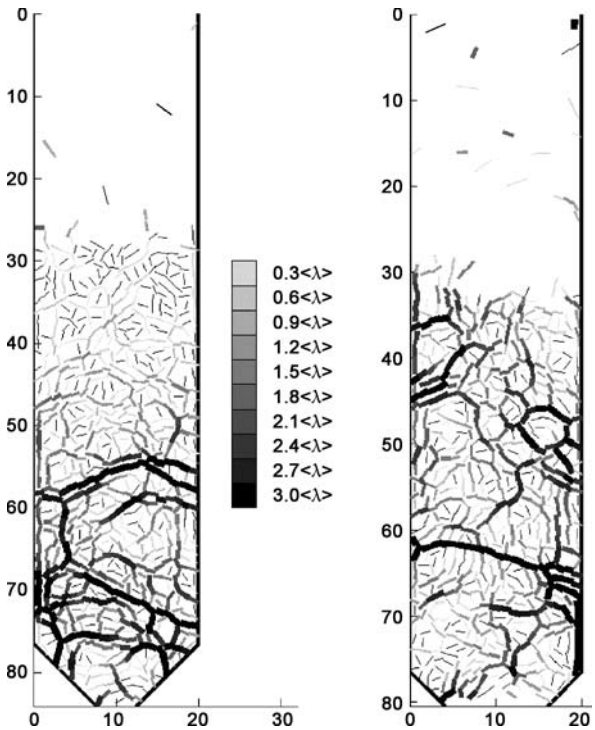

Jamming of Granular Matter, Figure 3

Stress chains. The grayscale plot is constructed by scaling the collisional stress by the average collisional stress ($\langle\lambda\rangle$) obtained by coarse graining over many collisions. Close to jamming, the coarse-graining time is much shorter than the time taken by a particle to fall through its own diameter [72]

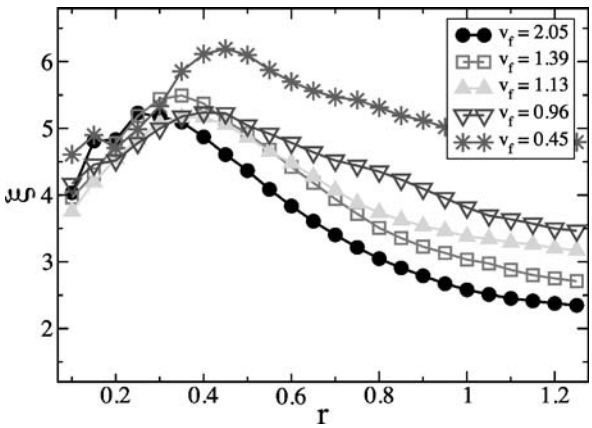

Jamming of Granular Matter, Figure 4

Lengths scale, ξ, associated with the heterogeneity of dynamics as a function of the mean square displacement, r, of particles in MD simulations of a two-dimensional hopper flow [20]. This length scale, extracted by analyzing the spatial correlation between displacements of particles [74,75], peaks at a characteristic displacement which can be related to a characteristic time at which the dynamics is most heterogeneous. This plot is qualitatively similar to ξ vs. time plots observed in the experiments of Durian et al. on air-driven beads, in the experiments of Dauchot et al. on particles driven by oscillating shear (see text), and in supercooled liquids

dynamical heterogeneities identified through the displacements of grains [72].

A length scale can be extracted from measurements of spatio-temporal correlations of these heterogeneities. As in supercooled liquids, there is a length scale that has a peak at a characteristic time. Both length and time scales depend on the average flow velocity, growing as the system approaches jamming. The increase in length, however, is not as dramatic as in supercooled liquids or in experiments on air-driven granular beads [9]. As an example of the characteristic shapes of the length versus time curves observed in all of these systems, supercooled liquids, inertial and quasistatic granular flows, we show a set of data from the MD simulations of hopper flow in Fig. 4 [20].

Pouliquen et al. have carried out a series of experiments on flow down chutes/inclined planes [11,76]. These studies have shown that there is a range of inclination angles, θ, for the chute for which it is possible to obtain steady state flow, and that the depth of the flowing layer, h, depends on θ. The flow stops if h is smaller then an inclination-angle-dependent function, $h_{\text{stop}}(\theta)$. Data for the depth-averaged velocity, u can then be expressed in terms of a flow rule, $u/(gh)^{1/2} = \beta h/h_{\text{stop}}(\theta)$, where β is a material-dependent $O(1)$ constant. Following a suggestion by Ertas and Halsey [77], Pouliquen [11] explored the possibility that there might be observable spatial correlations for the surface velocity which would signal the onset of jamming. Indeed, such correlations exist, and they grow as the inclination angle of the chute is lowered, i. e. as the system approaches the jammed state.

Kolb et al. [78] have studied the response of a jammed 2D layer to a localized cyclic displacement. This process was carried out quasi-statically, and in such a way as to locally unjam the system. More specifically, the experiment consisted of a bidisperse layer of disks, inclined from the vertical, so that the system was normally jammed. An intruder particle having a diameter corresponding to the larger of the two grain sizes, was displaced periodically in time by small amounts. These local displacements led to a much longer range set of displacements, part of which was reversible, but part of which was irreversible. This long-range response is suggestive of a critical-like response for states near jamming.

Drocco et al. [79] have used MD to to simulate the behavior of a 2D particle that is pushed through originally static bidisperse packings of similar particles. The pack-

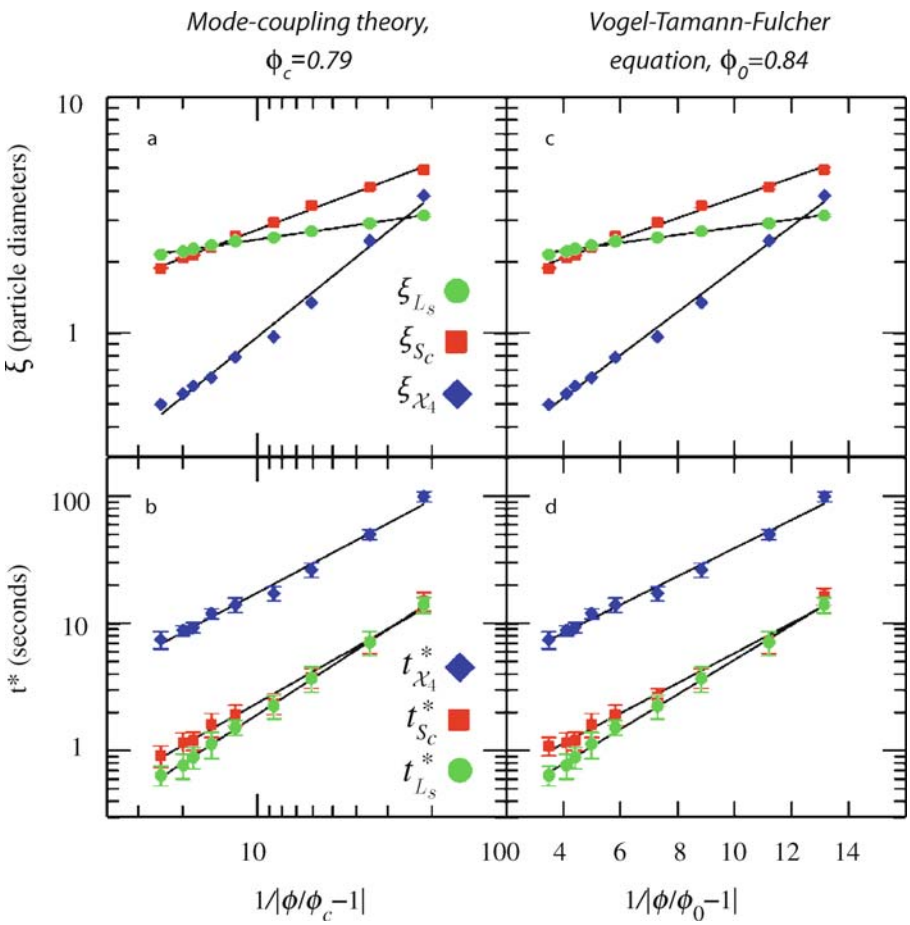

Jamming of Granular Matter, Figure 5

Data for length (ξ) and time (t^*) showing an increase in these scales associated with dynamical heterogeneities in a system of air-driven beads. Reprinted from [9]

ings reside in a square geometry with periodic boundary conditions, and are prepared at packing fractions below the jamming value for this system. The authors first focus on the intruder velocity, which becomes increasingly intermittent as $\phi \to \phi_c$ from below. To characterize the intermittency, Drocco et al. use multifractal analysis to compute moments, $M(q) = \int \mathrm{d}v P(v) v^{-q} \propto (\phi_c - \phi)^{\tau(q)}$, and present evidence for multiscaling. Of particular relevance here is a demonstration that as $\phi \to \phi_c$, the number of disks, n, that move in response to a fixed pushing distance for the intruder grows rapidly. These authors use data for the number of moving disks vs. ϕ to estimate a correlation length, which diverges as $\xi \propto (\phi_c \phi)^{-\nu}$, with $\nu = 0.71 \pm 0.12$. These numerical studies have an interesting parallel with experimental studies by Geng and Behringer [80] which yielded the force needed to push a disk through a channel of other disks in the jammed state. These data yielded a pushing force that also became increasingly intermittent on approach to ϕ_c, in this case from above, and a mean force that vanished as $(\phi - \phi_c)^\alpha$ with $\alpha = 1.5$.

Dauchot et al. [10] have studied correlations in systems of particles in 2D that are subject to small-amplitude oscillating shear. In this case, simple shear was applied, meaning that a rectangular sample was alternately tilted into a parallelogram to the right, then left. Dauchot et al. were particularly interested in characterizing the spatio-temporal fluctuations of systems near jamming. An image was obtained each time that the system was returned to the rectangular state, and the location of each particle was then determined. From these data, the authors first calculated a measure of individual particle motion, the self-intermediate scattering function, $F_s = \langle \hat{F}_s(k,t) \rangle = N^{-1} \Sigma_j \langle \exp[-ik(r_j(t) - r_j(0))] \rangle$. The results for $F_s(k,t) \propto \exp[-(t/\tau(k))^{\beta(k)}$ indicate Brownian diffusion at small k, but a different behavior at large k,

i. e. smaller spatial scales, where β is smaller than unity: a stretched exponential. They attribute this behavior to dynamical heterogeneities, and they further quantify the nature of these dynamical heterogeneities by analyzing length and time scales associated with fluctuations of $\hat{F}_s(k, t)$, as has been done for supercooled liquids. The analysis identifies a moderate length scale associated with the fluctuations, in agreement with the type of length scales that have been observed in supercooled liquids.

Durian et al. [9] have studied dynamical heterogeneities in a system of air-driven granular beads as a function of the packing density. Using multiple measures of lengths associated with dynamical heterogeneities, these authors demonstrate that there are length and time scales, which grow with the approach to Point J. They also show that the increase in these scales follows the Vogel–Fulcher–Tamann form: a form that is associated with supercooled liquids approaching the glass transition [81]. Figure 5 shows length and time scales extracted from different measures of dynamical heterogeneities as a function of the packing fraction. The fits are to the predictions of Mode-Coupling-Theory of the glass transitions and to the Vogel–Fulcher–Tamann form, which implies an exponential divergence at a packing fraction ϕ_0. Interestingly, the value of ϕ_0 is very close to the ϕ_c associated with Point J [9].

Force Distributions, Length and Time Scales in Jammed States near the Jamming Transition

An interesting premise is that the distribution of interparticle contact forces, $P(F)$, can provide insight into the nature of the global granular state of a system. In particular, it may be useful as a tool to distinguish jammed from unjammed or nearly unjammed states. It is also an important indicator of the overall stress state of the system, as demonstrated in experiments [68,82] and theory [83,84]. Since the transition to a deforming state in a dense granular material has often been obtained by shearing, there have been a number of studies that have addressed this case [12,13,14,16,17,18,85,86]. In particular, Howell et al. [13,14] have directly probed the transition that occurs when the density of a sheared granular sample is reduced to the point where stresses vanish. Other studies have probed the nature of steady granular shear [12,16, 18,85,86].

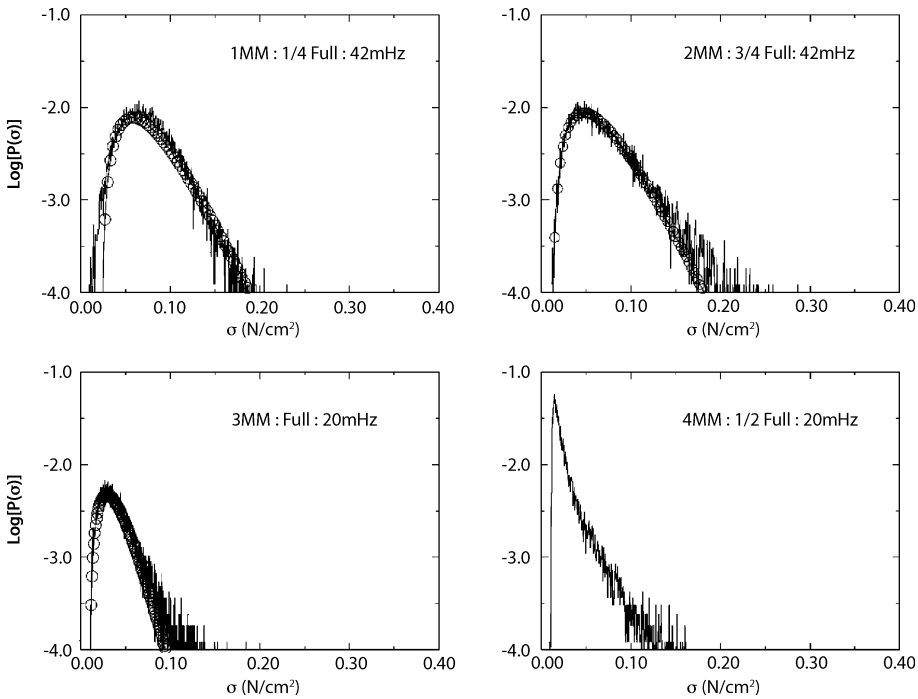

Jamming of Granular Matter, Figure 6

Distributions of forces measured at the base of a continuously sheared layer of glass spheres, for different sphere diameters of 1 mm, 2 mm, 3 mm and 4 mm, as indicated, and a fixed detector diameter of 1.0 cm. The other numbers give the depth of the granular layer as a fraction of the full height, 4.1 cm, and the shearing rate [12]

We discuss below several recent experimental studies which help elucidate this point. Here, we focus first on sheared, and then on isotropicically confined systems.

Sheared States

Fluctuations, their distributions and their correlations, are interesting for a number of reasons. First, they can reveal the nature of short and long range behavior. In addition, they provide a useful test of model behavior, and they help to identify key parameters. One of the earliest experimental characterization of force fluctuations in dense granular materials was by Miller et al. [12]. These experiments involved the shearing of an annular layer of glass spheres. A rough plate sheared the top of the annular layer and the pressure was measured at the bottom of the layer using a force gauge of fixed area. These studies are typical of many quasi-static shearing experiments. The system remains close to a static state, so that if the shear stress is reduced, the system typically reverts to a static state with only small changes in the particle configurations. However, enough shear is applied during steady-state motion that the system unjams intermittently, presumably associated with a short-term weakening of the shear modulus. In some sense, this type of motion straddles the jammed-unjammed boundary, first on one side, and then on the other. In addition, it is typical that a region of the material weakens and forms what is called a shear band. Because a shear band has lower shear strength than other regions, it tends to persist as a localized region where most of the shear deformation occurs. This process is typified by local structural rearrangements and frequently with large force fluctuations. The fluctuations in the experiments of Miller et al. showed a kind of rate-independence. They also yielded information on the force and pressure distributions, Fig. 6. The force detector was of fixed diameter, so by varying the particle diameter, it was possible to tune the number of particles contacting the detector from a small number, to ~ 100 particles. For the largest particles, this provided, at least roughly, information on $P(F)$. For the smallest particles, one might expect that the force fluctuations would be substantially averaged out, yielding something more like the mean pressure. We show data for the PDF's of the measured forces/stresses, in Fig. 6. If the forces acting on the detector from individual particles were uncorrelated, then one would expect that this would narrow as $N^{1/2}$, i. e. as the square root of the number of contacting particles, and evolve towards a gaussian. In fact, there is much less narrowing than would occur for uncorrelated forces from individual particles.

Two recent studies of 3D continuously sheared systems provide additional insight [16,17,18,86]. Both systems yield PDF's of forces at the boundaries, and it is interesting to contrast the two sets of results.

Corwin et al. [87] have recently presented extensive experiments using a photoelastic technique to measure forces at the bottom boundary of a cylindrical container filled with spherical particles and sheared from above. In the steady state, particles in the bottom layer located beyond a characteristic radius, R_b, exhibited dynamic shear flow, specifically, a shear band. Particles located closer to the center than this radius remained in a permanently jammed state and moved as a solid body. Corwin et al. obtained P(F)'s, with a particular focus on the region above R_b. These distributions, Fig. 7, show an enhancement for small F, and qualitatively resemble those obtained by Howell et al. for 2D shear flow, as discussed

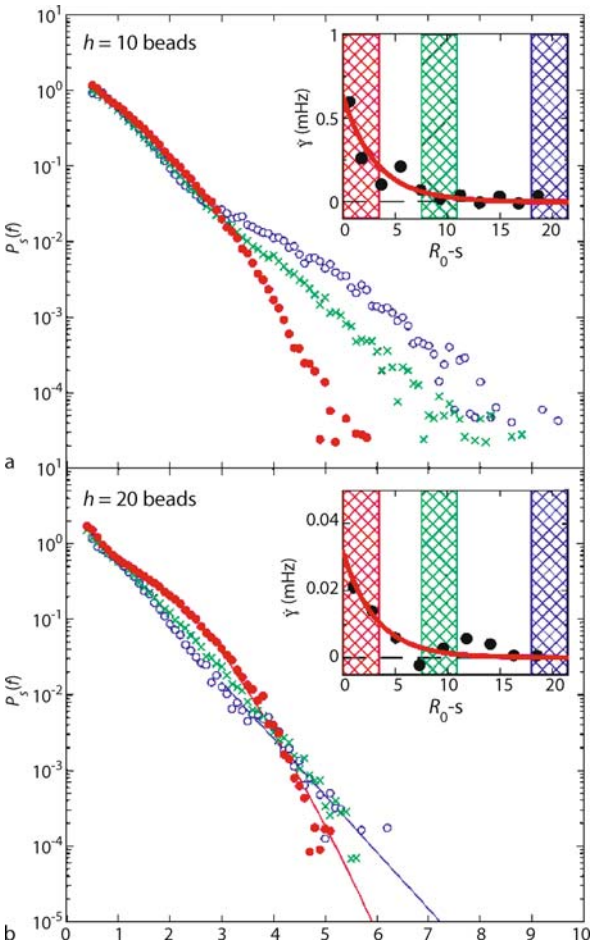

Jamming of Granular Matter, Figure 7
P(F) in sheared and non-sheared zones. Reprinted from [87]

below. Corwin et al. proposed that these distributions can be related to an effective temperature, T_{eff}, by noting that the distribution of forces and the radial correlation function, assuming forces described by a potential, $V(r)$, should satisfy $P(F)dF = G(r)dr$, where $G(r)dr$ is the radial distribution function. They then drew on the small-r thermal result $G(r) \propto r^{-2}\exp[-V(r)\beta]$ where $\beta = 1/(k_B T)$ (in this case, T should be replaced by T_{eff}). This argument leads to the prediction that at low forces, one should expect $P(F) \propto F^{-1/3}$, a prediction that describes their data well. The resulting effective temperatures obtained from this analysis are insensitive to shear rate and also to the height of the granular layer.

Other recent studies of sheared 3D particles, this time in an annular channel, were carried out by Daniels and Behringer [16,17,18]. In these experiments, the overall geometry was similar to Miller et al. [12] but in addition, the bottom boundary of the experiment was shaken with peak accelerations that typically exceeded the acceleration of gravity. The shaking motion allowed the system to find not only a jammed state, but actually a crystalline state. At high enough shear, the crystal melted, producing a shear-banded, disordered, and flowing state. This transition was clearly evident in $P(F)$. Here, F is the force exerted by particles on a transducer that is roughly three particle diameters across. In the crystalline state, $P(F)$, Fig. 8, had an overall envelope that was roughly gaussian, but that had two peaks which were induced by the vibrational motion. In the melted, disordered state, $P(F)$ resembled the distributions of Miller et al. As the transition to the ordered state was approached from the disordered state, the tail of $P(F)$ became increasingly extended. Associated with this long tail were increasingly large volume fluctuations. In fact, the variance of volume fluctuations and the various moments, including the kurtosis of the P(F), showed a cusp at the transition. This is particularly interesting in the present discussion, since the volume variance should be proportional to the derivative of the Edwards entropy (discussed in Sect. "Statistical Framework of Jamming") with respect to compactivity, i. e. the Edwards ensemble analogue of a specific heat.

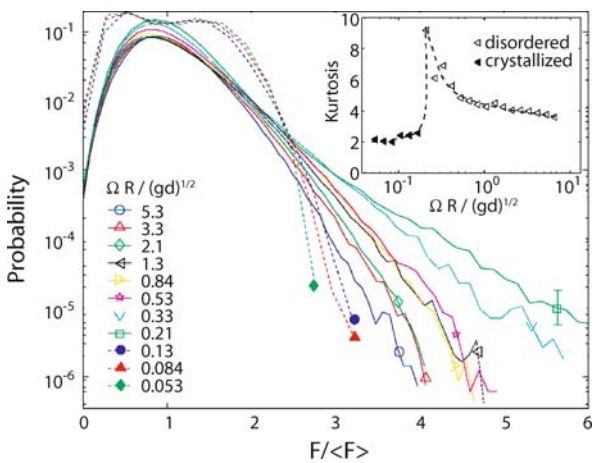

Jamming of Granular Matter, Figure 8
Distributions for the pressure/force at the bottom of an annular layer of spheres that is sheared at a rate Ω, from above, and that is vibrated from below with a peak acceleration of $\Gamma = 2.0$, in units of g. R is the mean radius of the annulus, and d is the particle diameter. The two-peaked distributions are in the crystalline phase, and the single-peaked distributions are in the disordered phase. The *inset* shows the Kurtosis of the distributions as a function of a scaled shear rate. The cusp in the kurtosis is caused by the stretching out of the distributions as Ω is decreased from a large value where the state is disordered

A relatively early demonstration of jamming properties was the work of Howell et al. [13,14] These experments consisted of photoelastic disks which were sheared in an annular Couette geometry, as in the sketch of Fig. 9. The boundaries of the apparatus consisted of a fixed outer ring, and in inner wheel whose rotations provided the shear. The particles were confined in the horizontal directions by the ring and wheel, and they rested on a smooth powder-lubricated horizontal Plexiglas sheet. Data were obtained in a steady state after the system had been sheared for roughly 30 minutes. The low shearing rate meant that that the process was quasi-static and hence always close to equilibrium. In particular, if the shearing was stopped, the majority of the force chains remained unchanged following an initial relaxation. Over long times, more of the force chains decayed, but that process was logarithmically slow [85]. In these experiments, the average force per particle (roughly a measure of the particle-scale pressure) was obtained by calibrating an applied compression to the photoelastic response of the particles. These experiments, as well as those of Daniels and Behringer [18,88], showed an increase of the mean stress with the shear rate that varied linearly as the logarithm of the shear rate. The logarithmic strengthening has been shown to be consistent with predictions of the stress-based ensemble, described in Sect. "Statistical Framework of Jamming" [89].

Several observations concerning these experiments are noteworthy. First, these experiments yielded the force distributions for the mean force on a particle, and also for averages over multiple particles. Second, they showed a kind of critical slowing down as the packing fraction, ϕ, approached the jamming transition from above, and third, they showed that a characteristic length scale associated with the mean length of force chains grew as $\phi \to \phi_c$ from above. We reproduce these results in Figs. 10 and 11 [13].

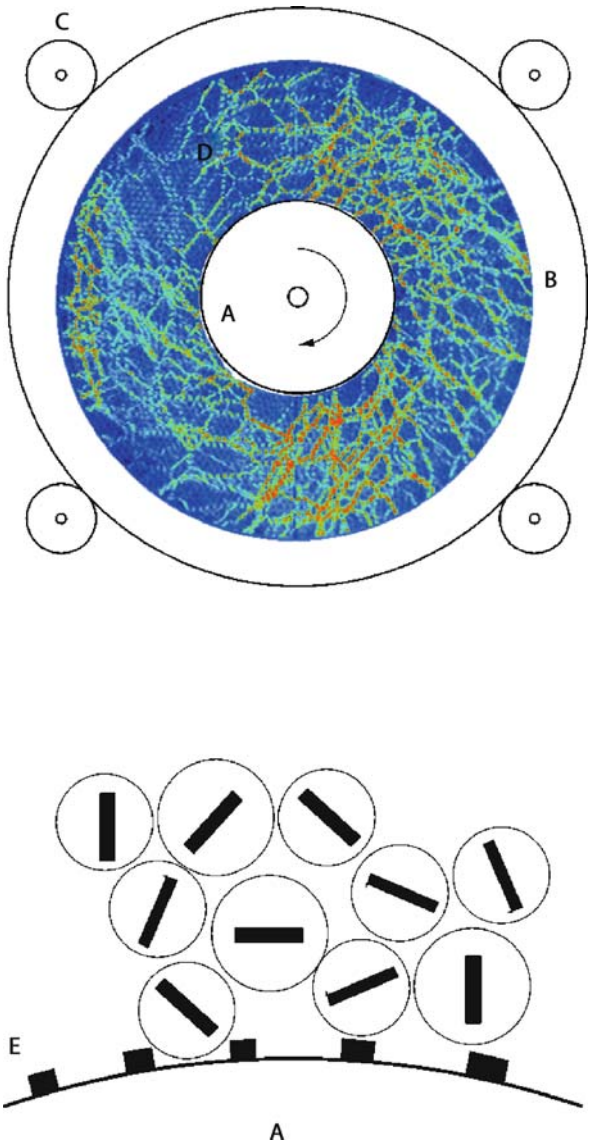

Jamming of Granular Matter, Figure 9

Sketch of the basic two-dimensional Couette shear apparatus, with an overlaid image showing the heterogeneous force structure that occurs. Photoelastic particles are confined within an annular region whose boundaries are a rotating inner wheel, and a fixed outer ring. Also shown is a blow-up sketch indicating the rough nature of the shearing wheel, and the fact that the photoelastic disks are marked with small bars for tracking purposes. In the false-color image from this experiment, *red* corresponds to particles experiencing a large force, and *blue* 0 to particles experiencing a small force [13,14]

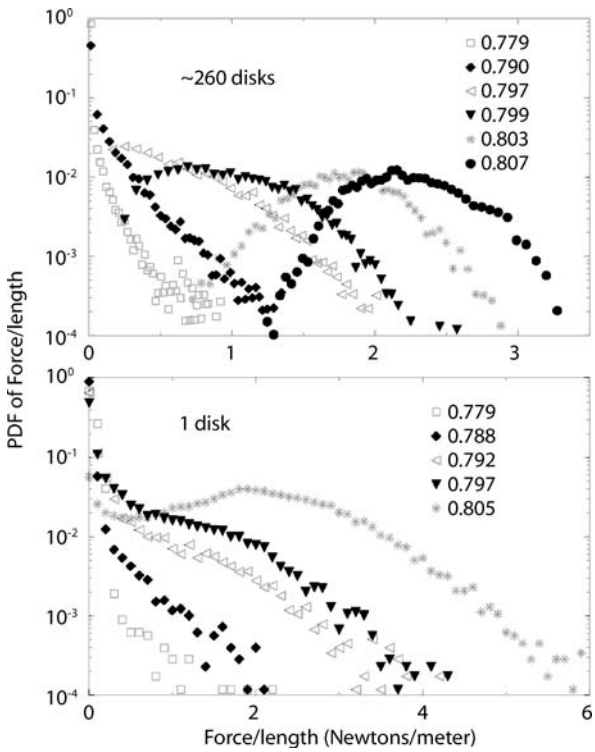

Jamming of Granular Matter, Figure 10

PDF's from the 2D Couette experiment for single particles (bottom) and for collections of particles lying within an extended region. Numbers indicate the packing fraction. This system has a critical value of $\phi = 0.776$ where stresses vanish. Note that the distributions of forces for single particles develops a maximum for large packing fractions. The distributions for forces for collections of roughly 260 particles in a contiguous region show a much stronger peak as ϕ increases, and no peak when ϕ is just above ϕ_c. This suggests that correlations in force grow as $\phi \to \phi_c$ [13]

The distributions for the single particle forces depend on the distance to ϕ_c. For ϕ close to ϕ_c, the distributions fall off roughly exponentially with large force, although there is an extra density of low force states. These distributions are nominally rather similar to single particle force distributions which were observed for particles at the boundaries of the 3D sheared system by Corwin et al. [86]. For larger ϕ, the distributions from the 2D shear experiments developed a peak which gradually migrated to larger force as the density grew. The distributions for the force on collections of particles also depend on the density. Close to jamming, they are similar to the single-particle distributions; at larger density, they evolve to a more gaussian shape. The multi-particle-force distributions are then interesting on several accounts. First, they provide a way to compare to earlier 3D pressure measurements (i. e. force measurements involving multiple particles) and they also give some sense of force correlations. That is, if the force on a given particle were uncorrelated with the force on other nearby particles, then the distribution for the forces

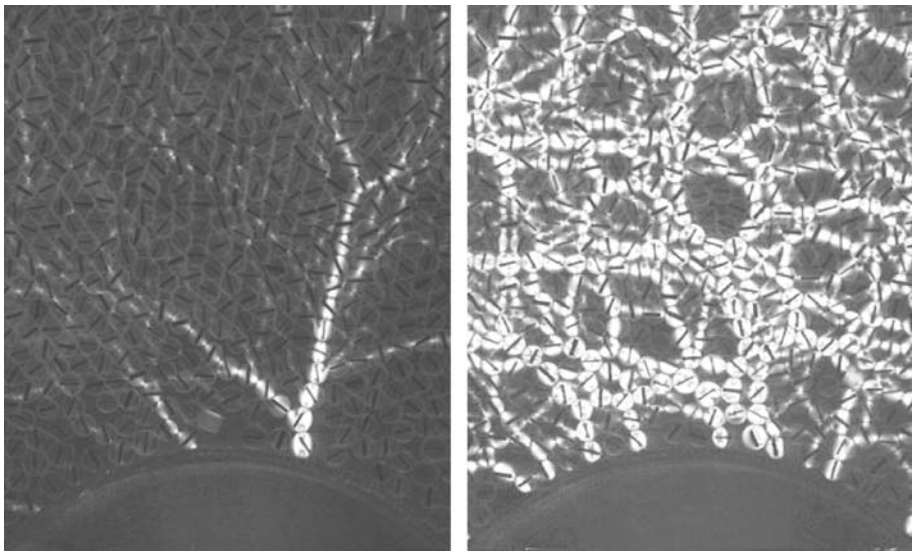

Jamming of Granular Matter, Figure 11
Photoelastic images from the Couette shear experiment at a low (*left*, $\phi - \phi_c = 0.001$) and high (*right*, $\phi - phi_c = 0.031$) distance from the unjamming point of this system. Note the long filimentary chains near ϕ_c and the tangled network far from ϕ_c [13,14]

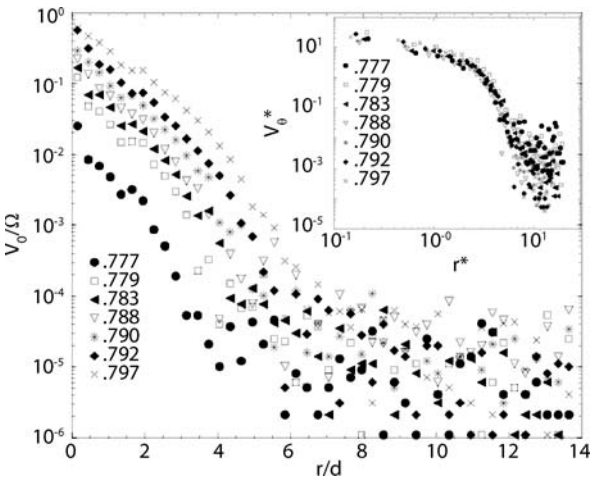

Jamming of Granular Matter, Figure 12
Data for the mean azimuthal velocity profiles vs. radial distance from the shearing wheel for the 2D Couette experiment. These data are normalized by the angular speed, Ω, of the shearing wheel. *Inset* shows that these data collapse onto a single curve when scaled a function $\propto (\phi - \phi_c)^1$ [13]

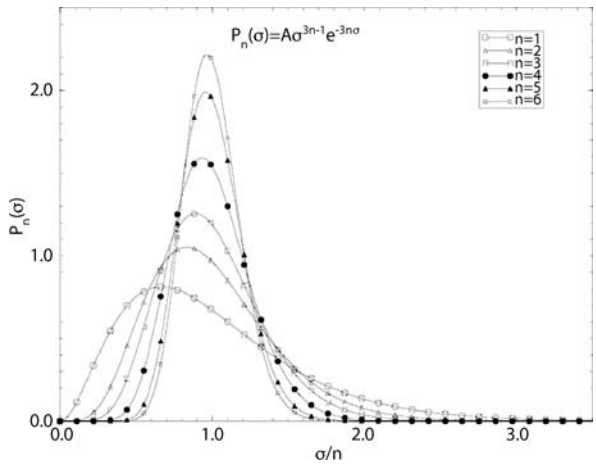

Jamming of Granular Matter, Figure 13
Computed PDF of the force per particle exerted by collections of n particles whose forces are uncorrleated and are drawn from exponential distributions. The absence of correlations leads to the expected narrowing by $n^{-1/2}$

experienced by a collection of particles would typically evolve to a guassian as the number of particles in the collection increases. This is consistent with what is observed for larger ϕ, but not with what is observed for ϕ near ϕ_c. Hence, by inference, there exist correlations for the particle-scale forces for near-critical ϕ's. To make this idea somewhat more precise, we show in Fig. 13 what happens to the PDF for the collective force for groups of particles acting on a detector if a) the forces exerted by each particle are chosen from q-model like distribution [103], and b) the forces exerted by any one particle are uncorrelated with any of the others. Specifically, the distribution narrows as $N^{-1/2}$.

The results from the 2D Couette shear for the velocity profiles vs. ϕ and also data for the characteristic force chain length both suggest that the system becomes increasingly inhomogeneous, in terms of force transmission as $\phi \to \phi_c$ from above. In particular, the typical force chain length clearly grows, although it does not necessarily diverge, in these experiments on approach to ϕ_c. In fact, given our discussion above concerning a $P - \tau$ phase diagram, we might well expect that in shear experiments one approaches point J along a path which lies above the P axis. Figure 11 contrasts a photoelastic image from Howell et al. [13] taken well above ϕ_c with an image for ϕ just slightly above ϕ_c. In the higher ϕ case, the force network is more nearly homogeneous, in contrast to the case just above ϕ_c. For the latter case, only a handful of particles are visibly in a force chain. (Here, some caution must be taken, since there is a force below which the photoelastic image is too weak to be resolved.) Nevertheless, only intermittently is there a strong enough contact at the shearing wheel so that a particle is entrained by the shearing wheel. This leads to critical slowing down which is evident in the mean velocity profiles, Fig. 12.

Isotropic vs. Anistropic Stress States

As discussed above, the nature of jamming depends, in what appears to be a significant way, on the presense or absence of shear stresses. The experiments and simulation discussed above have all involved sheared states. Here, we consider simulations and experiments which are for isotropic systems, and which focus on an approach to jamming that involves the dense/jammed side.

Numerical Simulations The phenomenon of jamming in isotropically stressed states has been extensively investigated through numerical simulations of frictionless, spherical grains in both two and three dimensions [49,90]. This work includes in particular, a series of MD simulations by O'Hern, Silbert, Liu and Nagel [49,91,92]. This series of simulations led to the introduction of the existence of a critical point at zero shear and a critical density, ϕ_c: Point J. The simulations probed the nature of the packings of spherical grains (disks in two dimensions), which interact via a short-range, soft-repulsive potential, meaning that there are no long-range interactions, and that there are purely repulsive normal forces which come into play when the grains are compressed. The packings were obtained by quenching from initial random states with a packing fraction $\phi = NV_p/V$, where N grains each with volume V_p were packed in a box of volume V. For polydispersed assemblies of grains, the definition of the packing fraction can be easily generalized. An interesting protocol that was developed in trying to identify Point J was that of inflation or deflation, in which the pressure of a quenched state was measured, and the radius of the grains were scaled up or down by small factors until the pressure was zero (within a numerical tolerance). For each initial configuration (ν) the zero pressure state corresponded to a particular packing fraction, ϕ_ν^c. At this packing fraction, the grains just touched and if the packing fraction was reduced below this, no mechanically stable states could be obtained. The crucial findings of these simulations are summarized below:

1. If properties such as pressure, shear modulus, and average number of contacts of the packings are measured as a function of $\phi_\nu - \phi_\nu^c$, then the properties are found to be independent of ν.
2. The pressure, bulk modulus and shear modulus all go to zero as some power of $\phi_\nu - \phi_\nu^c$. The exponent of the power law for the pressure and the bulk modulus follows from the force law but the shear modulus has a non-trivial exponent that indicates non-affine displacements [49,93].
3. The distribution of ϕ_ν^c becomes narrower with increasing system size and the mean approaches the Random Close Packing value [32].
4. Above ϕ_c, the average number of contact follows a power law: $\langle z \rangle - z_{\text{iso}} \propto (\phi - \phi_c)^{1/2}$.
5. The vibrational density of states exhibits increasing weight at low frequencies as Point J is approached, and the lowest frequency below which the packing behaves as a normal elastic material approaches zero [94].
6. Two different diverging lengths scales can be identified from analysis of the vibrational spectrum. These two length scales diverge with *different* exponents [95], and therefore indicate the existenc of multiple diverging correlation lengths at Point J.
7. The force distribution, $P(F)$ is sensitive to the distance from ϕ_c, and approaches an exponential as the packing fraction approaches ϕ_c

Experiments Regarding physical experiments for the isotropic case, we are aware of only one set of results, namely data by Majmudar and Behringer [68]. These results depend crucially on using photoelastic techniques in a much more precise way to obtain contact forces [68,82]. Hence, we discuss briefly how this approach works. The basic idea is the following. For given contact forces acting on a disk, the stress field within the disk is determined. The stress field in turn determines the photoelastic response. Specifically, for a ray that traverses a slab of

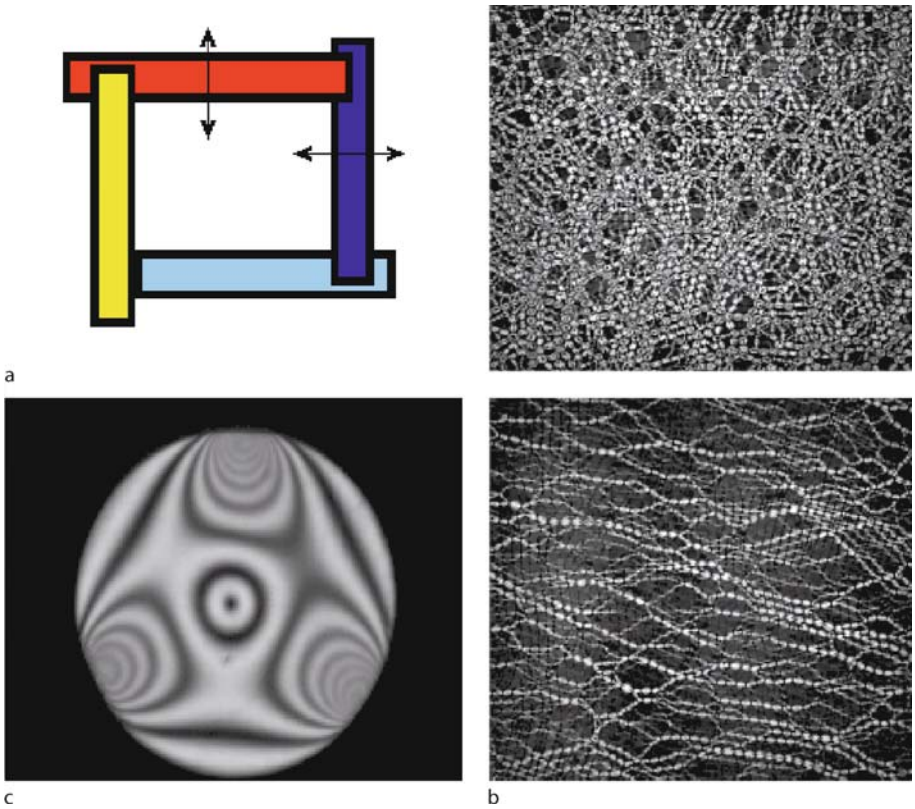

Jamming of Granular Matter, Figure 14
Biaxial experiment. a Sketch illustrating the fact that two walls of the experiment are moveable, allowing the creation of arbitrary (rectangular) deformations and stress states. b Two different stress states produced by top: isotropic compression, and bottom: pure shear, i. e. compression in one direction and equal dilation in the opposite. c A closeup image of a single photoelastic particle showing the detailed photoelastic pattern that is used to deduce contact forces [68]

photoelastic material of thickness L that is sandwiched between crossed circular polarizers, the transmitted intensity is $I = I_o \sin^2[(\sigma_2 - \sigma_1)CL/\lambda]$. Here, σ_2 and σ_1 are the principal stresses in the plane of the slab (or disk), C, the stress optic coefficient is a property of the material, and λ is the wavelength of the light with intensity I_o. Thus, contact forces determine stresses which in turn determine the photoelastic pattern. The idea is to carry out the inverse of this process. Specifically, from the photoelastic pattern, determine the applied forces. This can be done efficiently in the case of a disk because there is a closed form relation for the stress field generated by any number of contact forces.

MB have developed such an inverse process and applied it to systems of photoelastic disks that have been prepared in well defined stress/deformation states. The particularly important aspect of these experiments is that they have yielded the only experimental data, to our knowledge, for contact forces inside a granular sample, although a number of other experiments have yielded forces at boundaries. This point is important; theoretical studies by Snoeijer et al. [83,84] indicate that force distributions for contacts at boundaries and in the interior of a sample differ substantially.

Figure 14 shows a rough schematic of a biaxial tester (or biax) and resulting photoelastic response images for different types of applied stresses [68]. The purpose of the biax is to prepare states of well controlled strain or stress. The biax is constructed so that the space between opposing pairs of walls can be set to any convenient value. The particles in this sample are bidisperse disks, with about 80% having a smaller diameter (0.8cm) and 20% having a larger diameter (0.9 cm). Bidisperse packings of this sort typically have no long-range crystalline order, although they tend to show hexagonal bond order.

Manifestly, the force chain structures that result from pure shear vs. isotropic compression, Fig. 14b, are substantially different. Pure shear induces force chains that extend nearly straight and uninterrupted over the compressional

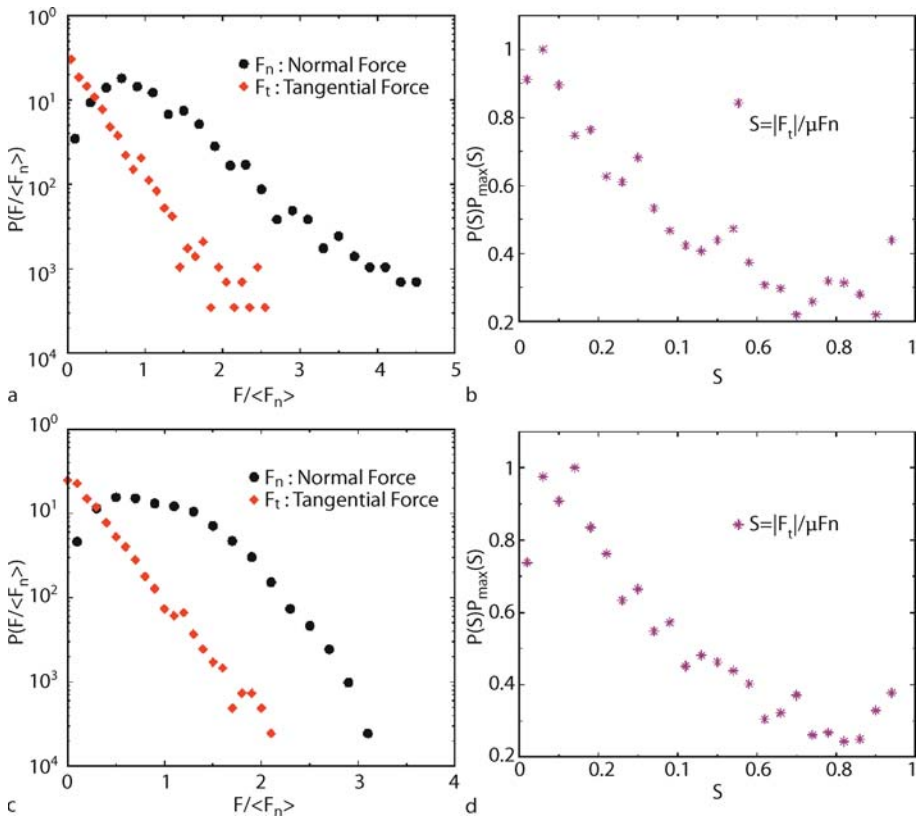

Jamming of Granular Matter, Figure 15

Distributions of forces for pure shear (*top*) and isotropic compression (*bottom*). Parts a and c give distributions of normal (F_n) and tangential (F_t, frictional) forces, all normalised by the appropriate mean normal force, $\langle F_n \rangle$. Parts b and d indicate the mobilization of friction, where the variable S indicates fully mobilized (at the point of slipping) friction when $S = 1$ [68]

direction of the biax. This is intuitively reasonable, since the pure shear state is achieved by compressing, hence strengthening contacts in one direction, while dilating the sample, thus weakening contacts, in the perpendicular direction. By contrast, for an isotropically compressed sample, the force network consists of a dense tangle of short force chain segments.

Various statistical measures reflect the fact that shear and isotropic compression yield qualitatively different states. We consider first, the distributions of contact forces, $P(F)$, which are given in Fig. 15. For convenience, forces are normalized by $\langle F_n \rangle$, the mean normal force. The figures show separate distributions for the normal and tangential contact forces. Although the distributions for the tangential forces are always exponentially distributed, regardless of the stress state, the same is not true for the normal force distribution. These clearly reflect the stress state, with a state of pure shear showing a roughly exponential fall-off at large F, and with a state of isotropic compression showing a much more rapid fall-off with F. In fact, these distributions are consistent with recent entropy-based arguments by Snoeijer et al. [83] and by Tighe et al. [96]. In both cases, the distributions for the normal forces show a peak at a force comparable to the mean. Perhaps a better measure of the difference between the shear and isotropic deformations is given by the force correlation function, which is significantly longer range along the force chain direction of the sheared case, than any direction for the isotropic case [68]. We show these results in Fig. 16.

Isostaticity and Point J

Isostaticity and Random Close Packing

This section is devoted to a geometrical picture which offers a perspective that is complementary to the statistical ensemble picture. The geometrical approach is focused on mathematically precise descriptions of packing of infinitely rigid particles [32,65]. In this statistical geometric picture, packings are characterized by the type of jamming: local, collective or strict. In the hierarchy of jammed states,

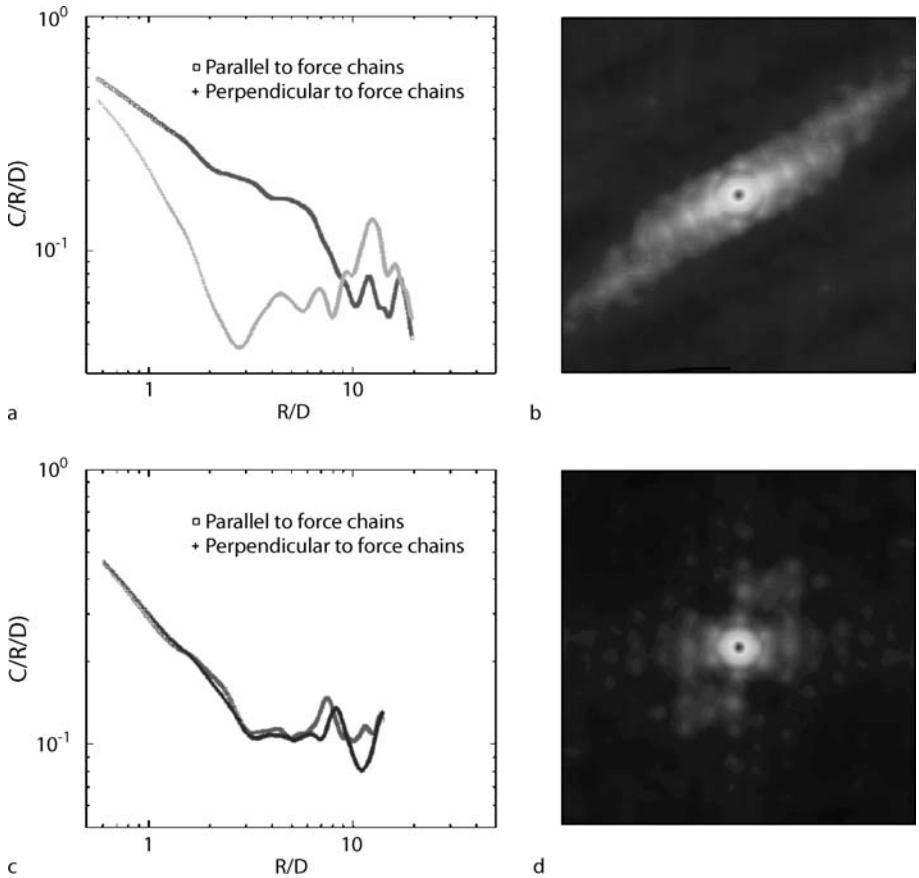

Jamming of Granular Matter, Figure 16

Force-force correlation functions obtained from 2D experiments. To compute these correlation functions, we compute the average force magnitude, $\langle F(r+r')F(r)\rangle$, acting on a particle. Since the system may be anisotropic, the average over r' must retain the angular information. We contrast data for a system that has been subjected to pure shear, top, with one that has been subject to isotropic compression, bottom. (See part b of Fig. 14). The right side of the figure shows a grayscale representation of the data. For the shear case, the correlation function has a roughly power-law decay (to the limits of the system size) for correlations along the strong force chain direction, and a rapid drop off for the transverse direction. For the isotropically compressed case, the correlations are identical in all directions, and decay rapidly [68]

locally jammed states are ones where each particle in the system is locally trapped by its neighbors. Collectively jammed states are ones where all finite subsets of particles are trapped by their neighbors, and strictly jammed states are collectively jammed configurations for which no global, volume-nonincreasing deformations are possible [32]. In addition, the degree of order in the packings is characterized by an order parameter or an order metric [97]. The emphasis in this approach is to understand the existence of packings, not their statistical weight in any dynamical protocol. The geometrical approach applies to infinitely rigid bodies which is an idealization of real particles, but the classification into jamming categories and a precise understanding of the nature of packings which can exist as the packing fraction is varied provides a framework onto which the statistical decsription can be superposed. There are a few special points on a phase diagram in the order-packing fraction space: (a) the maximally random jammed state (MRJ) is an extremal point corresponding to the least ordered, strictly jammed state, (b) the random-loose-packed (RLP) state is another extremal point corresponding to the lowest density at which a strictly jammed state can exist. This RLP state is more ordered than the MRJ state and is extremely fragile [97]. In contrast to the concept of random close packing (RCP) [32,97], the MRJ state is protocol-independent leading to a mathematical framework for studying randomeness in hard particle packings. The definition of MRJ does, however, depend on the choice of the order parameter, and further work needs to be done to explore appropriate order parameters.

Isostatic Packings are Marginal

It has become increasingly clear through theoretical analysis and simulations that isostatic packing of frictionless, isotropic particles are marginally stable. Simulations show that the vibrational spectrum of these packings have many soft modes and that the density of states of zero-frequency modes become non-zero as Point J (which is isostatic) is approached [49]. There is a diverging length scale associated with these vibrational modes, and this length scales as $1/(z - z_{\rm iso})$ [61,94]. The theoretical explanation for this divergence is rooted in the vanishing degrees of freedom as the isostatic point is approached from the jammed, hyperstatic side [60,61,93]. Stability analysis of the packing of deformable, isotropic grains, also shows that there is a marginal stability line along which, the pressure of the packing obeys $p/B = (z - z_{\rm iso})^2$, where p is the pressure and B is the bulk modulus of the packing [60,93]. Packings with fewer than the number of contacts specified by this relation are unstable. The question of whether isostacity and marginality always go hand in hand is an interesting question that is beginning to be explored [65,98].

Simulations and Theory

As discussed in Sect. "Isotropic vs. Anistropic Stress States", simulations of deformable, spherical grains [49,91] exhibit a special packing fraction, ϕ_c, below which it is impossible to construct a jammed packing, and interestingly, for large systems, ϕ_c approaches the RCP value. Recent theoretical work based on the isostatic nature of Point J [60,93], have provided an explanation for the diverging correlation length and the scaling relation between pressure and the number of contacts. A theory based on a minimum number of contacts needed for *local* stability is the K-core percolation model of Schwarz, Chayes and Liu [99]. This theory focusses on the mixed first-second order nature of the transition at Point J in terms of the order parameter, $\langle z\rangle$, which approaches $z_{\rm iso}$ with an exponent close to 1/2 as $\phi \to \phi_c^+$, but which is predicted to be zero for ϕ infinitesimally below ϕ_c. The meanfield exponents of this model agree with the exponents associated with Point J in the numerical simulations.

A field theory of jammed grain packings in two dimensions, and close to Point J has been constructed using the generalized stress-based ensemble (Sect. "Statistical Framework of Jamming"), and a fluctuating field related to the Airy Stress function [55]. This field theory [56], identifies two order parameters associated with the transition at Point J; the Airy stress function and the deviation of the number of contacts from the isostatic value. The field theory predicts a transition with a diverging length scale. Recent work [57] has focussed on refining this field theory by comparing its predictions to simulations of frictionless disks [49].

The stress-based ensemble described in Sect. "Statistical Framework of Jamming" can be used to understand the exponential form of $P(F)$, if one uses the fact that the packings at ϕ_c are isostatic. The starting point of this calculation is the canonical partition function of the stress-based ensemble: $Z(\alpha) = \sum_\nu {\rm e}^{-\alpha\Gamma_\nu}$, where α is the counterpart of the inverse temperature and $\Gamma = \sum_{ij} |r_{ij}|F_{ij}$ [53]. At ϕ_c, the spheres or disks are just touching, and therefore, the separations $|r_{ij}|$ can be replaced by the diameter of the grains. The sum over grain configurations, ν, therefore, involves a sum over the F_{ij}'s and the angles of the contact vectors. The isostatic point is special in that there is a one-to-one correspondence between geometry and forces. This means that for a chosen set of $\{F_{ij}\}$, there is only one geometry characterized by a set of contact angles that can be mechanically stable. The partition function then becomes:

$$Z(\alpha) = \sum_{\{F_{ij}\}} {\rm e}^{-\sum_{ij}\alpha F_{ij}} = \left[\int_0^\infty {\rm d}F {\rm e}^{-\alpha F}\right]^{z_{\rm iso}N/2} \tag{6}$$

The integral is easily performed, and the result can be used to relate α to the average contact force, $\langle F\rangle$: $\alpha = (z_{\rm iso}/2)\langle F\rangle$. Since the forces on different contacts are completely independent of each other at this isostatic point, as seen from Eq. (6), it follows that $P(F) \propto {\rm e}^{-\alpha F} = {\rm e}^{-z_{\rm iso}F/(2\langle F\rangle)}$, a pure exponential. This is a consequence of isostaticity. Away from the isostatic point, the correspondence between geometry and a set of contact forces is no longer one-to-one and distributions will acquire a non-exponential character, in agreement with observations that $P(F)$ of crystalline packings are more Gaussian than disordered packings, as discussed in Sect. "Force Distributions, Length and Time Scales in Jammed States near the Jamming Transition".

Analysis of simulations of frictionless disks, using this generalized ensemble led to a definitive functional form for the distribution of $\Gamma_m = \sum_{i=1}^m \sum_j r_{ij}F_{ij}$, the pressure of m particles inside an assembly of N grains, integrated over the volume occupied by the grains (Γ is known as the internal virial). The distribution $P_m(\Gamma_m)$ depends only on $x = N\Gamma_m/\Gamma_N$, where Γ_N is the internal virial of the whole assembly of N grains, and the functional form is [53]:

$$P_m(x) \propto x^{\rm ma}{\rm e}^{-ax}\ , \tag{7}$$

where $a = 2 + (\langle z\rangle - z_{\rm iso})^2$ This form indicates that the distribution would approach a Gaussian with a width which narrows as $\sqrt{m}$, in x space. In the space of the

unscaled variable Γ_m, however, the distribution could acquire a non-trivial shape and scaling with m if $\Gamma_N \to 0$, or equivalently, $\alpha \to \infty$. Since this is what happens as $\phi \to \phi_c$, one can expect non-trivial scaling of the pressure distribution. Equation (7) also shows that the exponential tail is maximally stretched at $\langle z \rangle = z_{\rm iso}$. Evidence for this may appear in the distributions of Fig. 8, where just at the transition, the exponential tail has become extremely extended.

There are many existing models for the exponential distribution of forces. In one view [87,91], the exponential distribution is related to the form of the pair correlation function $G(r)$, a function that measures the number of particles separated by a distance r, at small r. Using generic properties of $G(r)$ and the limit where grains are barely compressed, leads to a $P(F) \propto e^{-F^\kappa}$, where the exponent κ depends on the force law. In this approach, the exponential distribution is not related to isostaticity. This point of view was developed through the discussion of the experimental results of Corwin et al. [87]. A different set of approaches have considered the origin of the unidirectional transmission of forces (force chains) [100,101,102] by proposing a new class of constitutive relations arising from constraints on the stress tensor due to geometry of the packings. This approach has a natural connection to the generalized ensemble [28,54] and isostaticity [28,41,55]. An earlier, heuristic model, the q-model led to unidirectional propagation of forces, and an exponential distribution of contact forces [103]. More recently, Snoeijer et al. [83] and Tighe et al. [96] have predicted force distributions using the force ensemble approach (Sect. "Statistical Framework of Jamming"). The connection between the stress-based ensemble and force chains, away from isostaticity is still being explored.

Experimental Observations

Direct experimental investigation of Point J, approached from the jammed side, and the behavior in its vicinity have been more limited than computational and theoretical studies. We are aware of only one experiment by Majmudar et al. [59] that has directly probed Point-J from the jammed side. This work [59] has provided detailed experimental data for the mean contact number, Z, and the pressure, P vs. the packing fraction, ϕ_c. Hence, it is possible now to make direct comparison between a physical experiment and theory/model results. In these experiments, photoelastic disks were confined in the biaxial tester discussed above. The photoelastic approach allows the experimental determination of contact forces between pairs of particles or between particles and a boundary.

Figure 17 shows results for $Z(\phi)$ and $P(\phi)$. The data for Z show a fairly rapid increase in Z with increasing ϕ, but not a truly sharp discontinuity. However, assuming a reasonable choice of ϕ_c, the data indicate an increase of Z above the critical value which varies as $Z - Z_c \propto (\phi - \phi_c)^\alpha$ with an exponent $\alpha = 0.55 \pm 0.05$. This result is in agreement with the simulation of frictionless grains [49]. The pressure also follows a power-law in $\phi - \phi_c$ with an exponent of 1.1 ± 0.05, which is in agreement with Silbert et al. [49]. Finally, it is possible to compare to the stress-ensemble predictions of Henkes and Chakraborty by eliminating α in their predictions for $P(\alpha)$ and $Z(\alpha)$ to obtain an expression for $P(Z)$. The data, Fig. 18, are also in reasonable agreement with this prediction.

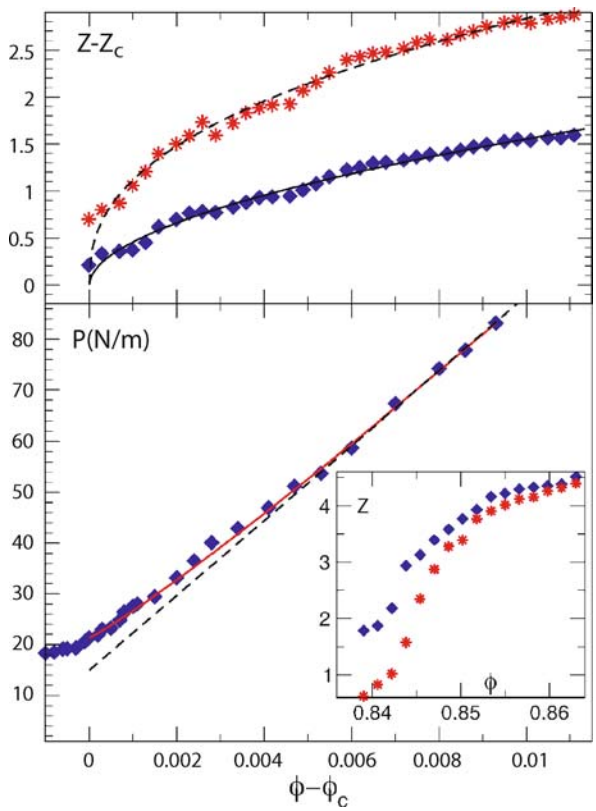

Jamming of Granular Matter, Figure 17
Data for the pressure and for the mean contact number per particle, Z vs. ϕ. The *inset* shows that Z vs. ϕ over a larger range than the *top* part of the figure. Data including rattlers as shown by asterisks, and data without rattlers by diamonds. Note that Z rises rapidly but not discontinuously at jamming. Power-law fits of P and $Z - Z_c$ vs. $\phi - \phi_c$ above jamming and for reasonable ϕ_c show expected exponents of 0.55 ± 0.05 for $Z - Z_c$ and 1.1 for P [59]

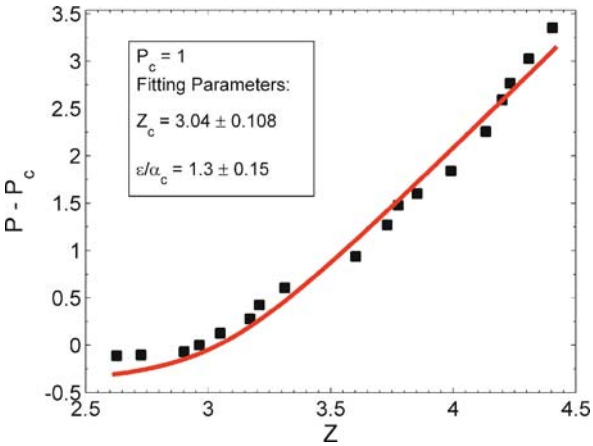

Jamming of Granular Matter, Figure 18
Data of Majmudar et al. for *P* vs. *Z* showing the generally good agreement with the predictions of Henkes and Chakraborty [59]

Future Directions

From the combined experimental, theoretical, and simulation studies of the last decade, a picture of the nature of jamming in granular matter is beginning to emerge, although many questions remain. In our discussion, we distinguish jamming/unjamming under isotropic and anisotropic stress conditions. Many recent simulations have considered the isotropic approach to Point J. A number of experiments have explored jamming/unjamming, although most of these involved the succession of failures that occur under shear and away from Point J, which corresponds to processes with a heuristically 'first-order' character. We believe that it is important to distinguish these various cases. To our knowledge, no one has considered the approach to Point J along an anisotropic stress path.

There are clear indications of heterogeneities in granular matter. These have both a spatial and a temporal aspect, and they become increasingly important with the approach to jamming. They have been identified on both the fluid-like and jammed side of the transition.

One aspect of these heterogeneities is concerned with forces and their transmission. A clear manifestation is in force chains, which can show strong correlations in the sheared state, but very short range correlations in the isotropic stress state. In dynamic processes, force chains continually rearrange, leading to strong force fluctuations. Although force chains are clearly visible in a variety of 2D experiments that are carried out above jamming, incipient stress chains have been observed in simulations of hopper flow on the fluid-like side [20], and there is evidence of arch formation and stress chains in experiments studying jamming in hopper flow [104,105,106]. An open question concerns the role that such structures may play if Point J is approached along a path of anisotropic stress.

A different type of heterogeneity in granular flows is related to the mobilities of grains [9,10]. This situation is similar to heterogeneities in supercooled liquids.

The analogies between jamming and thermal phase transitions prompts questions about the extent of the similarities between the two. For instance, is there an order parameter associated with the transition? Studies of the special type of jamming at Point J suggest that pressure and the deviation of the number of contacts from the isostatic value are the two, possibly coupled, candidates for the order parameter.

The generic jamming/unjamming transition that takes place in the presence of non-zero shear stress is characterized by intermittent dynamics and is reminiscent of trap-like dynamics, where the shearing causes the system to "hop" from one jammed state to another and jamming occurs when the average time scale for exploring all the traps diverges [89,107]. The framework of soft-glassy-rheology [108] provides an approach to calculating the stress response of granular packings approaching jamming. In this picture, the jammed state is an intrinsically non-equilibrium state, which exhibits aging, meaning a slow evolution of its properties with time. The issues raised here are much the same as those arising in the context of the glass transition, and involve understanding the relation between fluctuations and response [109], through the definition of an effective temperature. This is an area of active research [110,111,112,113,114].

Understanding the jamming of non-spherical grains is much less advanced than that of spherical grains. In this regard, the geometrical approach of Torquato and Stillinger [65] is being applied to non-spherical grains. Experiments have probed the issue of isostaticity in non-spherical grains [115,116,117]. The stress-based ensemble described in this article is a promising approach for analyzing these issues.

In the context of frictional and frictionless packings, a question that needs to be addressed is what aspects of the jamming transition are sensitive to the presence of friction. Simulations and theories of jamming have mainly focussed on frictionless grains. The statistical ensemble approaches, however, are general and provide an avenue for a unified framework.

These observations raise many questions:

1. How are stress chains related to the the mobility of grains? Since force chains tend to lock grains in place, it may well be that there is anti-correlation between force chains and mobility.

2. Is there a basic dynamical principle leading to the occurrence of stress chains, or are they more strongly influenced by geometry?
3. What if any, is the relationship between the length and time scales on the jammed side to those observed on the flowing side?
4. Are incipient chains on the fluid-like side responsible for jamming as the transition is approached? Is jamming caused by a divergence of the lifetime of these chains?
5. Is there an extension to jamming in the presence of shear? That is, how does the path in P-τ space affect jamming?
6. What is the nature of jamming for nonspherical particles, for systems with a broad range of particle sizes, or for particles that interact with cohesive forces?

The advances in experimental techniques which have led to the measurement of grain-level forces, has been a tremendous boon for theorists. Simulations have led to detailed descriptions of fluctuations which provide means for testing theoretical frameworks. The recent advance in the statistical ensemble approach to jamming, the geometrical characterizations of packings of rigid grains, combined with the detailed experimental and simulation studies, is expected to answer many of the remaining questions and lead to a fuller understanding of the phenomenon of jamming.

Bibliography

1. Jaeger H, Nagel S, Behringer R (1996) Granular solids, liquids, and gases. Rev Mod Phys 68:1259–1273
2. Jaeger H, Nagel S, Behringer R (1996) The physics of granular materials. Phys Today 49:32–38
3. Kadanoff LP (1999) Built upon sand: Theoretical ideas inspired by granular flows. Rev Mod Phys 71:435
4. Weeks ER, Crocker JC, Levitt AC, Schofield A, Weitz DA (2000) Three-dimensional direct imaging of structural relaxation near the colloidal glass transition. Science 287:627
5. Donati C et al (1998) Stringlike cooperative motion in a supercooled liquid. Phys Rev Lett 80:2338
6. Donati C, Glotzer S, Poole P, Kob W, Plimpton S (1999) Spatial correlations of mobility and immobility in a glass-forming lennard-jones liquid. Phys Rev E 60:3107
7. Berthier L et al (2005) Direct experimental evidence of a growing length scale accompanying the glass transition. Science 310:1797–1800
8. Lacevic N, Starr F, Schroder T, Glotzer S (2003) Growing correlation length on cooling below the onset of caging in a simulated glass-forming liquid. J Chem Phys 119:7372
9. Keys AS, Abate AR, Glotzer SC, Durian DJ (2007) Direct observation of growing dynamical length scales and prediction of the jamming transition from dynamical heterogeneity in a granular system. Nat Phys 3:260
10. Dauchot O, Marty G, Biroli G (2005) Dynamical heterogeneity close to the jamming transition in a sheared granular material Phys Rev Lett 95:265701
11. Pouliquen O (2004) Velocity correlations in dense granular flows. Phys Rev Lett 93:248001
12. Miller B, O'Hern C, Behringer RP (1996) Stress fluctuations for continously sheared granular materials. Phys Rev Lett 77: 3110
13. Howell D, Behringer RP (1999) Fluctuations in a 2d granular Couette experiment: A critical transition. Phys Rev Lett 82: 5241
14. Veje C, Howell D, Behringer RP (1999) Kinematics of a two-dimensional granular couette experiment at the transition to shearing. Phys Rev E 59:739–745
15. Geng J, Behringer RP, Reydellet G, Clément E (2003) Green's function measurements of force transmission in 2d granular materials. Physica D 182:274
16. Daniels KE, Behringer RP (2005) Hysteresis and competition between disorder and crystallization in sheared and vibrated granular flow. Phys Rev Lett 94:168001
17. Daniels KE, Behringer RP (2005) Characterization of a freezing/melting transition in a vibrated and sheared granular medium. In: Garcia-Rojo R, Herrmann HJ, McNamara S (eds) Powders, Grains 05 357–360 Balkema, Rotterdam
18. Daniels KE, Behringer RP (2006) Characterization of a freezing/melting transition in a vibrated and sheared granular medium. J Stat Mech 7:P07018
19. Longhi E, Easwar N, Menon N (2002) Large force fluctuations in a flowing granular medium. Phys Rev Lett 89:0455011–0455014
20. Ferguson A, Chakraborty B (2007) Spatially heterogenous dynamics in dense, driven granular flows. Europhys Lett 78
21. Silbert LE, Ertas D, Grest GS, Halsey TC, Levine D (2002) Analogies between granular jamming and the liquid-glass transition. Phys Rev E 65:051307
22. Silbert L (2005) Temporally heterogeneous dynamics in granular flows. cond-mat/0501617
23. Silbert LE, Grest GS, Brewster R, Levine AJ (2007) Rheology and contact lifetimes in dense granular flows. Phys Rev Lett 99:068002
24. Chandler D (1987) Introduction to Modern Statistical Mechanics. Oxford University Press, New York
25. Dolnik M, Zhabotinsky A, Epstein I (1996) Modulated standing waves in a short reaction-diffusion system. J Physical Chem 100:6604–6607
26. Dhar D (2006) Theoretical studies of self-organized criticality. Phys A-Stat Mech Appl 369:29–70
27. Schmittmann B, Zia RKP (1995) Statistical Mechanics of Driven Diffusive Systems. In: Domb C, Lebowitz J (eds) Phase Transitions and Critical Phenomena, vol 17. Academic Press, New York
28. Edwards SF, Blumenfeld R (2007) The thermodynamics of granular materials. In: Mehta A (ed) Physics of Granular Materials, Cambridge University Press, Cambridge
29. Edwards SF, Grinev DV (1999) Statistical mechanics of stress transmission in disordered granular arrays. Phys Rev Lett 82:5397
30. Edwards SF, Oakeshott RBS (1989) Theory of powders. Phys A 157:1080
31. Edwards SF, Grinev DV (2001) Jamming and Rheology: Con-

strained Dynamics on Microscopic and Macroscopic Scales. Taylor, New York
32. Donev A, Torquato S, Stillinger F, Connelly R (2004) Jamming in hard sphere and disk packings. J Appl Phys 95:989–999
33. Barrat A, Kurchan J, Loreto V, Sellitto M (2001) Edwards' measures: A thermodynamic construction for dense granular media and glasses. Phys Rev E 6305:0513011–05130114
34. Barrat A, Kurchan J, Loreto V, Sellitto M (2000) Edwards' measures for powders and glasses. Phys Rev Lett 85:5034
35. Coniglio A, Fierro A, Nicodemi M (2002) Probability distribution of inherent states in models of granular media and glasses. Eur Phys J E 9:219
36. Coniglio A, Fierro A, Nicodemi M (2001) Applications of the statistical mechanics of inherent states to granular media. Phys a-Stat Mech Appl 302:193
37. Kurchan J (2001) Recent theories of glasses as out of equilibrium systems. Comptes Rendus Acad Sci Ser Iv Phys Astrophys 2:239–247
38. Makse H, Kurchan J (2002) Testing the thermodynamic approach to granular matter with a numerical model of a decisive experiment. Nature 415:614–617
39. Blumenfeld R, Edwards SF (2003) Granular entropy: Explicit calculations for planar assemblies. Phys Rev Lett 90:1143031–1143034
40. Snoeijer JH, Vlugt TJH, van Hecke M, van Saarloos W (2003) Force network ensemble: a new approach to static granular matter. Phys Rev Lett 91:072303
41. Tkachenko A, Witten T (1999) Stress propagation through frictionless granular material Phys Rev E 60:687
42. Snoeijer J, Vlugt T, van Hecke M, van Saarloos W (2004) Force network ensemble: A new approach to static granular matter. Phys Rev Lett 92:0543021–0543024
43. Snoeijer J, Ellenbroek W, Vlugt T, van Hecke M (2006) Sheared force networks: Anisotropies, yielding, and geometry. Phys Rev Lett 96:09800191–0980014
44. van Eerd ART, Ellenbroek WG, van Hecke M, Snoeijer JH, Vlugt TJH (2007) Tail of the contact force distribution in static granular materials. Phys Rev E 75:0603021–0603024
45. Snoeijer J, van Hecke M, Somfai E, van Saarloos W (2003) Force and weight distributions in granular media: Effects of contact geometry. Phys Rev E 67:0303021–0303024
46. Snoeijer J, van Hecke M, Somfai E, van Saarloos W (2004) Packing geometry and statistics of force networks in granular media. Phys Rev E 70:0113011–01130115
47. Snoeijer J, Vlugt T, Ellenbroek W, van Hecke M, van Leeuwen J (2004) Ensemble theory for force networks in hyperstatic granular matter. Phys Rev E 70:0613061–06130616
48. Tighe B, Socolar J, Schaeffer D, Mitchener W, Huber M (2005) Force distributions in a triangular lattice of rigid bars. Phys Rev E 72:0313061–03130610
49. O'Hern CS, Silbert LE, Liu AJ, Nagel SR (2003) Jamming at zero temperature and zero applied stress: The epitome of disorder. Phys Rev E 68:011306
50. Bertin E, Dauchot O, Droz M (2006) Definition and relevance of nonequilibrium intensive thermodynamic parameters. Phys Rev Lett 96:1206011–1206014
51. Bertin E, Dauchot O, Droz M (2005) Nonequilibrium temperatures in steady-state systems with conserved energy. Phys Rev E 71:0461401–04614014
52. Bertin E, Dauchot O, Droz M (2004) Temperature in nonequilibrium systems with conserved energy. Phys Rev Lett 93:2306011–2306014
53. Henkes S, O'Hern CS, Chakraborty B (2007) Entropy and temperature of a static granular assembly: An ab initio approach. Phys Rev Lett 99:0380021–0380024
54. Blumenfeld R (2007) On entropic characterization of granular materials. To appear in: Aste T, Tordesiillas A, Matteo T (eds) Lecture Notes. World Scientific, Singapore
55. Ball RC, Blumenfeld R (2002) Stress field in granular systems: Loop forces and potential formulation. Phys Rev Lett 88:115505
56. Henkes S, Chakraborty B (2005) Jamming as a critical phenomenon: A field theory of zero-temperature grain packings. Phys Rev Lett 95:1980021–1980024
57. Henkes S, Chakraborty B (2008) Field theory, soft modes and the nature of jamming the critical point. Phys Rev E (to appear)
58. Liu AJ, Nagel SR (1998) Jamming is not just cool anymore. Nature 396:21
59. Majmudar TS, Sperl M, Luding S, Behringer RP (2007) Jamming transition in granular systems. Phys Rev Lett 98:058001
60. Wyart M (2005) On the rigidity of amorphous solids. Ann Phys 30:1–96
61. Wyart M, Nagel S, Witten T (2005) Geometric origin of excess low-frequency vibrational modes in weakly connected amorphous solids. Europhys Lett 72:486–492
62. Kirkpatrick TR, Thirumalai D, Wolynes PG (1989) Scaling concepts for the dynamics of viscous liquids near an ideal glassy state. Phys Rev A 40:1045
63. Xia X, Wolynes PG (2001) Fragilities of liquids predicted from the random first order transition theory of glasses. Phys Rev Lett 86:5526
64. Bouchaud J, Biroli G (2004) On the adam-gibbs-kirkpatrick-thirumalai-wolynes scenario for the viscosity increase in glasses. J Chem Phys 121:7347–7354
65. Donev A, Connelly R, Stillinger FH, Torquato S (2007) Underconstrained jammed packings of nonspherical hard particles: Ellipses and ellipsoids. Phys Rev E 75:0513041–05130432
66. Reynolds O (1885) On the dilatancy of media composed of rigid particles in contact. Philos Mag Ser 5 50–20:469
67. Nedderman RM (1992) Statics and kinematics of granular materials. Cambridge University Press, Cambridge
68. Majmudar TS, Behringer RP (2005) Contact force measurements and stress-induced anisotropy in granular materials. Nature 435:1079–1082
69. Blume M, Emery V, Griffiths RB (1971) Ising model for the lambda transition... Phys Rev A 4:1071
70. Lois G, Lemaitre A, Carlson JM (2007) Spatial force correlations in granular shear flow. i. numerical evidence. Phys Rev E 76:0213021–02130212
71. Lois G, Lemaitre A, Carlson JM (2007) Spatial force correlations in granular shear flow. ii. theoretical implications. Phys Rev E 76:0213031–02130314
72. Ferguson A, Chakraborty B (2006) Stress and large-scale spatial structures in dense, driven granular flows. Phys Rev E 73:0113031–0113037
73. Ferguson A, Fisher B, Chakraborty B (2004) Impulse distributions in dense granular flows: Signatures of large-scale spatial structures. Europhys Lett 66:277–283
74. Hurley M, Harrowell P (1995) Kinetic structure of a two-dimensional liquid. Phys Rev E 52:1694–1698

75. Perera D, Harrowell P (1996) Kinetic structure of a two-dimensional liquid. Phys Rev E 54:1652
76. Pouliquen O (1999) Scaling laws in granular flows down rough inclined planes. Phys Fluid 11:542–548
77. Ertas D, Halsey T (2002) Granular gravitational collapse and chute flow. Europhys Lett 60:931–937
78. Kolb E, Cviklinski J, Lanuza J, Clauding P, Clement E (2004) Reorganizationof a dense granular assembly: The unjamming response function. Phys Rev E 69:031306
79. Drocco JA, Hastings MB, Reichardt CJO, Reichardt C (2005) Multiscaling at point j: Jamming is a critical phenomenon. Phys Rev Lett 95:088001
80. Geng J, Behringer RP (2005) Slow drag in two-dimensional granular media. Phys Rev E 71:011302
81. Ediger MD, Angell CA, Nagel SR (1996) Supercooled liquids and glasses. J Phys Chem 100:13200
82. Majmudar TS, Behringer RP (2005) Contact forces and stress induced anisotropy. In: Garcia-Rojo R, Herrmann HJ, McNamara S (eds) Powders and Grains. 65 AA Balkema, Leiden
83. Snoeijer JH, van Hecke M, Somfai E, van Saarloos W (2004) Force and weight distributions in granulr media: Effects of contact geometry. Phys Rev E 67:030302
84. Snoeijer JH, Vlugt TJH, van Hecke M, van Saarloos W (2004) Force network ensemble: A new approach to static granular matter. Phys Rev Lett 92:054302
85. Hartley RR, Behringer RP (2003) Logarithmic rate dependence of force networks in sheared granular materials. Nature 421:928
86. Corwin EI, Jaeger HM, Nagel SR (2005) Structural signature of jamming in granular media. Nature 435:1075–1078
87. Corwin E, Jaeger H, Nagel S (2005) Structural signature of jamming in granular media. Nature 435:1075–1078
88. Daniels KE, Behringer RP (2005) Hysteresis and competition between disorder and crystallization in sheared and vibrated granular flow: Hysteresis and competition between disorder and crystallization in sheared and vibrated granular flow. Phys Rev Lett 94:168001
89. Behringer RP, Chakraborty B, Henkes S, Hartley RR (2008) Why do granular materials stiffen with shear rate? a test of novel stress-based statistics. Phys Rev Lett (to appear)
90. Makse H, Johnson D, Schwartz L (2000) Packing of compressible granular materials. Phys Rev Lett 84:4160–4163
91. O'Hern C, Langer S, Liu A, Nagel S (2001) Force distributions near jamming and glass transitions. Phys Rev Lett 86:111
92. O'Hern C, Langer S, Liu A, Nagel S (2002) Random packings of frictionless particles. Phys Rev Lett 88:075507
93. Ellenbroek WG (2007) Response of Granular Media near the Jamming Transition. Ph.D thesis, Leiden University
94. Wyart M, Silbert LE, Nagel SR, Witten TA (2005) Effects of compression on the vibrational modes of marginally jammed solids. Phys Rev E 72:051306
95. Silbert LE, Liu AJ, Nagel SR (2005) Vibrations and diverging length scales near the unjamming transition. Phys Rev Lett 95:098301
96. Tighe BP, Socolar JES, Schaeffeer DG, Mitchener WG, Huber ML (2005) Force distributions in a triangular lattice of rigid bars. Phys Rev E 72:031306
97. Torquato S, Truskett T, Debenedetti P (2000) Is random close packing of spheres well defined? Phys Rev Lett 84:2064–2067
98. Krzakala F, Kurchan J (2007) Landscape analysis of constraint satisfaction problems. Phys Rev E 76:0210021–02100213
99. Schwartz J, Liu A, Chayes L (2006) The onset of jamming as the sudden emergence of an infinite k-core cluster. Europhys Lett 73:560–566
100. Cates M, Wittmer J, Bouchaud J, Claudin P (1998) Jamming, force chains, and fragile matter. Phys Rev Lett 81:1841–1844
101. Cates M, Wittmer J, Bouchaud J, Claudin P (1998) Development of stresses in cohesionless poured sand. Philos Trans Royal Soc London Ser A-Math Phys Eng Sci 356:2535–2560
102. Cates ME, Wittmer JP, Bouchaud JP, Claudin P (1999) Jamming and static stress transmission in granular materials. Chaos 9:511–522
103. Coppersmith S, Liu C, Majumdar S, Narayan O, Witten T (1996) Model for force fluctuations in bead packs. Phys Rev E 53:4673–4685
104. To K (2005) Jamming transition in two-dimensional hoppers and silos. Phys Rev E Stat Nonlin Soft Matter Phys 71:060301
105. Zuriguel I, Garcimartin A, Maza D, Pugnaloni LA, astor JM (2005) Jamming during the discharge of granular matter from a silo. Phys Rev E Stat Nonlin Soft Matter Phys 71:051303
106. Easwar N Private Communication
107. Monthus C, Bouchaud J-P (1996) Models of traps and glass phenomenology. J Phys A 29:3847
108. Sollich P (1998) Rheological constitutive equation for a model of soft glassy materials. Phys Rev E 58:738
109. Bouchaud J, Cugliandolo L, Kurchan J, Mezard M (1996) Mode-coupling approximations, glass theory and disordered systems. Physica A 226:243–273
110. Song C, Wang P, Potiguar F, Makse H (2005) Experimental and computational studies of jamming. J Phys-Condens Matter 17:S2755–S2770
111. Song C, Wang P, Makse H (2005) Experimental measurement of an effective temperature for jammed granular materials. Proc National Acad Sci USA 102:2299–2304
112. Potiguar F, Makse H (2006) Effective temperature and jamming transition in dense, gently sheared granular assemblies. Euro Phys J E 19:171–183
113. Ono I et al (2002) Effective temperatures of a driven system near jamming. Phys Rev Lett 89:0957031–0957034
114. O'Hern C, Liu A, Nagel S (2004) Effective temperatures in driven systems: Static versus time-dependent relations. Phys Rev Lett 93:1657021–1657024
115. Desmond K, Franklin SV (2006) Jamming of three-dimensional prolate granular materials. Phys Rev E Stat Nonlin Soft Matter Phys 73:031306
116. Man W et al (2005) Experiments on random packings of ellipsoids. Phys Rev Lett 94:198001
117. Blouwolff J, Fraden S (2006) The coordination number of granular cylinders. Europhys Lett 76:1095

Books and Reviews

Blumenfeld R (2004) Stresses in isostatic granular systems and emergence of force chains. Phys Rev Lett 93:108301

Bouchaud JP (2003) Granular media: Some ideas from statistical physics. In: Barrat JL, Dalibard J, Feigelman M, Kurchan J (eds) Slow relaxations and nonequilibrium dynamics in condensed matter. Springer, Berlin

Bouchaud JP, Claudin P, Levine D, Otto M (2001) Force chain splitting in granular materials: A mechanism for large-scale pseudo-elastic behaviour. Eur Phys J E 4:451–457

Coniglio A, Fierro A, Herrmann H, Nicodemi M (eds) (2004) Unifying concepts in granular media and glasses, 1st edn. Elsevier, Amsterdam
Mehta A (1994) Granular matter: an interdisciplinary approach. Springer, New York
Halsey TC, Mehta A (2002) Challenges in granular physics. World Scientific, Singapore
Herrmann HJ, Hovi JP, Luding S (1998) Physics of dry granular media. In: NATOASI series. Series E, Applied sciences, vol 350. Kluwer Academic, Dordrecht
Jiang Y, Liu M (2007) A brief review of "granular elasticity": why and how far is sand elastic? Eur Phys JE Soft Matter 22:255–260
Krimer DO, Pfitzner M, Brauer K, Jiang Y, Liu M (2006) Granular elasticity: general considerations and the stress dip in sand piles. Phys Rev E Stat Nonlin Soft Matter Phys 74:061310
Otto M, Bouchaud JP, Claudin P, Socolar JES (2003) Anisotropy in granular media: classical elasticity and directed-force chain network. Phys Rev E Stat Nonlin Soft Matter Phys 67:031302
Ovarlez G, Fond C, Clement E (2003) Overshoot effect in the janssen granular column: a crucial test for granular mechanics. Phys Rev E Stat Nonlin Soft Matter Phys 67:060302
Torquato S, Donev A, Stillinger F (2003) Breakdown of elasticity theory for jammed hard-particle packings: conical nonlinear constitutive theory. Int J Solid Struct 40:7143–7153

Jerky Motion in Slowly Driven Magnetic and Earthquake Fault Systems, Physics of

Karin A. Dahmen[1], Yehuda Ben-Zion[2]
[1] Department of Physics, University of Illinois at Urbana-Champaign, Urbana, USA
[2] Department of Earth Sciences, University of Southern California, Los Angeles, USA

Article Outline

Glossary
Definition of the Subject
Introduction
Models
Theoretical Results
Summary
Future Directions
Acknowledgments
Bibliography

Glossary

Mean field theory A theoretical approximation with an interaction field that has constant strength and infinite range. In mean field approximation every domain interacts equally strongly with every other domain, regardless of their relative distance.

Critical point A (phase transition) point in the parameter space of a physical system where the length scale characteristic of its structure, called the correlation length ξ, becomes infinite and the system displays power law scaling behavior on all available scales. The associated critical power law exponents are universal, i. e. they are independent of the microscopic details of the system.

Universality Power law scaling exponents and scaling functions near a critical point are the same for a class of systems, referred to as universality class, independent of the microscopic details. Universal aspects typically depend only on a few basic physical attributes, such as symmetries, range of interactions, dimensions, and dynamics.

Tuning parameters Parameters such as disorder, temperature, pressure, driving force etc. that span phase diagrams. Critical values of the tuning parameters describe critical points of the phase diagrams.

Renormalization group (RG) A set of mathematical tools and concepts used to describe the change of physics with the observation scale. Renormalization Group techniques can be used to identify critical points of a system as fixed points under a coarse graining transformation, and to calculate the associated critical power law exponents and the relevant tuning parameters. They can also be used to determine what changes to the system will leave the scaling exponents unchanged, and thus to establish the extent of the associated universality class of the critical point.

Earthquake quantities The most common form of earthquake data consists of seismic catalogs that list the time, location, and size of earthquakes in a given space-time domain. The size of earthquakes is usually specified by magnitudes associated with spectral amplitudes of seismograms at a given frequency and site-instrument conditions. The seismic potency and moment provide better physical characterizations for the overall size of earthquakes. Additional important quantities are the geometry of faulting (e. g., strike slip), stress drop at the source region, and radiated seismic energy.

Seismic potency A physical measure for the size of earthquakes given by the integral of slip over the rupture area during a seismic event.

Seismic moment A physical measure of earthquakes given by the rigidity at the source region times the seismic potency.

Strike slip fault A style of faulting involving pure horizontal tangential motion, predicted for situations where the maximum and minimum principal stresses are both horizontal. Prominent examples include the

San Andreas fault in California, the Dead Sea transform in the Levant and the North Anatolian fault in Turkey.

Definition of the Subject

Observations indicate that earthquakes and avalanches in magnetic systems (Barkhausen Noise) exhibit broad regimes of power law size distributions and related scale-invariant quantities. We review results of simple models for earthquakes in heterogeneous fault zones and avalanches in magnets that belong to the same universality class, and hence have many similarities. The studies highlight the roles of tuning parameters, associated with dynamic effects and property disorder, and the existence of several general dynamic regimes. The models suggest that changes in the values of the tuning parameters can modify the frequency size event statistics from a broad power law regime to a distribution of small events combined with characteristic system size events (characteristic distribution). In a certain parameter range, the earthquake model exhibits mode switching between both distributions. The properties of individual events undergo corresponding changes in different dynamic regimes. Universal scaling functions for the temporal evolution of individual events provide similar predictions for the earthquake and magnet systems. The theoretical results are generally in good agreement with observations. Additional developments may lead to improved understanding of the dynamics of earthquakes, avalanches in magnets, and the jerky response to slow driving in other systems.

Introduction

Global Statistics and Power Law Scaling

Earthquakes occur in a broad spectrum of sizes, ranging from unnoticeable tremors to catastrophic events. While short term earthquake prediction is still beyond reach, understanding the statistics of earthquakes might facilitate longer term prediction of large earthquakes and statistical estimates of seismic hazard. Gutenberg and Richter [29] found that the frequency of observed regional and global earthquakes versus magnitude forms a regular function over a very large range of scales (see Fig. 1). When the measure for the earthquake size is the seismic potency or moment (see "Glossary"), the frequency size statistics of regional and global earthquakes follow a power law distribution. Precise definitions and details on the seismic potency and moment are given in [1] and [3]. (In this paper we assume a unit nominal rigidity and will therefore use potency and moment interchangeably.) Omori [57] found

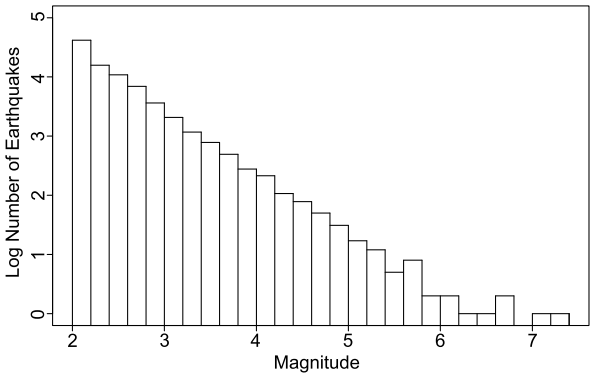

Jerky Motion in Slowly Driven Magnetic and Earthquake Fault Systems, Physics of, Figure 1
Histogram of earthquakes with magnitude 2.0 or larger recorded by the Southern California network during 1984–2002. The earthquake catalog is available at http://www.data.scec.org/research/SHLK.html

that the decay rate of aftershocks with time follows a power law distribution. One would expect that there might be a simple explanation for why earthquakes occur in a broad range of sizes and follow regular statistical patterns!

In the last two decades it has become increasingly evident that there are many other systems that respond to slowly changing external conditions with events on extremely large ranges of scales ("crackling noise"). An example of particular interest here involves magnets, which respond to a slowly varying external field by changing their magnetization in a series of bursts or "avalanches" called Barkhausen Noise. Just like earthquakes, these avalanches come in many sizes, ranging from microscopic to macroscopic and are distributed according to a regular function over the entire range. The spectra of the source time function of earthquakes is approximately flat up to a corner frequency related to the rupture size, followed by a power law decay at higher frequencies [1,3]. Similarly, the spectra of the number of spins flipping per time during an avalanche in magnets has high frequency power law decay with a low frequency roll off [68]. For certain values of tuning parameters, earthquake and magnet quantities are associated with scale invariant functions (power laws). In such cases each individual magnetic avalanche or earthquake slip has fractal spatial structure (see Fig. 2 for magnets and Fig. 5a for earthquakes). Other systems with similar "collective events" of all available sizes include, among others, superconductors, charge density waves, and group decision making [66].

While there are several interesting recent reviews, pointing out the similarities between systems with power law event size distributions, the goal of this paper is to de-

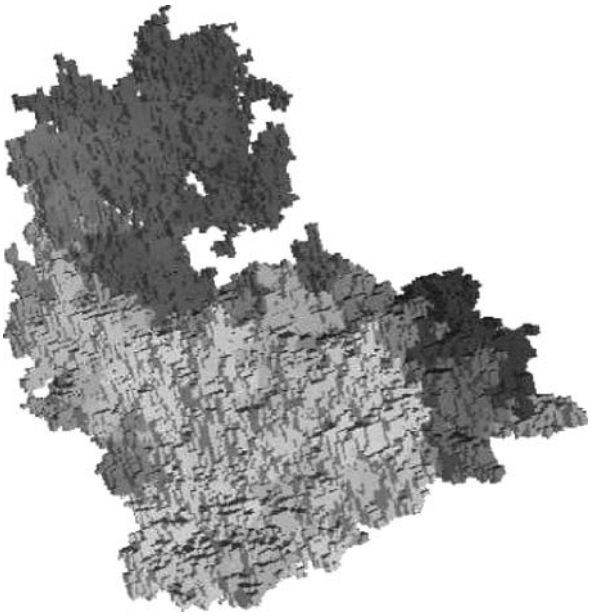

Jerky Motion in Slowly Driven Magnetic and Earthquake Fault Systems, Physics of, Figure 2
Fractal spatial structure of a medium sized avalanche of 282 785 domain flips in the 3 dimensional random field Ising model [66]. Fractal structures and power laws are characteristic of systems at their critical point. The shading represents time of the domain flips: the first domains to flip are at the right end of the avalanche, the last towards the left. The short range of the ferromagnetic interactions causes the avalanche to be spatially connected (see [66])

velop in detail some of the connections and analysis methods in earthquake and magnetic systems. Expanding on some of our earlier results, we focus especially on the role of disorder and dynamic changes in the strength threshold as potential tuning parameters to drive the system toward power law scaling behavior or away from it. Table 1 summarizes some of the similarities between magnets and earthquakes that are discussed in this review.

In Sect. "Models" we describe several magnet and earthquake models that are simple enough to make the connections transparent and easy to recognize. In Sect. "Theoretical Results" we review theoretical results obtained from these models and their comparison to experimental or observational data. Finally in Sect. "Summary" we summarize the results and discuss future work, both observationally and theoretically, that can help to improve our understanding of the dynamics of earthquakes and magnets.

Models

Models for Barkhausen Noise in Magnets

Hysteresis and avalanches in disordered magnetic materials have been modeled using several variants of the nonequilibrium, zero-temperature random-field Ising model (RFIM), which is one of the simplest models of magnetism, with applications far beyond magnetic systems (for a review, see [66], and also [15,56,58]). In contrast to some other hysteresis models, like the Preisach model [44] and the Stoner–Wohlfarth model [33], where interactions between the individual hysteretic units (grains) are not included and collective behavior in the form of avalanches is not addressed, in the RFIM the inter grain coupling is an essential feature and cause for hysteresis and avalanche effects.

The Random Field Ising Model (RFIM) The *equilibrium* RFIM was originally introduced to study disordered magnetic materials in thermal equilibrium. We study the *nonequilibrium* version, to model hysteresis and

Jerky Motion in Slowly Driven Magnetic and Earthquake Fault Systems, Physics of, Table 1
Some scaling features that are similar for magnets and earthquakes. More details on the various properties are given in the indicated sections

	Earthquake system	Magnetic system
Frequency size statistics	Power law near criticality, characteristic distribution away from criticality (Sect. "Results on the Monotonic Version of the Model")	Same as earthquakes (Sect. "Results on the Monotonic Version of the Model")
Scaling of source shape functions	Parabola for moment rate shape of events with fixed duration T in simulations, scaling function skewed to the left for observational data (Sect. "Moment Rate Shapes for Monotonic Models")	Same as earthquakes (Sect. "Moment Rate Shapes for Monotonic Models")
Spatial properties of individual events	Fractal near criticality, compact away from criticality (Sect. "Non-monotonic Models" and Fig. 5)	Same as earthquakes (Sects. "Non-monotonic Models"" and "Phase Diagram"" and Fig. 2)
Spectral decay of source function of individual events	Flat up to a corner frequency followed by power law decay (Sect. "Introduction")	Same as earthquakes (Sect. "Introduction")

avalanches observed *far from thermal equilibrium*. Even though the model is a toy version of the microscopic details in a magnet, near the critical point it correctly describes the large scale behavior of systems with the same general properties such as symmetries, dimensions, interaction ranges and dynamics [15], as follows from renormalization group arguments.

In the RFIM, to each site i in a simple cubic lattice is assigned a variable s_i, a so called "spin", which can take two different values, $s_i = +1$ ("up") or $s_i = -1$ ("down"). (This corresponds to a real magnet where a crystal anisotropy prefers the magnetic moments or elementary domains, represented by the spins, to point along a certain easy axis.) Each spin interacts with its nearest neighbors on the lattice through a positive exchange interaction, J_{nn}, which favors parallel alignment. (For the behavior on large scales the exact range of the microscopic interaction is irrelevant, so long as it is finite.) Some variations of the RFIM also include *long range* interactions due to the demagnetizing field and the dipole-dipole interactions. A general form of the Hamiltonian can be written as [37]

$$\mathcal{H} = -\sum_{\mathrm{nn}} J_{\mathrm{nn}} s_i s_j - \sum_i H s_i - \sum_i h_i s_i + \sum_i \frac{J_{\mathrm{inf}}}{N} s_i - \sum_{\{i,j\}} J_{\mathrm{dipole}} \frac{3\cos(\theta_{ij}) - 1}{r_{ij}^3} s_i s_j \,, \quad (1)$$

where H is the homogeneous external magnetic driving field, h_i is a local, uncorrelated random field, that models the disorder in the system, J_{inf} is the strength of an infinite range demagnetizing field, N is the total number of spins in the system, and J_{dipole} is the strength of the dipole-dipole interactions. The power laws of generated events are independent of the particular choice for the distribution $\rho(h_i)$ of random fields, for a large variety of distributions. Usually a Gaussian distribution of random fields is used, with a standard deviation ("disorder") R. As a simple approximation the model is studied at zero temperature, far from equilibrium, to describe materials with sufficiently high barriers to equilibration, so that temperature fluctuations are negligible on experimental time scales. As the magnetic field is adiabatically slowly changed between $H = -\infty$ to $H = +\infty$ two different *local* dynamics have been considered:

(1) in the first ("bulk") dynamics, each spin s_i flips while decreasing its own energy. We have studied this dynamics for the original RFIM without long range interactions, i. e. for $J_{\mathrm{inf}} = J_{\mathrm{dipole}} = 0$ [15,58]. This dynamics allows for *both* domain nucleation (when a spin s_i surrounded by equal valued spins flips in the opposite direction), *and* for domain wall motion (when a spin flips on the surface of a preexisting cluster of uniform spins in a background of opposite valued spins). A spin flip can trigger neighboring (or more generally, coupled) spins to flip as well, leading to an avalanche of spin flips, analogous to a real Barkhausen pulse. During an avalanche the external field is kept constant until the avalanche is finished, in accordance with the assumed adiabatic limit. The model is completely deterministic – two successive sweeps through the hysteresis loop produce the exact same sequence of avalanches (since the temperature is set to zero). This dynamics may be appropriate to describe for example hard magnetic materials with strong anisotropies. The analogue earthquake system may be associated with fault regions or fault networks that have strong geometrical and material heterogeneities.

(2) The second dynamics is a "front propagation dynamics" in which only the spins on the edge of an existing front (interface between up and down spins) flip if that decreases their energy. This dynamics can be used to model soft magnetic materials with a single or several noninteracting advancing domain walls and negligible new domain nucleation, due to antiferromagnetic demagnetizing fields. The front propagation model without long range interactions ($J_{\mathrm{inf}} = J_{\mathrm{dipole}} = 0$) was originally introduced by Robbins et al. to model fluids invading porous media [43]. The analogue earthquake system for this case may be associated with a single fault zone.

Simple Models for Inhomogeneous Earthquake Faults

Much of the previous work on simple earthquake models has involved variants of the Burridge–Knopoff (or "sliderblock") model, in which complex behavior is generated in a system with many degrees of freedom, and where inertia, friction laws and inherent discreteness play important roles [11,38,61]. These systems appear to exhibit power-law statistics over some range with a cutoff beyond some magnitude, and with most of the slip occurring in larger system-size events. However the understanding of the origin of the power law behavior is limited. Our approach here is to obtain an analytic understanding of a class of models and then to add in various additional features by analytic scaling arguments using tools from the theory of phase transition and the renormalization group, aided by numerical studies. There are interesting related studies using tools from statistical physics [12,63]. Some studies suggest that the power law scaling is connected to a spinodal [34]. Various cellular automata models have also been used for modeling earthquakes [40]. Rather than reviewing a large number of models, we will focus on a subgroup

of models, that we found particularly well suited to clarify the connection between earthquake and magnetic systems with a jerky response to slowly changing external conditions.

The Ben-Zion and Rice Model A representative of the class of models that we consider is a model developed originally by Ben-Zion and Rice [2,5,6], referred to below as the BZR model. The model assumes that a narrow irregular strike-slip fault zone of horizontal length L and vertical depth W may be represented by an array of $N \sim LW$ cells in a two dimensional planar region of length L and width W, with long range interaction, abrupt transitions in the threshold dynamics during failure, and constitutive parameters that vary from cell to cell to model the disorder (offsets etc.) of the fault zone structure (Fig. 3).

The cells represent brittle patches on the interface between two tectonic blocks that move with slow transverse velocity v in the x direction at a great distance from the fault. The interaction between cells during slip events is governed by 3-D elasticity and falls off with a distance r from the failure zone as $1/r^3$. The cells remain stuck while the stress τ_i on each cell is increased gradually as a result of the external loading which grows adiabatically (that is we take the limit $v \to 0$). When the stress on a cell i reaches its local failure threshold $\tau_{s,i}$, the cell slips until the stress is reduced to its local arrest stress $\tau_{a,i}$. Both failure stress and arrest stress are distributed according to some bounded probability distribution. The stress drop resulting from a cell failure is redistributed to the other cells according to the long range elastic stress transfer function. The resulting stress increase on the other cells can cause some of them to slip as well, leading to an avalanche of cell slips, or a model earthquake. A review of extensive numerical simulations with various versions of the BZR model, in relation to observed features of seismicity, criticality, and other dynamic regimes, is given in [75].

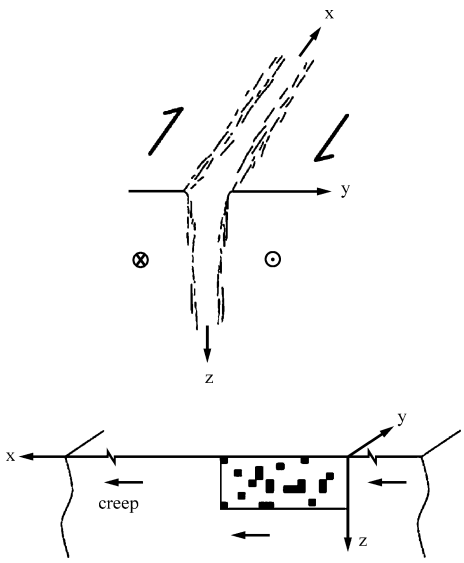

Jerky Motion in Slowly Driven Magnetic and Earthquake Fault Systems, Physics of, Figure 3
Illustration of the Ben-Zion and Rice (BZR) model: projection of a 3D fault zone (*top*) onto a 2D interface embedded in a 3D elastic halfspace (*bottom*). The geometrical inhomogeneities of the physical fault zone are modeled by spatially varying constitutive parameters of the brittle patches (see [46])

Dynamical Weakening The model includes dynamic weakening effects during the failure process [2,5,6]: after an initial slip in an earthquake, the strength of a failed cell is reduced to a *dynamical* value:

$$\tau_{d,i} \equiv \tau_{s,i} - \epsilon(\tau_{s,i} - \tau_{a,i}), \tag{2}$$

with $0 \le \epsilon \le 1$ parametrizing the relative importance of the dynamical weakening in the system. This weakening represents the transition from static friction to dynamic friction during the rupture. The strength of a failed cell remains at its dynamic value throughout the remainder of the earthquake. In the time intervals between earthquakes all failure thresholds heal back to their static value $\tau_{s,i}$.

Dynamical Strengthening The model can be expanded further to include dynamic strengthening represented by $\epsilon < 0$. Multidisciplinary observations indicate [7] that brittle failure of rock has an initial transient phase associated with strengthening, distributed deformation, and creation of new structures. Detailed frictional studies also show an initial strengthening phase associated with the creation of a new population of asperity contacts [3,19]. In mean field studies of our model (Fig. 3) discussed in Sect. "Results on Aftershocks", we associate $\epsilon < 0$ with regions off the main fault segments that are in an early deformation stage. The events that are triggered as the failure stresses are lowered back in the following weakening period are referred to as *aftershocks*. The Omori law [3,69,70] is obtained if we assume that the increased failure stress thresholds $\tau_{f,i}$ are slowly lowered with time as $\log(t)$ towards their earlier static values $\tau_{s,i}$, and that the stresses are distributed over a wide range of values [46].

Related General Continuum Equations of Motion The above model is a special case of a more general class of models for infinite systems driven by a constant drive force F [27]. We consider general equations of motion of

the form:

$$\eta \partial u(\mathbf{r}, t)/\partial t = F + \sigma(\mathbf{r}, t) - f_R[u(\mathbf{r}, t), \mathbf{r}, \{u(\mathbf{r}, t' < t)\}] \quad (3)$$

where

$$\sigma(\mathbf{r}, t) = \int_{-\infty}^{t} \mathrm{d}t' \int \mathrm{d}^d r' J(\mathbf{r} - \mathbf{r}', t - t') \cdot [u(\mathbf{r}', t') - u(\mathbf{r}, t)] \quad (4)$$

is the stress and f_R is a quenched random "pinning" force crudely representing inhomogeneities in the friction, asperities, stepovers etc., which in general can depend on the local past history (e. g. as in velocity dependent friction). The dynamical variables $u(\mathbf{r}, t)$ are assumed to represent the discontinuity across the fault plane in the component of the displacement in the direction of slip. The dynamics depend on the local history dependence of the pinning force, the stress transfer function $J(\mathbf{r}, t)$, and the coefficient η that represents the fault impedance. (In an elastic medium, the impedance depends on mass density, the elastic parameters, and directional parameters [1].) Equation (3) can be considered a continuum description of the rules of the BZR model. Integrating out the degrees of freedom due to the bulk material on either side of the d=2 dimensional fault plane leaves us with effective long range static stress transfer: $J_s(r) \equiv \int \mathrm{d}t J(r, t) \sim 1/r^{d+\Gamma} \sim 1/r^3$. For a planar fault in an elastic half space, $d = 2$ and $\Gamma = 1$ [2,6]. The correlations in f_R are generally assumed to be short-range in u and $\mathbf{r}$. (For results on the BZR model with long range correlations in the disorder, see [2,27,77] and Sect. "Theoretical Results".) In a version of the BZR earthquake model with a constant driving force F, the loading may be replaced by driving through a weak spring with spring constant $K \sim 1/L$ coupled to the slowly moving continents far away (i. e. replacing F in Eq. (3) by $F(\mathbf{r}, t) = K[vt - u(\mathbf{r}, t)]$, with $v \to 0$).

Monotonic Models Substantial simplifications occur if f_R is history independent and $J(\mathbf{r}, t) \geq 0$ for all $(\mathbf{r}, t)$; leading to *monotonic* models [27]. Related monotonic models have been studied extensively in various other contexts [25,53]. Examples include elastic depinning models for contact lines, vortex lines, liquids invading porous materials, and elastic charge density waves. Their crucial simplifying feature is that the steady state velocity $\overline{v} \equiv \langle \partial u/\partial t \rangle$ is a history independent function of F [48]. In the context of the BZR model this corresponds to the case with zero weakening ($\epsilon = 0$) and non-negative J. A crucial feature of monotonic models is that the slip profile $\Delta u(\mathbf{r})$ of a quake is *independent of the dynamics* [48]. However, several interesting dynamical issues discussed below are associated with the effects left out of the monotonic models that can make this feature break down.

Non-monotonic Models (a) *Weakening*: We first consider including some weakening effects of sections which have already slipped in a given quake. This is best studied in the discrete model. In analogy to the dynamic weakening in the BZR model discussed above, we choose [27]

$$f_R = \tilde{f}_R[u(\mathbf{r}), \mathbf{r}]\{1 - \epsilon \Theta[u(\mathbf{r}, t) - u(\mathbf{r}, t - T)]\} \quad (5)$$

with T a cutoff time much longer than the duration of the largest quakes, but much smaller than the interval between the quakes. Here $\Theta(x)$ is the Heavyside step function. As mentioned, the case $\epsilon > 0$ represents the difference between static and dynamic friction. The effects of small weakening ($\epsilon > 0$) can be analyzed perturbatively (see Sect. "Theoretical Results").
(b) *Stress Pulses*: A similar but more subtle effect can be caused by stress pulses that result from non-positive $J(\mathbf{r}, t)$; these arise naturally when one includes elastodynamic effects. We consider

$$J(\mathbf{r}, t) \sim \frac{\delta\left(t - \frac{r}{c}\right)}{r^{d+\Gamma}} + \frac{\alpha \delta'\left(t - \frac{r}{c}\right)}{c r^{d+\gamma}} \quad (6)$$

with c the sound speed, $\delta(t)$ the Dirac delta distribution, and $\delta'(t) = \mathrm{d}\delta(t)/\mathrm{d}t$. The scalar approximation to elasticity in a half space corresponds to $d = 2$, $\Gamma = 1$, $\gamma = 0$, and $\alpha = 1$ [27]. If a region slips forward, the stress at another point first has a short pulse at the sound arrival time from the second term in Eq. (6), and then settles down to its smaller static value, i. e. it is non-monotonic. The magnitude of these stress pulses and their duration is set by various aspects of the models; for example larger η in Eq. (3) implies weaker stress pulses as the local motion will be slower.

Theoretical Results

Both the magnet and earthquake models of the previous section are capable of producing a large range of power law scaling of event sizes, and related scale invariant quantities in response to a slowly varying driving force or field. This section highlights similarities between these different physical systems and attempts to explain them.

The Universality Class of the BZR Model

We first review results for the simplified monotonic case, starting with scaling relations for driving with fixed force

and far field plate motion and continuing with moment rate shapes. We then discuss additional results associated with non monotonic versions of the model, including mode-switching and aftershocks.

Results on the Monotonic Version of the Model

General results: Depinning transition As mentioned above, substantial simplifications occur for the monotonic version of the model, i. e. if f_R is history independent and $J(\mathbf{r}, t) \geq 0$ for all $(\mathbf{r}, t)$. In [25,27,53] it is shown that for F greater than a critical force F_c the displacement grows continuously in a "sliding state" for which the mean velocity $\overline{v} \equiv \langle \partial u/\partial t \rangle \sim (F - F_c)^\beta$. Here β is a universal exponent that is independent of the microscopic details of the system. It only depends on a few fundamental properties, such as symmetries, spatial dimensions d, range of interactions, etc. [53]. Long time dynamic properties such as β depend in addition on the small ω dependence of $J(\mathbf{q}, \omega)$ [54].

For F less than the critical force F_c, the mean velocity is $\overline{v} \equiv 0$. If F is adiabatically slowly increased towards F_c, the system moves from one metastable configuration to another by a sequence of "quakes" of various sizes. The "quakes" can be characterized by their radius R, the d-dimensional area A which slips (by more than some small cutoff), their potency or moment $M \equiv \int_A \mathrm{d}^d \mathbf{r} \Delta u(\mathbf{r})$, a typical displacement $\Delta u \sim M/A$, and a duration τ. The critical force F_c marks a second order phase transition point. Such phase transitions are typically associated with power law scaling behavior.

In the class of earthquake models with long range interactions along the fault involving the static stress transfer $J_s(r) \equiv \int \mathrm{d}t J(r, t) \sim 1/r^3$, the equations are very similar to those of a model for contact line depinning studied in ref. [25]. Using renormalization group methods it was shown in [25] that for a physical two dimensional interface (or "fault") in a 3 dimensional elastic half space, these long range interactions are so long that the scaling behavior near F_c is correctly described by mean field theory (up to logarithmic corrections, since $d = 2$ is the "upper critical dimension"). The main assumption in mean field theory is that the spatial and temporal fluctuations in the displacement field $u(\mathbf{r}, t)$ are so small that the local displacement $u(\mathbf{r}, t)$ can be replaced by a time dependent spatial average $u(t)$, which then needs to be determined self consistently from the behavior of the neighboring regions that contribute to the stress at a chosen point $\mathbf{r}$ [26]. The same mean field equations are obtained when the long range interaction is approximated to be constant in space $J(\mathbf{r}, t) = J_{mft}(t)/(LW)$. With this approximation Eqs. (3) and (4) become

$$\eta \partial u(\mathbf{r}, t)/\partial t = F + \sigma_{mft}(\mathbf{r}, t) - f_R[u(\mathbf{r}, t), \mathbf{r}, \{u(\mathbf{r}, t' < t)\}] \quad (7)$$

where

$$\sigma_{mft}(\mathbf{r}, t) = \int_{-\infty}^{t} \mathrm{d}t' J_{mft}(t - t')[u(t') - u(\mathbf{r}, t)] \quad (8)$$

and the self consistency requirement is

$$\int u(\mathbf{r}, t) \mathrm{d}^2 r/(LW) = u(t) \quad (9)$$

Many scaling exponents and scaling functions can be calculated exactly in mean field theory by solving these simplified equations of the model. In [15,26,42], several illustrative examples are given for solving similar self consistent mean field theories. There are various approaches that one may use, ranging from numerical simulations to analytical expansion and scaling analysis near a phase transition point where universal power law scaling occurs. The approach of choice to solve the mean field equations depends on the quantity under consideration. To obtain exact results for the scaling behavior of the frequency size statistics of earthquake or avalanche events, a fairly simple approach is to use a discrete version of the model in which we treat the fault as a discrete set of dislocation patches, coupled to a mean displacement and an external driving force that slowly increases with time. (The stress τ_i at each patch is given by Eq. (16) of Sect. "Mode–Switching" below.) As shown in [17], the sequence that describes the distance from failure of the rescaled stress variables resembles a biased random walk. The scaling behavior of the resulting random walk is known exactly from the literature. Using this mapping it then becomes straightforward to derive universal scaling predictions for the mean field earthquake frequency size distribution [17].

Furthermore, as shown in [13,25], their (and thus also our) model have the same scaling behavior as a front propagation model for a two dimensional domain wall in a soft magnet with long range dipolar magnetic interactions, driven by a slowly changing external field (see Sect. "Models"). A flipping spin in the magnet model corresponds to a slipping dislocation patch in the earthquake model. The long range elastic interactions in the earthquake model are similar to the long range dipolar magnetic interactions in the magnet model. The driven two dimensional magnetic domain wall in the (three dimensional) magnet model corresponds to the driven two dimensional earthquake fault

in a three dimensional elastic half space. Since the scaling behavior of the earthquake model and that of [25] and [73] are identical, we may simply copy their results and translate them into quantities that can be extracted from seismic data. Using tools from phase transitions, such as the renormalization group (RG), near the critical force the following scaling results were derived by [13,25,53,54,73] and others:

$$\Delta u \sim R^{\zeta} \ ,$$
$$A \sim R^{d_f} \ \text{ with } \ d_f \leq 2 \ \text{ a fractal dimension} \ ,$$
$$M \sim R^{d_f+\zeta} \ ,$$
$$\text{and } \ \tau \sim R^{z} \ .$$

The differential distribution $P(M)$ of moments M is shown in [25,54] and [26,27] to scale as

$$P(M)\mathrm{d}M \sim \mathrm{d}M/M^{1+B}\rho_{\infty}(M/\hat{M}) \tag{10}$$

with ρ_{∞} a universal scaling function which decays exponentially for large argument. The cutoff $\hat{M}$ for large moments is characterized by a correlation length – the largest likely radius – $\xi \sim 1/(F_c - F)^{\nu}$ with $\hat{M} \sim \xi^{d_f+\zeta}$.

In the same references it is shown that in mean-field theory, $B = 1/2$, $1/\nu = 1$, $z = 1$ and the quakes are fractal with displacements of order the range of correlations in $f_R(u)$, i. e. $\zeta = 0$.

These mean-field exponents are valid for a $d = 2$ dimensional planar fault in a three dimensional elastic half space [7], since the physical fault operates at the upper critical dimension. As usual, at the upper critical dimension, there are logarithmic corrections to mean-field results. Using renormalization group methods one can calculate these corrections [27] and finds barely fractal quakes with $A \sim R^2/\ln R$ so that the fraction of the area slipped decreases only as $1/\ln r$ away from the "hypocenter". The typical slip is $\Delta u \sim (\ln R)^{1/3}$ so that $M \sim R^2/(\ln R)^{2/3}$. The scaling form of $P(M)$ is the same as Eq. (10) with the mean-field ρ_{∞}, although for $M \ll \hat{M}$, $P(M) \sim (\ln M)^{1/3}/M^{3/2}$ so that B will be virtually indistinguishable from 1/2 [27]. A similar form of moment distribution and exponent value $B = 1/2$ were obtained also for a critical stochastic branching model [71].

More realistic driving of a fault We now consider more realistic drive and finite-fault-size effects. As mentioned, driving the fault by very slow motion far away from the fault is roughly equivalent to driving it with a weak spring, i. e. replacing F in Eq. (3) by $F(\mathbf{r}, t) = K[vt - u(\mathbf{r}, t)]$. With $v \to 0$ the system must then operate with the spring stretched to make $F(\mathbf{r}, t) \lesssim F_c$ at least on average, to ensure $\overline{v} = 0$; depending on the stiffness of the spring, it will actually operate just below F_c, as shown below. If in constant force drive the force is increased by a small amount ΔF, the average resulting slip per area, $\langle \Delta u \rangle \equiv \sum_i \Delta u_i/(LW)$ is given by the total potency/moment per total area $M \equiv \int \mathrm{d}^d\mathbf{r}\Delta u(\mathbf{r})/(LW)$. The total moment per area observed in response to a small force increase equals the number $n\Delta F$ of earthquakes per area that are triggered by the increase ΔF, multiplied with the average observed moment of a single earthquake $\langle M \rangle = \int MP(M)\mathrm{d}M$. The result is

$$\langle \Delta u \rangle = n\Delta F \int MP(M)\mathrm{d}M \tag{11}$$

where n is the number of quakes per unit area per force increase ΔF. It has been shown that $n(F)$ is non-singular at F_c [53], so it can be treated like a constant near F_c. Plugging in Eq. (10) and the scaling laws written above and below that equation, we obtain

$$\langle \Delta u \rangle \sim \Delta F \xi^{(2\tilde{\Gamma}+\zeta)(1-B)} \sim \Delta F \xi \tag{12}$$

for our case where mean field results can be used for the critical exponents. For consistency, we must have in steady state with the spring drive, $Kv\Delta t = \Delta F = K\Delta u$ so that the system will operate with a correlation length $\xi \sim 1/K^{1/\tilde{\Gamma}}$, i. e. $1/K$ for our case. For a fault section with linear dimensions of order L, drive either from uniformly moving fault boundaries or from a distance $\sim L$ perpendicularly away from the fault plane will be like $K \sim 1/L$ so the power-law quake distribution will extend out to roughly the system size $\xi \sim L$. For smaller quakes, i. e. $R \ll L$, the behavior will be the same as in the infinite system with constant F drive, but the cutoff of the distribution of moments will be like Eq. (10) with a different cutoff function ρ that depends on the shape of the fault, how it is driven, and the boundary conditions.

We have tested these conclusions numerically by simulating the BZR model, which is a discrete space, time, and displacement version of a monotonic Eq. (3), with quasistatic stress transfer appropriate for an elastic half space [2,5]. The slip, u, is purely in the horizontal direction along the fault and $f_R[u(\mathbf{r})]$ is a series of equal height spikes with spacings which are a random function of $\mathbf{r}$. When $\sigma(\mathbf{r}, t) > f_R[u(\mathbf{r}, t]$, $u(\mathbf{r})$ jumps to the next spike. This provides a way of implementing the random stress drops of the BZR model. The boundary conditions on the bottom and sides are uniform creep or slip – ($u = vt$) with infinitesimal v – and stress free on the top (Fig 3). The statistics of the moments of the quakes are shown by the triangles in Fig. 4. Although the uncertainties are appreciable, relatively good agreement is found with the prediction $B = 1/2$. One typical large quake is illustrated in

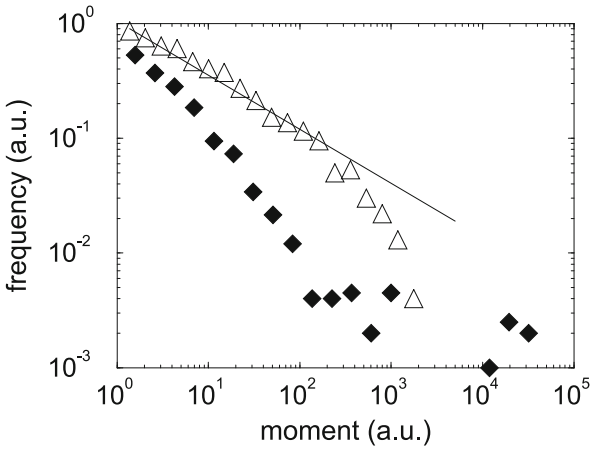

Jerky Motion in Slowly Driven Magnetic and Earthquake Fault Systems, Physics of, Figure 4
Histograms of moments for a simulation of a rectangular fault with 32 x 128 cells for the discrete monotonic quasistatic model (with arbitrary units (a.u.)). Triangles: without dynamical weakening ($\epsilon = 0$). Diamonds: with dynamic weakening of $\epsilon = 0.95$. (ϵ is defined in Eq. (5).) The straight line indicates the predicted slope $B = 1/2$ (from [27])

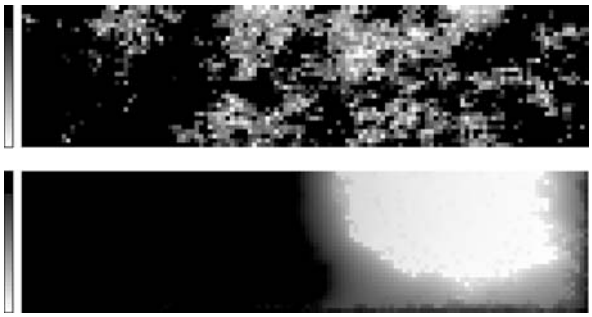

Jerky Motion in Slowly Driven Magnetic and Earthquake Fault Systems, Physics of, Figure 5
Distribution of horizontal slip, *u*, along a fault with 32 x 128 cells for a *single* large quake event. Lighter shading represents larger slip during the quake. *Top*: almost fractal quake with a total moment of 1750 (and 1691 cells failing) for the monotonic model without any dynamical effects ($\epsilon = 0$). *Bottom*: "crack like" quake with a total moment of 16922 (and 2095 cells failing) for the model with dynamic weakening ($\epsilon = 0.95$). In both cases the system is driven by horizontally creeping fault boundaries (*sides* and *bottom*) while the top boundary is free (from [27])

Fig. 5 (top); it appears almost fractal as predicted, and tends to stay away from the bottom and sides due to the specific loading that we chose. The ratios of the moments of quakes to their areas have been studied and found to grow only very slowly with the area, as predicted from the logarithmic corrections listed below Eq. (3). This is in striking contrast to earthquakes in conventional crack models which are compact (Fig. 5 (bottom)) and have $\Delta u \sim R$ (i. e. $\zeta = 1$), so that $M/A \sim \sqrt{A}$. As discussed by [8], however, the scaling $M \sim A$ appears to be consistent with observational results for small earthquakes which presumably propagate and are arrested in rough stress fields. More observational data on the scaling of the moment M with the slipping area A for smaller earthquakes would be highly desirable to test this prediction more precisely.

Because the system is at its critical dimension, the cutoff function ρ of the moment distribution appropriate to the boundary conditions, as well as various aspects of the shapes and dynamics of quakes can be computed using tools from the theory of phase transitions [26,27]. For quasistatic stress transfer, $J(\mathbf{r}, t) \sim \delta(t)/r^3$, in the infinite system the quake durations are found to scale as $\tau \sim R^z$ with $z = 1$ for a $d = 2$ dimensional fault, with logarithmic corrections [25]. (A more physical dynamics with sound-travel-time delay has slower growth of the quakes with $z = 1$ in all dimensions.) Due to the geometrical disorder included in the model, in either case the growth will be very irregular – including regions starting and stopping – in contrast to crack models and what is often assumed in seismological analysis of earthquakes on more regular faults. Similar fractal-like quakes were simulated by Zöller et al. [75,76], for a quasi-dynamic version of the BZR model that includes stress redistribution with a finite communication speed.

Moment Rate Shapes for Monotonic Models In both magnet and earthquake models it has been shown that there are not just universal scaling exponents but also some experimentally accessible universal scaling functions [66]. By comparing theoretical predictions for these functions to experiments or observations, one can often test models much more accurately than by merely comparing a finite set of discrete exponents. Two such functions were first discovered for Barkhausen Noise in magnets [47,66]. The analogy between magnets and earthquakes then lead to the development of the corresponding functions for earthquakes. For slowly driven magnets, consider the time history $V(t)$ of the number of domains flipping per unit time (Barkhausen train). It is called V because it is usually measured as a voltage in a pickup coil. An example of a Barkhausen train for a single avalanche is shown in Fig. 6.

The voltage function $V(t)$ in magnets is the analogue of the moment rate $\mathrm{d}m/\mathrm{d}t(t)$, or the slip per unit time for earthquakes. Recent analysis allowed researchers to obtain the moment rate $\mathrm{d}m_0(t)/\mathrm{d}t$, during the propagation of earthquake rupture for hundreds of large seismic events recorded on global networks [9,31]. The moment rates

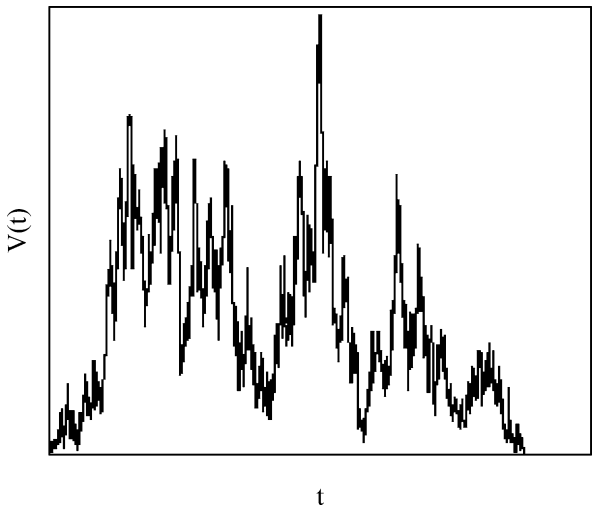

Jerky Motion in Slowly Driven Magnetic and Earthquake Fault Systems, Physics of, Figure 6
Voltage train of a typical large avalanche. Note that the voltage fluctuates drastically and the avalanche nearly stopped several times (from [37]). The analogous moment rate time trace for earthquakes (though measured with lower resolution) is shown in the right inset marked "RAW" of Fig. 8

shown below are derived from inversions of teleseismically recorded seismograms on a global seismic network [62]. (The frequency-moment distribution, $D(M_0) \sim M_0^{-1-\beta}$ of the observed data [9] has three decades of scaling and an exponent of $\beta = 1/2 \pm 0.05$, in close agreement with the BZR model near $\epsilon = 0$ [46].)

For both magnets and earthquakes there are large fluctuations in $V(t)$ and $\mathrm{d}m/\mathrm{d}t(t)$ respectively (Fig. 6). However averaging the signal over many avalanches, leads to typical shapes. Figure 7 shows the average over all avalanches of fixed duration T, $\langle V\rangle(T,t)$ obtained from simulations of two variants of the RFIM (a), and from three different Barkhausen noise experiments (b). Figure 8 shows $\langle \mathrm{d}m/\mathrm{d}t\rangle(T,t)$ obtained for the BZR earthquake model and derived from earthquake observations respectively. The renormalization group and scaling theory [66] predict that for a self similar system at a critical point with power law size and duration distributions for avalanches, there are self similar average avalanche profiles. As shown in [46,66] one finds

$$\langle \mathrm{d}m/\mathrm{d}t\rangle(T,t) \sim T^{b'} g(t/T) \tag{13}$$

where the function $g(x)$ is a universal scaling prediction and $b' \equiv 1/(\sigma\nu z) - 1 = 1$ for the BZR earthquake model (as obtained from mean field theory). The corresponding value for b' for magnets in three dimensions is smaller – the values used for the corresponding collapses can be read off for the different versions of the RFIM from the caption of Fig. 7.

Based on universality one would expect these theoretical predictions to agree with experimental results, apart from an overall shift in time and voltage or moment rate scales. For the moment rate of earthquakes this means

$$\langle \mathrm{d}m/\mathrm{d}t\rangle_{\mathrm{observation}}(T,t) = A\langle \mathrm{d}m/\mathrm{d}t\rangle_{\mathrm{theory}}(T/B, t/B) \tag{14}$$

for some rescaling factors A and B, and similarly for the average voltage $\langle V\rangle(t,T)$ in magnets. In both cases the theory predicts a symmetric looking profile. The mean field prediction for $g(x)$ is in fact a parabola [46,66] – the theoretical prediction thus is that events grow as quickly as they decay. As seen in Figs. 7b and 8 the experimental/observational profile in both cases, however, appear skewed – the real events tend to grow more quickly than they decay! A similar asymmetry has also been observed in avalanches associated with plastic deformation [39].

For magnets this apparent disagreement has been resolved by taking greater account of a microscopic detail involving eddy currents that had been neglected by previous models. Eddy currents are transient current loops that arise in conducting magnets in response to the reorientation of a magnetic domain. These currents temporarily prevent neighboring domains from being triggered to realign in the same direction in an avalanche of domain reversals. The eddy currents decay after a microscopic time τ given by the resistance of the material. Their delay effect thus also decays after a time τ. If the avalanche duration is large compared to τ this effect is negligible and the mean profile approaches the predicted symmetrical shape (see Fig. 7c and d).

The source of asymmetry in the mean moment rate profile may be similar for earthquakes [16]. It has been suggested that triggering delays – arising from a noticeable earthquake nucleation time, or an increase in the failure threshold during the formation of new cracks and subsequent weakening as rock damage increases – could be responsible for aftershocks that often follow large earthquakes [46]. On long time scales a large mainshock with smaller aftershocks can be seen as a similar asymmetry to that seen in magnets, possibly with a similar explanation.

There is a second scaling function that may be extracted from the same data: Fig. 9 shows the average over all earthquakes of fixed total moment $M\langle \mathrm{d}m/\mathrm{d}t\rangle(M,t)$, both for observations and the BZR model prediction. As shown in [46,66] the theory predicts

$$\langle \mathrm{d}m/\mathrm{d}t\rangle(M,t) \sim M^{1/2} q(t/M^{1/2}) \tag{15}$$

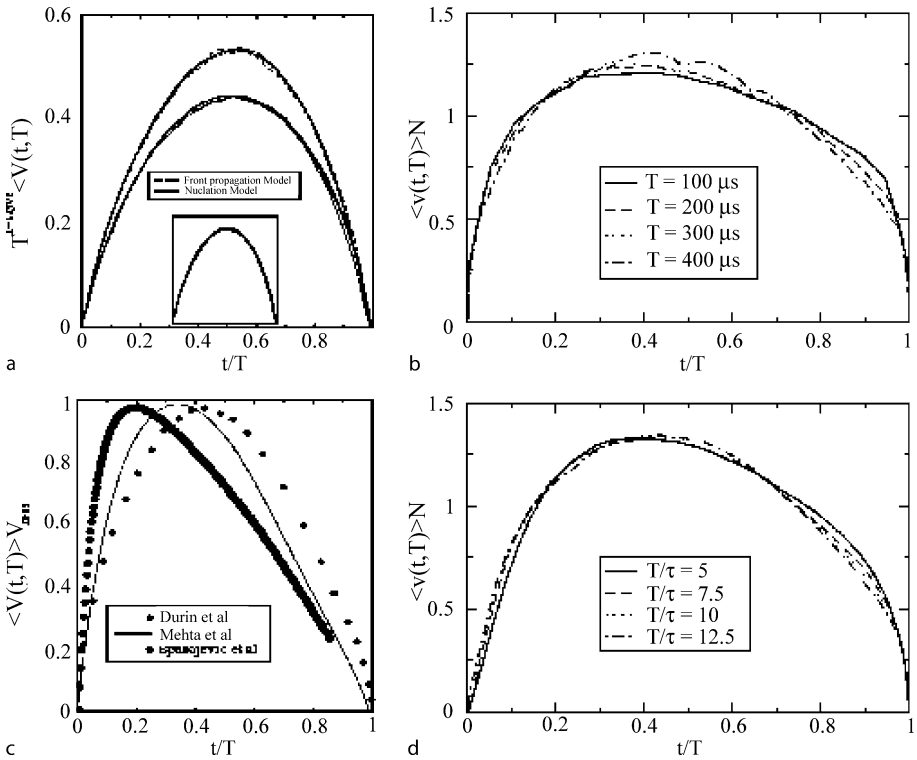

Jerky Motion in Slowly Driven Magnetic and Earthquake Fault Systems, Physics of, Figure 7

a Theoretical average avalanche shape scaling functions for fixed avalanche durations T **denoted with** $g(t/T)$ **in the text, for the nucleation and the front propagation RFIM [47]. The overall height is non universal, the curves for the two models are otherwise extremely similar. The front propagation model has** $1/\sigma\nu z = 1.72$ **and, the nucleation model has** $1/\sigma\nu z = 1.75$ **in this collapse. The** *inset* **shows the two curves rescaled to the same (non universal) height: the two curves are quantitatively different, but far more similar one to another than either is to the experimental curve in b. b Experimental average pulse shapes from three different experiments for fixed pulse duration, as measured by three different groups [21,23,47,67]. Notice that both theory curves are much more symmetric than those of the experiments. Notice also that the three experiments do not agree. At first this result represented a serious challenge to the idea about universality of the dynamics of crackling noise [66]. c Pulse shape asymmetry experiment [72]. Careful experiments show a weak but systematic duration dependence in the collapse of the average Barkhausen pulse shape. The longer pulses (larger avalanches) are systematically more symmetric (approaching the theoretical prediction). d Pulse shape asymmetry theory [72]. Incorporating the delay effects of eddy currents into the theoretical model produces a similar systematic effect. The non-universal effects of eddy currents are in principle irrelevant for extremely large avalanches (from [64])**

where the universal scaling function $q(x) = Ax\exp -Bx^2/2$ and the universal exponents are obtained from the mean field theory for the BZR earthquake model. A comparison between prediction and observational results for this scaling function is shown in Fig. 9.

Clearly, more data, especially for small earthquakes, are needed to decrease the statistical error bars of the observational data and determine the degree of agreement between theory and observations. An alternative scaling approach to moment rate data was given by [31] and a comparison between both approaches is discussed in [46].

Non-Monotonic Models We first consider including weakening of the cell failure threshold by an amount ϵ for sections which have already slipped in a given quake. This crudely models the difference in static versus dynamic friction (see Sect. "Models", Eq. (5)). In between quakes all thus weakened thresholds heal back to their static strength. The effects of small weakening can be analyzed perturbatively.

With $\epsilon = 0$, consider a quake of diameter R_1 ($\ll L$ *or* ξ), with moment M_1 and area A_1: i. e. A_1 sites have slipped. If a small ϵ is turned on at the end of the quake, all slipped sites that are within ϵ of slipping will now slip again – this will be $N_2^{ex} \sim \epsilon A_1$ sites. The simplest justifiable guess is that each of these will cause an approximately independent secondary quake. The total moment of these secondary quakes will be dominated by the largest one, so the extra moment will be $M_2^{ex} \sim (\epsilon A_1)^{1/B}$. (For a very large or

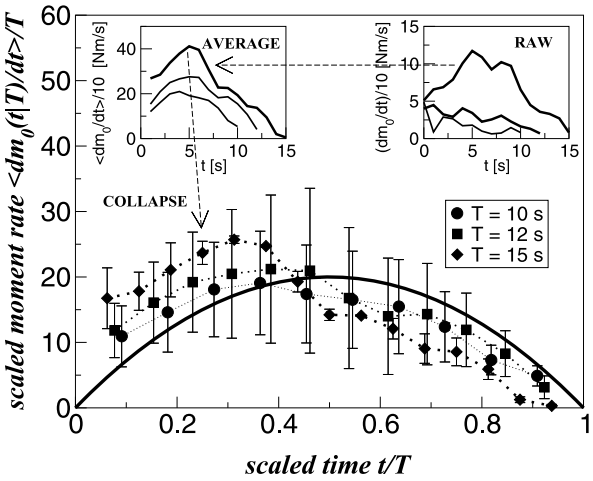

Jerky Motion in Slowly Driven Magnetic and Earthquake Fault Systems, Physics of, Figure 8

A collapse of averaged earthquake pulse shapes, $\langle dm_0(t|M_0)/dt\rangle$ with a duration of T (seconds) within 10% (given in legend), is shown. The collapse was obtained using the mean field scaling relation [37]: $\langle dm_0(t|T)/dt\rangle \sim g(t/T)$. In order to obtain each collapsed pulse shape, two to ten earthquakes were averaged for each value of T. In our mean field theory the universal scaling function is $g_{mf}(x) = Ax(1-x)$ with $x = t/T$. We plot this functional form (bold curve) with $A = 80$. Note the apparent asymmetry to the left in the observed data while the theoretical curve is symmetric around its maximum. *Inset*: The raw data and the averaged data (before collapsed) (from [46])

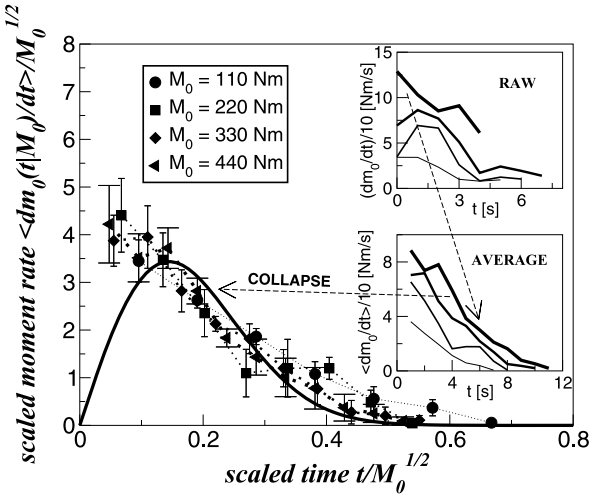

Jerky Motion in Slowly Driven Magnetic and Earthquake Fault Systems, Physics of, Figure 9

A collapse of averaged earthquake pulse shapes, $\langle dm_0(t|M_0)/dt\rangle$, with the size of the moment M_0 in Newton meters within 10% of each size given in the legend respectively. In order to obtain each collapsed moment rate shape, five to ten earthquakes were averaged for each value of M_0. The collapse was obtained using the mean field scaling relation [27]: $\langle dm_0(t|M_0)/dt\rangle/M_0^{1/2} \sim f(t/M_0^{1/2})$. In our mean field theory the universal scaling function is $f_{mf}(x) = Axe^{-Bx^2/2}$ where $x = t/M_0^{1/2}$. We plot this functional form (bold curve) with $A = 4$ and $B = 4.9$. *Inset*: The raw data and the averaged data (before collapsed) (see [46])

infinite fault this is obtained from $1 = N_2^{ex}\int_{M_2^{ex}}^{\infty} P(M)\mathrm{d}M$, and inserting Eq. (10).) If $M_2^{ex} \ll M_1$ this process can continue but will not increase the total moment substantially. If $M_2^{ex} \sim M_1$, however, the process can continue with a larger area A_2 and hence a larger M^{ex}, leading to a catastrophic runaway event. From the above exponent relations and scaling laws we obtain $B = 1/2$ and $A \sim M$, so that for any ϵ, for large enough M_1, $M_1 \gtrsim M_D \sim \epsilon^{-2}$, M_2^{ex} will be comparable to M_1 and the quake will become much larger (runaway). In the force driven infinite system for $F \lesssim F_c$, quakes of size ξ will runaway and become infinite if $\xi > \epsilon^{-1}$. Since $\xi \sim (F - F_c)^{-\nu}$ and $1/\nu = 1$, this will occur for $F_c - F < C_w\epsilon$ with some constant C_w. This result is very intuitive and justifies a posteriori the assumptions leading to it: Since on slipping, the random pinning forces, f_R in a region are reduced by order ϵ, the effective critical force F_c for continuous slip will have been reduced by order ϵ; thus if $F > F_c(\epsilon) = F_c - C_w\epsilon$, the mean velocity $\overline{v}$ will be nonzero. A similar effect can be caused by stress pulses associated with Eq. (6). By considering which of the sites in a long quake with $\alpha = 0$ can be caused to slip further by such stress pulses one finds that runaway will occur for $M \geq M_D \sim \alpha^{-4}$ for the physical case [27]. This has been checked in $d = 1$ with $\Gamma = 1$ and $\gamma = 0$, finding the predicted reduced critical force $F_c(\alpha) \sim F_c - C_p\alpha^2$ as shown in Fig. 10 [27]. These 1-d simulations also reveal a hysteretic $\overline{v}(F)$ curve in finite systems. This is expected to also occur with the model with weakening discussed above. Related higher dimensional systems are discussed in [60] and in [30].

We can now understand what should happen with either weakening or stress pulses in finite systems driven with a weak spring or with slowly moving boundaries. As the system is loaded, quakes of increasing size are observed. If the system is small enough that it cannot sustain quakes with $M > M_D(\epsilon, \alpha)$, i. e. even events within the power law scaling regime of the event size distribution, with $M \leq M_D(\epsilon, \alpha)$, are system spanning, then the behavior will not be much different from the monotonic case with $\epsilon = \alpha = 0$. In both cases there is a power law event size distribution all the way to the largest events, that are determined by the system size. This will occur if the dominant linear system size L is less than the maximum possible linear extent of an earthquake that does not become a runaway event: $L < R_D(\epsilon, \alpha) \sim M_D^{1/2} \sim \max(C_\alpha/\alpha^2, C_\epsilon/\epsilon)$ with appropriate coefficients C_α, C_ϵ, which will depend on

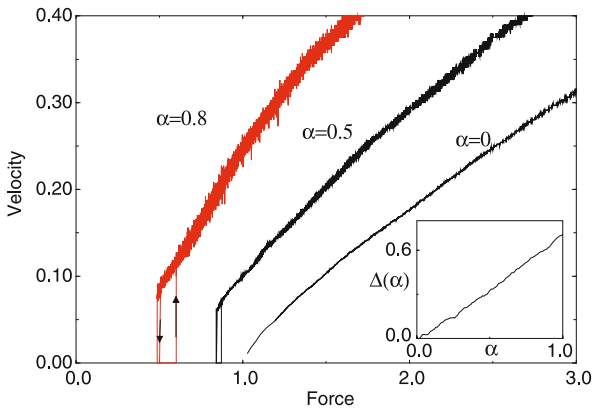

Jerky Motion in Slowly Driven Magnetic and Earthquake Fault Systems, Physics of, Figure 10

Mean velocity vs. force for one dimensional system with a non-monotonic kernel $J(x,t) = \delta(t-x)/x^2 + \alpha\delta'(t-x)/x$ for $\alpha = 0.8, 0.5, 0$. A spring or boundary loaded system will traverse the hysteresis loops in the direction indicated. *Inset*: the threshold force, $F_c^{\uparrow}(\alpha)$, on increasing the load; $\Delta_\alpha = [1 - F_c^{\uparrow}(\alpha)/F_c^{\uparrow}(\alpha = 0)]^{1/2}$ is plotted vs. α (from [27])

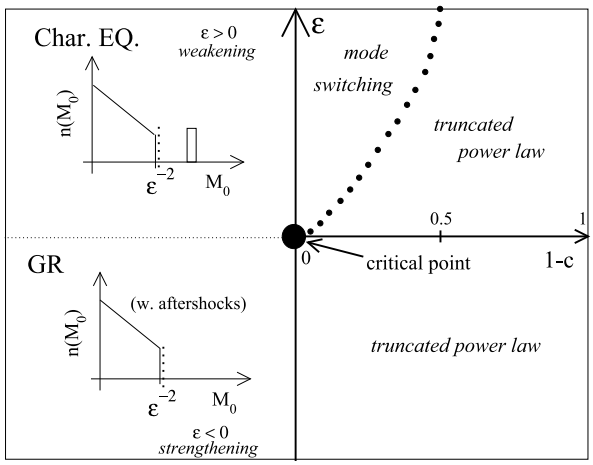

Jerky Motion in Slowly Driven Magnetic and Earthquake Fault Systems, Physics of, Figure 11

Phase Diagram of the BZR model, described in the text. The range $\epsilon > 0$ represents dynamic weakening, while $\epsilon < 0$ represents strengthening. The parameter $1 - c$ quantifies the deviation from stress conservation in the mean field approximation of the model

the amount of randomness in the fault. On the other hand, if $L > R_D$, quakes of size of order R_D will runaway and most of the system will slip, stopping only when the load has decreased enough to make the loading forces less than the *lower* end of the hysteresis loop in $\overline{v}(F)$ (as in Fig. 10).

Because of the tendency of regions that have already slipped to slip further, and the consequent buildup of larger stresses near the boundaries of the slipped regions, large events in systems with dynamic weakening will be much more crack like than in monotonic models, probably with $\Delta u \sim L$. Statistics of quakes with weakening, ϵ, reasonably large, but no stress pulses ($\alpha = 0$) are shown in Fig. 4 and in [2,5,6]; note the absence of quakes with intermediate moments. A typical large event in this case is shown in Fig. 5b; it appears to be crack-like.

In this section we have shown that simple models of heterogeneous faults – with the dimensionality and long-range elastic interactions properly included – can give rise to either power-law statistics of earthquake moments or a distribution of small events combined with characteristic system size events. Which behavior – or intermediate behavior – obtains is found to depend on a number of physical properties such as frictional weakening and dynamic stress transfer, analogs of which should definitely exist in real systems. In the power-law-regime the conventionally defined Gutenberg–Richter exponent $b \equiv 3B/2$ [3] is is found to be $b = 3/4$. This is close to the observed b-value of global strike-slip earthquakes at depth less than 50 km [28].

Mode–Switching In [17] the mean field approximation of infinite range elastic interaction in the BZR model with $N = LW$ (with $W \sim L$) geometrically equal cells on the fault, is used to write the local stress τ_i on cell i as

$$\begin{aligned}\tau_i &= J/N \sum_j (u_j - u_i) + K_L(vt - u_i) \\ &= J\bar{u} + K_L vt - (K_L + J)u_i \,, \end{aligned} \tag{16}$$

where u_i is the total fault offset of cell i in the horizontal (x) direction, $\bar{u} = (\sum_j u_j)/N$, J/N is the elastic coupling between cells in the mean-field approximation, and K_L is the effective loading stiffness of the bulk material surrounding the fault patch. Instead of the loading spring stiffness K_L, a conservation parameter $c \equiv J/(K_L + J)$ is introduced, which equals the fraction of the stress drop of the failing cell, that is retained in the system after the slip. There, it is shown that for the physical loading spring stiffness $K_L \sim 1/L$, one has $1 - c \sim O(1/\sqrt{N})$. A value $c < 1$ for a large system would be physically realized if the external drive is closer to the fault than its linear extent. To be precise, mean field theory only gives the correct physical scaling behavior near the critical point at zero weakening $\epsilon \to 0$ and for $c \to 1$. In [17] it is shown, however, that in a certain parameter regime for $\epsilon > 0$ and $0.5 < c < 1$ indicated in the phase diagram of Fig. 11 one finds a mode switching behavior between Gutenberg–Richter statistics and characteristic earthquake statistics. Similar mode switching behavior has also been seen in

a more realistic three dimensional model for coupled evolution of earthquakes and faults [4,41], and in numerical simulations with the BZR model that includes elastic stress transfer [76]. In the mean field BZR model, the activity switching results from episodic global reorganization of the mode of strain energy release of the fault system, reflected in a "configurational entropy" of stress states on the fault [17]. This is associated with a statistical competition between a tendency of a synchronized behavior leading to clusters of large earthquakes and the characteristic earthquake distribution, and a tendency for disordered response leading to Gutenberg–Richter type statistics without a preferred event size. Mode switching happens when these two opposite tendencies are roughly equal in strength. Some possible observational evidence for mode switching in earthquake data are discussed in [4].

Results on Aftershocks As mentioned in Sect. "Simple Models for Inhomogeneous Earthquake Faults", we associate regions off the main fault segments that are in an early deformation stage with dynamic strengthening $\epsilon < 0$. To capture basic aspects of brittle deformation on such regions in the three-dimensional volume around the main fault (Fig. 3), we change the model as follows: when any cell i slips during an earthquake, and thereby reduces its stress by $\Delta\tau_i \equiv \tau_{f,i} - \tau_{a,i}$, the failure stress $\tau_{f,j}$ of *every* cell $j = 1, \ldots, N$ is *strengthened* by an amount $|\epsilon|\Delta\tau_i/N$. Once the earthquake is complete, the failure stress of each cell is slowly lowered back to its original value. This represents in a simple way the brittle deformation that occurs during an earthquake in the off-fault regions, which are first in a strengthening regime, compared to the main fault, and then have a weakening process. The events that are triggered as the failure stresses are lowered in the weakening period are referred to as *aftershocks*. The occurrence of aftershocks in this version of the model for off-fault regions is in agreement with the observation that a large fraction of observed aftershocks typically occur in off-fault regions [70]. For this version of the model with $\epsilon < 0$, both the primary earthquakes (i. e., mainshocks) and the triggered aftershocks are distributed according to the Gutenberg–Richter distribution, up to a cutoff moment scaling as $1/\epsilon^2$. Assuming that the increased failure stress thresholds $\tau_{f,i}$ are slowly lowered with time as $\log(t)$ towards their earlier static values $\tau_{s,i}$, and that the stresses are distributed over a wide range of values, we show analytically in [46] that the temporal decay of aftershock rates at long times is proportional to $1/t$, as in the modified Omori law $\Delta N/\Delta t K/(t+c)^p$ with $p = 1$ [3,69,70], where N is the cumulative number of aftershocks, t is the time after the mainshock, and K, c, and p are empirical constants.

Remarkably, the long length scale behavior of this model can be shown [45] to be the same as the behavior of the mean field BZR model given in Eq. (16) with an added "antiferroelastic" term $(-|\epsilon|J\bar{u})$:

$$\tau_i = J\bar{u} + K_L v t - (K_L + J)u_i - |\epsilon|J\bar{u}\,. \tag{17}$$

In Eq. (17) every time a cell fails, it slips by an amount Δu_i that leads to stress loading of the other cells, lessened by $|\epsilon|J\Delta u_i/N$ compared to our original model (Eq. (16)). On the other hand, in the global strengthening model (described above) when a cell slips the failure stresses of all cells are strengthened by $|\epsilon|J\Delta u_i/N$. On long length scales the global strengthening of the failure stress has equivalent effects on the earthquake statistics as the dissipation of the redistributed stress, up to corrections of order $O(1/N)$, so the scaling behavior for large events of both models are the same. Moreover, Eq. (17) can be rewritten as:

$$\tau_i = J[1 - |\epsilon|][\bar{u} - u_i] + K_L v t - [K_L + J|\epsilon|]u_i\,. \tag{18}$$

We can now absorb $|\epsilon|$ by defining $J' = J(1 - |\epsilon|)$ and $K'_L = K_L + J|\epsilon|$. Rewriting Eq. (18) with the new definitions, and dropping the $|\epsilon|$ contribution in $[K'_L - J|\epsilon|]vt$ since $v \to 0$, we find:

$$\tau_i = J'\bar{u} + K'_L v t - (K'_L + J')u_i\,. \tag{19}$$

Therefore we recover Eq. (16) with $J \to J'$ and $K_L \to K'_L$. This amounts to changing the stress conservation parameter c (from reference [17]). For Eq. (19):

$$c = J'/(K'_L + J') = 1 - |\epsilon| \tag{20}$$

where $K_L \to 0$ since we are concerned with the adiabatic limit. We also know (from reference [17]) that the cutoff S_{cf} for the Gutenberg–Richter distribution scales as $S_{cf} \sim 1/(1-c)^2$. Thus, from Eq. (20) we find that the cutoff for Eq. (17) will scale as $\sim 1/|\epsilon|^2$.

Mapping to Single Interface Magnet Model The mean field version of the single interface magnet model with infinite range antiferromagnetic interactions is given by [22,74]:

$$\dot{h}_i(t) = J[\bar{h} - h_i(t)] + H(t) - k\bar{h} + \eta_i(h) \tag{21}$$

where $h_i(t)$ is the position of the domain wall, $H(t)$ is the external driving field, k is the coefficient of the antiferromagnetic term, and $\eta_i(h)$ is the pinning field. In the paper by Fisher et al. [27] it has been shown that the scaling behavior on long length scales resulting from Eq. (5), without the $-|\epsilon|J\bar{u}$ term, is same as that of Eq. (21) without the

antiferromagnetic term $-k\bar{h}$. Furthermore, upon inspection we see the following correspondence between the single interface magnet model (Eq. (21)), and the mean field earthquake model (Eq. (17)):

$$-k\bar{h} \Longleftrightarrow -|\epsilon|J\bar{u} \tag{22}$$

In other words, the coefficient of the antiferromagnetic term k plays the same role in the magnet model (Eq. (21)), as the coefficient of strengthening $|\epsilon|J$ does in the earthquake model (Eq. (17)).

Summary

Phase Diagram

The regimes with various statistics produced by the model are summarized by the phase diagram given in Fig. 11. The range $\epsilon > 0$ corresponds to "mature" localized faults with a weakening rheology and characteristic earthquake statistics. The value $\epsilon = 0$ corresponds to "immature" strongly inhomogeneous fault zones and fault networks with power law statistics and scale invariant rupture properties. The range $\epsilon < 0$ corresponds to the fracture and fault networks around large rupture zones, characterized by strengthening due to the creation of new structures and associated emerging aftershocks. The right side of the diagram summarizes the mean field theory results on mode switching described in Sect. "Mode–Switching". The left side of the phase diagram resembles the phase diagram for avalanches in the nucleation RFIM for magnets [65]. There, too, increasing the disorder from small to large (compared to the ferromagnetic coupling between the individual domains) drives the system from a characteristic avalanche size distribution to a truncated power law, with a disorder induced critical point separating the two regimes.

It may be surprising that the discussed simple BZR model can capture many of the essential general features of earthquake statistics (or other systems with avalanches, such as driven magnetic domain walls). This can be understood through the renormalization group [10,66], a powerful mathematical tool to coarse grain a system and extract its effective behavior on long space-time scales. Many microscopic details of a system are averaged out under coarse graining, and universal aspects of the behavior on long scales depend only on a few basic properties such as symmetries, dimensions, range of interactions, weakening/strengthening, etc. When a model correctly captures those basic features, the results provide proper predictions for statistics, critical exponents, and universal scaling functions near the critical point. Consequently, many models that are in the same universality class lead to the same statistics and exponents [10,17,27,66].

Conclusions

The phenomenology of earthquakes and avalanches in magnets exhibit a number of power law distributions and scale-invariant functions (Table 1). In search of basic model ingredients that can explain these results, we have focused on models that are rich enough to produce a diversity of observed features, while being simple enough to allow analytical predictions on long spatio-temporal scales. For the earthquake system we use the BZR model for a heterogeneous fault with threshold dynamics and long range stress-transfer interactions [2,5,6]. For the magnet system we use variants of the RFIM model with threshold dynamics and both short range and long range interactions [37,65,66,74]. In both classes of models, changes in the property disorder and dynamic effects lead to different dynamic regimes (Fig. 11). For different ranges of parameters, the earthquake model produces fractal and crack-like slip functions, power law frequency-size statistics, characteristic earthquake distribution, mode switching, and aftershocks. Similar features are found with the magnet models. We discussed two universal scaling functions of moment rates near criticality as a stronger test of the theory against observations than mere scaling exponents that have large error bars. As in magnetic systems, we find that our analysis for earthquakes provides a good overall agreement between theory and observations, but with a potential discrepancy in one particular universal scaling function for mean moment-rate shapes at fixed duration. The discrepancy has an interesting precedent in the context of avalanches in magnetic systems, and has been explained there in terms of non-universal time retardation effects due to eddy currents. Similar retardation effects may be due to triggering delays or strengthening effects that are responsible for aftershocks in earthquake faults. More observational data, in particular on small earthquakes would be needed to test some of the predictions in detail.

Future Directions

We have highlighted some interesting connections between earthquake and magnet systems with a jerky response to a slowly varying driving force. Future useful studies include analysis of factors controlling nucleation processes, transitions to instabilities and final event sizes, along with a more detailed analysis of the effects of geometrical heterogeneities in the fault structure on the statistics of earthquakes. Additional observational data, particularly for small earthquakes, are needed to test predictions for the scaling of the earthquake duration and rupture area with moment, and for accurately testing our mean field predictions for moment rate shapes. Developing analytical

corrections to the mean field earthquake models can provide additional important insights. Testing similar ideas in other systems with crackling noise would improve and deepen our understanding of universal behavior in disordered nonequilibrium systems.

Acknowledgments

We thank Daniel S. Fisher, James R. Rice, James P. Sethna, Michael B. Weissman, Deniz Ertas, Matthias Holschneider, Amit Mehta, Gert Zöller and many others for very helpful discussions. K.D. acknowledges support from the National Science Foundation, the NSF funded Materials Computation Center, and IBM. YBZ acknowledges support from the National Science Foundation, the United States Geological Survey, and the Southern California Earthquake Center.

Bibliography

Primary Literature

1. Aki K, Richards PG (2002) Quantitative Seismology, 2nd edn. University Science Books, Sausalito
2. Ben-Zion Y (1996) Stress slip and earthquakes in models of complex single-fault systems incorporating brittle and creep deformations. J Geophys Res 101:5677–5706
3. Ben-Zion Y (2003) Appendix 2, Key Formulas in Earthquake Seismology. In: Lee WHK, Kanamori H, Jennings PC, Kisslinger C (eds) International Handbook of Earthquake and Engineering Seismology, Part B. Academic Press, San Diego, pp 1857–1875
4. Ben-Zion Y, Dahmen K, Lyakhovsky V, Ertaş D, Agnon A (1999) Self Driven Mode Switching of Earthquake Activity on a Fault System. Earth Planet Sci Lett 172(1–2):11–21
5. Ben-Zion Y, Rice JR (1993) Earthquake failure sequences along a cellular fault zone in a three-dimensional elastic solid containing asperity and nonasperity regions. J Geophys Res 98:14109–14131
6. Ben-Zion Y, Rice JR (1995) Slip patterns and earthquake populations along different classes of faults in elastic solids. J Geophys Res 100:12959–12983
7. Ben-Zion Y, Sammis CG (2003) Characterization of Fault Zones. Pure Appl Geophys 160:677–715
8. Ben-Zion Y, Zhu L (2002) Potency-magnitude Scaling Relations for Southern California Earthquakes with $1.0 < ML < 7.0$. Geophys J Int 148:F1-F5
9. Bilek SL (2001) Earthquake rupture processes in circum-Pacific subduction zones. Ph D thesis, University of California
10. Binney JJ, Dowrick NJ, Fisher AJ, Newman MEJ (1993) The theory of critical phenomena. Oxford University Press
11. Carlson JM, Langer JS, Shaw BE (1994) Dynamics of earthquake faults. Rev Mod Phys 66:658–70, and references therein
12. Chen K, Bak P, Obukhov SP (1991) Phys Rev A 43:625
13. Cizeau P, Zapperi S, Durin G, Stanley HE (1997) Phys Rev Lett 79:4669–4672
14. Cowie PA, Vanette C, Sornette D (1993) J Geophys Res 98:21809
15. Dahmen K (1995) Hysteresis, Avalanches, and Disorder Induced Critical Scaling: A Renormalization Group Approach, Ph D Thesis, Cornell University
16. Dahmen K (2005) Nature Physics 1:13–14
17. Dahmen K, Ertaş D, Ben-Zion Y (1998) Gutenberg–Richter and Characteristic Earthquake behavior in a Simple Mean-Field Model of Heterogeneous Faults. Phys Rev E 58:1494–1501
18. Dahmen KA, Sethna JP (1996) Hysteresis, Avalanches, and Disorder Induced Critical Scaling: A Renormalization Group Approach. Phys Rev B 53:14872
19. Dieterich JH (1979) J Geophys Res 84:2161–2168
20. Dieterich JH (1981) Amer Geophys Union Monog 24:103–120
21. Durin G, Zapperi S (2000) Scaling exponents for barkhausen avalanches in polycrystalline and amorphous ferromagnets. Phys Rev Lett 84:4705–4708
22. Durin G, Zapperi S (2001) J Magn Mat 1085:242–245
23. Durin G, Zapperi S (2002) Low field hysteresis in disordered ferromagnets. Phys Rev B 65:144441
24. Ertaş D, Kardar M (1994) Critical dynamics of contact line depinning. Phys Rev E 49:R2532–5
25. Ertaş D, Kardar M (1994) Phys Rev E 49:R2532. (1994) Phys Rev Lett 73:1703
26. Fisher DS (1998) Phys Rep 301:113
27. Fisher DS, Dahmen K, Ramanathan S, Ben-Zion Y (1997) Phys Rev Lett 78:4885–4888
28. Frohlich C, Davis SD (1993) J Geophys Res 98:631
29. Gutenberg B, Richter CF (1954) Seismicity of Earth and Associated Phenomena. Princeton Univ. Press, Princeton
30. Hillers G, Mai PM, Ben-Zion Y, Ampuero J-P (2007) Statistical Properties of Seismicity Along Fault Zones at Different Evolutionary Stages. Geophys J Int 169:515 V533. doi: 10.1111/j.1365-246X.2006.03275.x
31. Houston H (2001) Influence of depth, focal mechanism, and tectonic setting on the shape and duration of earthquake source time functions. J Geophys Res 106(B6):11137–11150
32. Ji H, Robbins MO (1992) Percolative, self-affine, and faceted domain growth in random three-dimensional magnets. Phys Rev B 46:14519–27
33. Jiles D (1991) Introduction to Magnetism and Magnetic Materials. Chapman and Hall
34. Klein W, Rundle JB, Ferguson CD (1997) Scaling and Nucleation in Models of Earthquake Faults. Phys Rev Lett 78:3793–3796
35. Koiller B, Ji H, Robbins MO (1992) Fluid wetting properties and the invasion of square networks. ibid 45:7762–7
36. Koiller B, Ji H, Robbins MO (1992) Effect of disorder and lattice type on domain-wall motion in two dimensions. Phys Rev B 46:5258–65
37. Kuntz MC, Sethna JP (2000) Phys Rev B 62:11699–11708
38. Langer JS, Carlson JM, Myers CR, Shaw BE (1996) Slip complexity in dynamic models of earthquake faults. Proc Natl Acad Sci 93:3825–3829
39. Laurson L, Alava MJ (2006) $1/f$ noise and avalanche scaling in plastic deformation. Phys Rev E 74:066106
40. Lomnitz-Adler J (1993) Automaton models of seismic fracture: constraints imposed by the magnitude-frequency relation. J Geophys Res 98:17745–17756
41. Lyakhovsky V, Ben-Zion Y, and Agnon A (2001) Earthquake Cycle, Fault Zones, and Seismicity Patterns in a Rheologically Layered Litosphere. J Geophys Res 106:4103–4120
42. Marchetti MC, Middleton AA, Prellberg T (2000) Viscoelastic

Depinning of Driven Systems: Mean-Field Plastic Scallops. Phys Rev Lett 85:1104–1107
43. Martys N, Robbins MO, Cieplak M (1991) Scaling relations for interface motion through disordered media: application to two-dimensional fluid invasion. Phys Rev B 44:12294–306
44. Mayergoyz ID (1991) Mathematical Models of Hysteresis. Springer
45. Mehta AP (2005) Ph D Thesis, University of Illinois at Urbana Champaign
46. Mehta AP, Dahmen KA, Ben-Zion Y (2006) Universal mean moment rate Profiles of earthquake ruptures. Phys Rev E 73:056104
47. Mehta AP, Mills AC, Dahmen KA, Sethna JP (2002) Phy Rev E 65:46139/1–6
48. Middleton AA (1992) Phys Rev Lett 68:670
49. Miltenberger P, Sornette D, Vanette C (1993) Phys Rev Lett 71:3604
50. Myers CR, Sethna JP (1993) Collective dynamics in a model of sliding charge-density waves. I. Critical behavior. Phys Rev B 47:11171–93
51. Myers CR, Sethna JP (1993) Collective dynamics in a model of sliding charge-density waves. II. Finite-size effects. Phys Rev B 47:11194–203
52. Narayan O, Fisher DS (1992) Critical behavior of sliding charge-density waves in $4-\epsilon$ dimensions, Phys Rev B 46:11520–49
53. Narayan O, Fisher DS (1992) Dynamics of sliding charge-density waves in $4-\epsilon$ dimensions. Phys Rev Lett 68:3615–8
54. Narayan O, Fisher DS (1993) Threshold critical dynamics of driven interfaces in random media. Phys Rev B 48:7030–42
55. Narayan O, Middleton AA (1994) Avalanches and the renormalization group for pinned charge-density waves. Phys Rev B 49:244
56. Nattermann T (1997) Theory of the Random Field Ising Model. In: Young AP (ed) Spin Glasses and Random Fields. World Scientific, Singapore
57. Omori F (1894) On the aftershocks of earthquakes. J Coll Sci Imp Univ Tokyo 7:111–200
58. Perković O, Dahmen K, Sethna JP (1995) Avalanches, Barkhausen Noise, and Plain Old Criticality. Phys Rev Lett 75:4528–31
59. Perković O, Dahmen K, Sethna JP (1999) Disorder-Induced Critical Phenomena in Hysteresis: Numerical Scaling in Three and Higher Dimensions. Phys Rev B 59:6106–19
60. Ramanathan S, Fisher DS (1998) Phys Rev B 58:6026
61. Rice JR, Ben-Zion Y (1996) Slip complexity in earthquake fault models. Proc Natl Acad Sci 93:3811–3818
62. Ruff LJ, Miller AD (1994) Pure Appl Geophys 142:101
63. Schwarz JM, Fisher DS (2001) Depinning with Dynamic Stress Overshoots: Mean Field Theory. Phys Rev Lett 87:096107/1–4
64. Sethna JP (2006) Les Houches Summer School notes. Crackling Noise and Avalanches: Scaling, Critical Phenomena, and the Renormalization Group. e-print at http://xxx.lanl.gov/pdf/cond-mat/0612418
65. Sethna JP, Dahmen K, Kartha S, Krumhansl JA, Roberts BW, Shore JD (1993) Hysteresis and Hierarchies: Dynamics of Disorder Driven First Order Phase Transformations. Phys Rev Lett 70:3347
66. Sethna JP, Dahmen KA, Myers CR (2001) Nature 410:242–250
67. Spasojevic D, Bukvic S, Milosevic S, Stanley HE (1996) Barkhausen noise: Elementary signals. power laws, and scaling relations. Phys Rev E 54:2531–2546
68. Travesset A, White RA, Dahmen KA (2002) Phys Rev B 66:024430
69. Utsu T (2002) Statistical features of seismology. In: Lee WHK, Kanamori H, Jennings PC, Kisslinger C (eds) International Handbook of Earthquake and Engineering Seismology, Part A. pp 719–732
70. Utsu Y, Ogata Y, Matsu'uara RS (1995) The centenary of the Omori Formula for a decay law of aftershock activity. J Phys Earth 43:1–33
71. Vere-Jones D (1976) A branching model for crack propagation. Pure Appl Geophys 114(4):711–726
72. Zapperi S, Castellano C, Calaiori F, Durin G (2005) Signature of effective mass in crackling-noise asymmetry. Nature Phys 1:46–49
73. Zapperi S, Cizeau P, Durin G, Stanley HE (1998) Dynamics of a ferromagnetic domain wall: Avalanches, depinning transition, and the Barkhausen effect. Phys Rev B 58:6353–66
74. Zapperi S, Cizeau P, Durin G, Stanley HE (1998) Phys Rev B 58(10):6353–6366
75. Zöller G, Hainzl S, Ben-Zion Y, Holschneider M (2009) Critical states of seismicity: From models to practical seismic hazard estimates. In: Encyclopedia of Complexity and System Science
76. Zöller G, Holschneider M, Ben-Zion Y (2004) Quasi-static and Quasi-dynamic modeling of earthquake failure at intermediate scales. Pure Appl Geophys 161:2103–2118
77. Zöller G, Holschneider M, Ben-Zion Y (2005) The role of heterogeneities as a tuning parameter of earthquake dynamics. Pure Appl Geophys 162:1027 V1049. doi: 10.1007s00024-004-2660-9

Joinings in Ergodic Theory

Thierry de la Rue
Laboratoire de Mathématiques Raphaël Salem,
CNRS – Université de Rouen,
Saint Étienne du Rouvray, France

Article Outline

Glossary
Definition of the Subject
Introduction
Joinings of Two or More Dynamical Systems
Self-Joinings
Some Applications and Future Directions
Bibliography

Glossary

Disjoint measure-preserving systems The two measure-preserving dynamical systems $(X, \mathcal{A}, \mu, T)$ and $(Y, \mathcal{B}, \nu, S)$ are said to be *disjoint* if their only joining is the product measure $\mu \otimes \nu$.

Joining Let I be a finite or countable set, and for each $i \in I$, let $(X_i, \mathcal{A}_i, \mu_i, T_i)$ be a measure-preserving dynamical system. A *joining* of these systems is a probability measure on the Cartesian product $\prod_{i\in I} X_i$, which has the μ_i's as marginals, and which is invariant under the product transformation $\bigotimes_{i\in I} T_i$.

Marginal of a probability measure on a product space Let λ be a probability measure on the Cartesian product of a finite or countable collection of measurable spaces $\left(\prod_{i\in I} X_i, \bigotimes_{i\in I} \mathcal{A}_i\right)$, and let $J = \{j_1, \ldots, j_k\}$ be a finite subset of I. The *k-fold marginal* of λ on $X_{j_1}, \ldots, X_{j_k}$ is the probability measure μ defined by:

$$\forall A_1 \in \mathcal{A}_{j_1}, \ldots, A_k \in \mathcal{A}_{j_k}\,,$$
$$\mu(A_1 \times \cdots \times A_k) := \lambda\left(A_1 \times \cdots \times A_k \times \prod_{i\in I\setminus J} X_i\right).$$

Markov intertwining Let $(X, \mathcal{A}, \mu, T)$ and $(Y, \mathcal{B}, \nu, S)$ be two measure-preserving dynamical systems. We call *Markov intertwining* of T and S any operator $P\colon L^2(X,\mu) \to L^2(Y,\nu)$ enjoying the following properties:

- $PU_T = U_S P$, where U_T and U_S are the unitary operators on $L^2(X,\mu)$ and $L^2(Y,\nu)$ associated respectively to T and S (i. e. $U_T f(x) = f(Tx)$, and $U_S g(y) = g(Sy)$).
- $P\mathbb{1}_X = \mathbb{1}_Y$,
- $f \geq 0$ implies $Pf \geq 0$, and $g \geq 0$ implies $P^* g \geq 0$, where P^* is the adjoint operator of P.

Minimal self-joinings Let $k \geq 2$ be an integer. The ergodic measure-preserving dynamical system T has *k-fold minimal self-joinings* if, for any ergodic joining λ of k copies of T, we can partition the set $\{1, \ldots, k\}$ of coordinates into subsets $J_1, \ldots, J_\ell$ such that

1. For j_1 and j_2 belonging to the same J_i, the marginal of λ on the coordinates j_1 and j_2 is supported on the graph of T^n for some integer n (depending on j_1 and j_2);
2. For $j_1 \in J_1, \ldots, j_\ell \in J_\ell$, the coordinates $j_1, \ldots, j_\ell$ are independent.

We say that T has *minimal self-joinings* if T has k-fold minimal self-joinings for every $k \geq 2$.

Off-diagonal self-joinings Let $(X, \mathcal{A}, \mu, T)$ be a measure-preserving dynamical system, and S be an invertible measure-preserving transformation of $(X, \mathcal{A}, \mu)$ commuting with T. Then the probability measure Δ_S defined on $X \times X$ by

$$\Delta_S(A \times B) := \mu(A \cap S^{-1}B) \tag{1}$$

is a 2-fold self-joining of T supported on the graph of S. We call it an *off-diagonal self-joining of T*.

Process in a measure-preserving dynamical systems Let $(X, \mathcal{A}, \mu, T)$ be a measure-preserving dynamical system, and let $(E, \mathcal{B}(E))$ be a measurable space (which may be a finite or countable set, or $\mathbb{R}^d$, or $\mathbb{C}^d \ldots$). For any E-valued random variable ξ defined on the probability space $(X, \mathcal{A}, \mu)$, we can consider the stochastic process $(\xi_i)_{i\in\mathbb{Z}}$ defined by

$$\xi_i := \xi \circ T^i\,.$$

Since T preserves the probability measure μ, $(\xi_i)_{i\in\mathbb{Z}}$ is a *stationary process*: For any ℓ and n, the distribution of $(\xi_0, \ldots, \xi_\ell)$ is the same as the probability distribution of $(\xi_n, \ldots, \xi_{n+\ell})$.

Self-joining Let T be a measure-preserving dynamical system. A *self-joining* of T is a joining of a family $(X_i, \mathcal{A}_i, \mu_i, T_i)_{i\in I}$ of systems where each T_i is a copy of T. If I is finite and has cardinal k, we speak of a *k-fold* self-joining of T.

Simplicity For $k \geq 2$, we say that the ergodic measure-preserving dynamical system T is *k-fold simple* if, for any ergodic joining λ of k copies of T, we can partition the set $\{1, \ldots, k\}$ of coordinates into subsets $J_1, \ldots, J_\ell$ such that

1. for j_1 and j_2 belonging to the same J_i, the marginal of λ on the coordinates j_1 and j_2 is supported on the graph of some $S \in C(T)$ (depending on j_1 and j_2);
2. for $j_1 \in J_1, \ldots, j_\ell \in J_\ell$, the coordinates $j_1, \ldots, j_\ell$ are independent.

We say that T is *simple* if T is k-fold simple for every $k \geq 2$.

Definition of the Subject

The word *joining* can be considered as the counterpart in ergodic theory of the notion of *coupling* in probability theory (see e. g. [48]): Given two or more processes defined on different spaces, what are the possibilities of embedding them together in the same space? There always exists the solution of making them independent of each other, but interesting cases arise when we can do this in other ways. The notion of joining originates in ergodic theory from pioneering works of H. Furstenberg [14], who introduced the fundamental notion of *disjointness*, and D.J. Rudolph, who laid the basis of joining theory in his article on minimal self-joinings [41]. It has today become an essential tool

in the classification of measure-preserving dynamical systems and in the study of their intrinsic properties.

Introduction

A central question in ergodic theory is to tell when two measure-preserving dynamical systems are essentially the same, i. e. when they are *isomorphic*. When this is not the case, a finer analysis consists of asking what these two systems could share in common: For example, do there exist stationary processes which can be observed in both systems? This latter question can also be asked in the following equivalent way: Do these two systems have a *common factor*? The arithmetical flavor of this question is not fortuitous: There are deep analogies between the arithmetic of integers and the classification of measure-preserving dynamical systems, and these analogies were at the starting point of the study of joinings in ergodic theory.

In the seminal paper [14] which introduced the concept of joinings in ergodic theory, H. Furstenberg observed that two operations can be done with dynamical systems: We can consider the *product* of two dynamical systems, and we can also take a *factor* of a given system. Like the multiplication of integers, the product of dynamical systems is commutative, associative, it possesses a neutral element (the trivial single-point system), and the systems S and T are both factors of their product $S \times T$. It was then natural to introduce the property for two measure-preserving systems to be *relatively prime*. As far as integers are concerned, there are two equivalent ways of characterizing the relative primeness: First, the integers a and b are *relatively prime* if their unique positive common factor is 1. Second, a and b are *relatively prime* if, each time both a and b are factors of an integer c, their product ab is also a factor of c. It is a well-known theorem in number theory that these two properties are equivalent, but this was not clear for their analog in ergodic theory. Furstenberg reckoned that the second way of defining relative primeness was the most interesting property in ergodic theory, and called it *disjointness* of measure-preserving systems (we will discuss precisely in Subsect. "From Disjointness to Isomorphy" what the correct analog is in the setting of ergodic theory). He also asked whether the non-existence of a non-trivial common factor between two systems was equivalent to their disjointness. He was able to prove that disjointness implies the impossibility of a non-trivial common factor, but not the converse. And in fact, the converse turns out to be false: In 1979, D.J. Rudolph exhibited a counterexample in his paper introducing the important notion of *minimal self-joinings*. The relationships between disjointness and the lack of common factor will be presented in details in Sect. "Joinings and Factors".

Given two measure-preserving dynamical systems S and T, the study of their disjointness naturally leads one to consider all the possible ways these two systems can be both seen as factors of a third system. As we shall see, this is precisely the study of their *joinings*. The concept of joining turns out to be related to many important questions in ergodic theory, and a large number of deep results can be stated and proved inside the theory of joinings. For example, the fact that the dynamical systems S and T are isomorphic is equivalent to the existence of a special joining between S and T, and this can be used to give a joining proof of Krieger's finite generator theorem, as well as Ornstein's isomorphism theorem (see Sect. "Joinings Proofs of Ornstein's and Krieger's Theorems"). As it already appears in Furstenberg's article, joinings provide a powerful tool in the classification of measure-preserving dynamical systems: Many classes of systems can be characterized in terms of their disjointness with other systems. Joinings are also strongly connected with difficult questions arising in the study of the convergence almost everywhere of non-conventional averages (see Sect. "Joinings and Pointwise Convergence").

Amazingly, a situation in which the study of joinings leads to the most interesting results consists of considering two or more *identical* systems. We then speak of the *self-joinings* of the dynamical system T. Again, the study of self-joinings is closely related to many ergodic properties of the system: Its mixing properties, the structure of its factors, the transformations which commute with T, and so on... We already mentioned minimal self-joinings, and we will see in Sect. "Minimal Self-Joinings" how this property may be used to get many interesting examples, such as a transformation with no root, or a process with no non-trivial factor. In the same section we will also discuss a very interesting generalization of minimal self-joinings: the property of being *simple*.

The range of applications of joinings in ergodic theory is very large; only some of them will be given in Sect. "Some Applications and Future Directions": The use of joinings in proving Krieger's and Ornstein's theorems, the links between joinings and some questions of pointwise convergence, and the strong connections between the study of self-joinings and Rohlin's famous question on multifold mixing, which was first posed in 1949 [39].

Joinings of Two or More Dynamical Systems

In the following, we are given a finite or countable family $(X_i, \mathcal{A}_i, \mu_i, T_i)_{i \in I}$ of measure-preserving dynamical

systems: T_i is an invertible measure-preserving transformation of the standard Borel probability space $(X_i, \mathcal{A}_i, \mu_i)$. When it is not ambiguous, we shall often use the symbol T_i to denote both the transformation and the system.

A *joining* λ of the T_i's (see the definition in the Glossary) defines a new measure-preserving dynamical system: The product transformation

$$\bigotimes_{i\in I} T_i : (x_i)_{i\in I} \longmapsto (T_i x_i)_{i\in I}$$

acting on the Cartesian product $\prod_{i\in I} X_i$, and preserving the probability measure λ. We will denote this big system by $\left(\bigotimes_{i\in I} T_i\right)_\lambda$. Since all marginals of λ are given by the original probabilities μ_i, observing only the coordinate i in the big system is the same as observing only the system T_i. Thus, each system T_i is a factor of $\left(\bigotimes_{i\in I} T_i\right)_\lambda$, via the homomorphism π_i which maps any point in the Cartesian product to its ith coordinate.

Conversely, if we are given a measure-preserving dynamical system (Z, C, ρ, R) admitting each T_i as a factor via some homomorphism $\varphi_i : Z \to X_i$, then we can construct the map $\varphi : Z \to \prod_{i\in I} X_i$ sending z to $(\varphi_i(z))_{i\in I}$. We can easily check that the image of the probability measure ρ is then a joining of the T_i's.

Therefore, studying the joinings of a family of measure-preserving dynamical system amounts to studying all the possible ways these systems can be seen together as factors in another big system.

The Set of Joinings

The set of all joinings of the T_i's will be denoted by $J(T_i, i \in I)$. Before anything else, we have to observe that this set is never empty. Indeed, whatever the systems are, the product measure $\bigotimes_{i\in I} \mu_i$ always belongs to this set. Note also that any convex combination of joinings is a joining: $J(T_i, i \in I)$ is a convex set.

The set of joinings is turned into a compact metrizable space, equipped with the topology defined by the following notion of convergence: $\lambda_n \xrightarrow[n\to\infty]{} \underline{\lambda}$ if and only if, for all families of measurable subsets $(A_i)_{i\in I} \in \prod_{i\in I} \mathcal{A}_i$, finitely many of them being different from X_i, we have

$$\lambda_n\left(\prod_{i\in I} A_i\right) \xrightarrow[n\to\infty]{} \underline{\lambda}\left(\prod_{i\in I} A_i\right). \tag{2}$$

We can easily construct a distance defining this topology by observing that it is enough to check (2) when each of the A_i's is chosen in some countable algebra C_i generating the σ-algebra $\mathcal{A}_i$. We can also point out that, when the X_i's are themselves compact metric spaces, this topology on the set of joinings is nothing but the restriction to $J(T_i, i \in I)$ of the usual weak* topology.

It is particularly interesting to study *ergodic* joinings of the T_i's, whose set will be denoted by $J_e(T_i, i \in I)$. Since any factor of an ergodic system is itself ergodic, a necessary condition for $J_e(T_i, i \in I)$ not to be empty is that all the T_i's be themselves ergodic. Conversely, if all the T_i's are ergodic, we can prove by considering the ergodic decomposition of the product measure $\bigotimes_{i\in I} \mu_i$ that ergodic joinings do exist: Any ergodic measure appearing in the ergodic decomposition of some joining has to be itself a joining. This result can also be stated in the following way:

Proposition 1 *If all the T_i's are ergodic, the set of their ergodic joinings is the set of extremal points in the compact convex set $J(T_i, i \in I)$.*

From Disjointness to Isomorphy

In this section, as in many others in this article, we are focusing on the case where our family of dynamical systems is reduced to two systems. We will then rather call them S and T, standing for $(Y, \mathcal{B}, \nu, S)$ and $(X, \mathcal{A}, \mu, T)$. We are interested here in two extremal cases for the set of joinings $J(T, S)$. The first one occurs when the two systems are as far as possible from each other: They have nothing to share in common, and therefore their set of joinings is reduced to the singleton $\{\mu \otimes \nu\}$: This is called the *disjointness* of S and T. The second one arises when the two systems are isomorphic, and we will see how this property shows through $J(T, S)$.

Disjointness Many situations where disjointness arises were already given by Furstenberg in [14]. Particularly interesting is the fact that classes of dynamical systems can be characterized through disjointness properties. We list here some of the main examples of disjoint classes of measure-preserving systems.

Theorem 2

1. *T is ergodic if and only if it is disjoint from every identity map.*
2. *T is weakly mixing if and only if it is disjoint from any rotation on the circle.*
3. *T has zero entropy if and only if it is disjoint from any Bernoulli shift.*
4. *T is a K-system if and only if it is disjoint from any zero-entropy system.*

The first result is the easiest, but is quite important, in particular when it is stated in the following form: If λ is a join-

ing of T and S, with T ergodic, and if λ is invariant by $T \times \mathrm{Id}$, then $\lambda = \mu \otimes \nu$.

The second, third and fourth results were originally proved by Furstenberg. They can also be seen as corollaries of the theorems presented in Sect. "Joinings and Factors", linking the non-disjointness property with the existence of a particular factor.

Both the first and the second results can be derived from the next theorem, giving a general spectral condition in which disjointness arises. The proof of this theorem can be found in [49]. It is a direct consequence of the fact that, if f and g are square-integrable functions in a given dynamical system, and if their spectral measures are mutually singular, then f and g are orthogonal in L^2.

Theorem 3 *If the reduced maximum spectral types of T and S are mutually singular, then T and S are disjoint.*

As we already said in the introduction, disjointness was recognized by Furstenberg as the most pertinent way to define the analog of the arithmetic property "a and b are relatively prime" in the context of measure-preserving dynamical systems. We must however point out that the statement

(i) S and T are disjoint

is, in general, strictly stronger than the straightforward translation of the arithmetic property:

(ii) Each time both S and T appear as factors in a third dynamical system, then their product $S \times T$ also appears as a factor in this system.

Indeed, contrary to the situation in ordinary arithmetic, there exist non-trivial dynamical systems T which are isomorphic to $T \times T$: For example, this is the case when T is the product of countably many copies of a single non-trivial system. Now, if T is such a system and if we take $S = T$, then S and T do not satisfy statement (i): A non-trivial system is never disjoint from itself, as we will see in the next Section. However they obviously satisfy the statement (ii).

A correct translation of the arithmetic property is the following: S and T are disjoint if and only if, each time T and S appear as factors in some dynamical system through the respective homomorphisms π_T and π_S, $T \times S$ also appears as a factor through a homomorphism $\pi_{T\times S}$ such that $\pi_X \circ \pi_{T\times S} = \pi_T$ and $\pi_Y \circ \pi_{T\times S} = \pi_S$, where π_X and π_Y are the projections on the coordinates in the Cartesian product $X \times Y$ (see the diagram below).

$$\begin{tikzcd}
 & Z \arrow[dl, "\pi_T"'] \arrow[d, "\pi_{T\times S}"] \arrow[dr, "\pi_S"] & \\
X & X \times Y \arrow[l, "\pi_X"] \arrow[r, "\pi_Y"'] & Y
\end{tikzcd}$$

Joinings and Isomorphism We first introduce some notations: For any probability measure λ on a measurable space, let '$A \overset{\lambda}{=} B$' stand for '$\lambda(A\Delta B) = 0$'. Similarly, if $\mathcal{C}$ and $\mathcal{D}$ are σ-algebras of measurable sets, we write '$\mathcal{C} \overset{\lambda}{\subset} \mathcal{D}$' if, for any $C \in \mathcal{C}$, we can find some $D \in \mathcal{D}$ such that $C \overset{\lambda}{=} D$, and by '$\mathcal{C} \overset{\lambda}{=} \mathcal{D}$' we naturally mean that both $\mathcal{C} \overset{\lambda}{\subset} \mathcal{D}$ and $\mathcal{D} \overset{\lambda}{\subset} \mathcal{C}$ hold.

Let us assume now that our two systems S and T are isomorphic: This means that we can find some measurable one-to-one map $\varphi\colon X \to Y$, with $T(\mu) = \nu$, and $\varphi \circ T = S \circ \varphi$. With such a φ, we construct the measurable map $\psi : X \to X \times Y$ by setting

$$\psi(x) := \big((x, \varphi(x)\big) .$$

Let Δ_φ be the image measure of μ by ψ. This measure is supported on the graph of φ, and is also characterized by

$$\forall A \in \mathcal{A}\,, \forall B \in \mathcal{B}\,, \Delta_\varphi(A \times B) = \mu(A \cap \varphi^{-1}B) . \quad (3)$$

We can easily check that, φ being an isomorphism of T and S, Δ_φ is a joining of T and S. And this joining satisfies very special properties:

- For any measurable $A \subset X$, $A \times Y \overset{\Delta_\varphi}{=} X \times \varphi(A)$;
- Conversely, for any measurable $B \subset Y$, $X \times B \overset{\Delta_\varphi}{=} \varphi^{-1}(B) \times Y$.

Thus, in the case where S and T are isomorphic, we can find a special joining of S and T, which is supported on the graph of an isomorphism, and which identifies the two σ-algebras generated by the two coordinates. What is remarkable is that the converse is true: The existence of an isomorphism between S and T is characterized by the existence of such a joining, and we have the following theorem:

Theorem 4 *The measure-preserving dynamical systems S and T are isomorphic if and only if there exists a joining λ of S and T such that*

$$\{X, \emptyset\} \otimes \mathcal{B} \overset{\lambda}{=} \mathcal{A} \otimes \{Y, \emptyset\} . \quad (4)$$

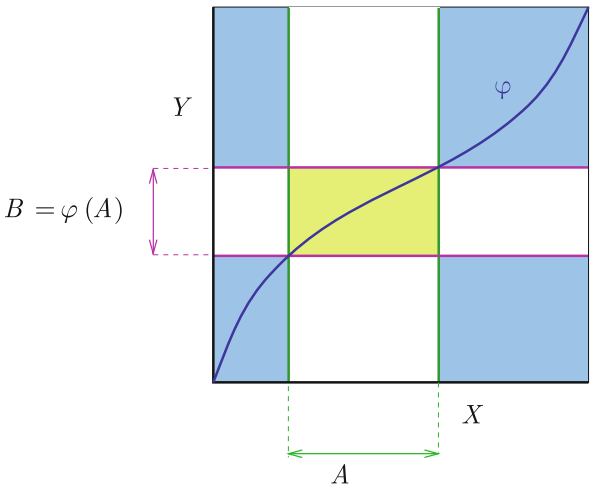

Joinings in Ergodic Theory, Figure 1
The joining Δ_φ identifies the sets $A \times Y$ and $X \times \varphi(A)$

When λ is such a joining, it is supported on the graph of an isomorphism of T and S, and both systems are isomorphic to the joint system $(T \otimes S)_\lambda$.

This theorem finds nice applications in the proof of classical isomorphism results. For example, it can be used to prove that two discrete-spectrum systems which are spectrally isomorphic are isomorphic (see [49] or [6]). We will also see in Sect.“ Joinings Proofs of Ornstein's and Krieger's Theorems” how it can be applied in the proofs of Krieger's and Ornstein's deep theorems.

Consider now the case were T and S are no longer isomorphic, but where S is only a factor of T. Then we have a factor map $\pi : X \to Y$ which has the same properties as an isomorphism φ, except that it is not one-to-one (π is only onto). The measure Δ_π, constructed in the same way as Δ_φ, is still a joining supported on the graph of π, but it does not identify the two σ-algebras generated by the two coordinates anymore: Instead of condition (4), Δ_π only satisfies the weaker one:

$$\{X, \emptyset\} \otimes \mathcal{B} \overset{\Delta_\pi}{\subset} \mathcal{A} \otimes \{Y, \emptyset\} . \tag{5}$$

The existence of a joining satisfying (5) is a criterion for S being a factor of T.

For more details on the results stated in this section, we refer the reader to [6].

Joinings and Factors

The purpose of this section is to investigate the relationships between the disjointness of two systems S and T, and the lack of a common factor. The crucial fact which was pointed out by Furstenberg is that the existence of a common factor enables one to construct a very special joining of S and T: The *relatively independent joining over this factor*.

Let us assume that our systems S and T share a common factor (Z, C, ρ, R), which means that we have measurable onto maps $\pi_X : X \to Z$ and $\pi_Y : Y \to Z$, respectively sending μ and ν to ρ, and satisfying $\pi_X \circ T = R \circ \pi_X$ and $\pi_Y \circ S = R \circ \pi_Y$. We can then consider the joinings supported on their graphs $\Delta_{\pi_X} \in J(T, R)$ and $\Delta_{\pi_Y} \in J(S, R)$, as defined in the preceding section. Next, we construct a joining λ of the three systems S, T and R. Heuristically, λ is the probability distribution of the triple (x, y, z) when we first pick z according to the probability distribution ρ, then x and y according to their conditional distribution knowing z in the respective joinings Δ_{π_X} and Δ_{π_Y}, but independently of each other. More precisely, λ is defined by setting, for all $A \in \mathcal{A}$, $B \in \mathcal{B}$ and $C \in C$

$$\lambda(A \times B \times C) := \int_C \mathbb{E}_{\Delta_{\pi_X}}[\mathbb{1}_{x \in A}|z]\mathbb{E}_{\Delta_{\pi_Y}}[\mathbb{1}_{y \in B}|z]\,\mathrm{d}\rho(z) . \tag{6}$$

Observe that the two-fold marginals of λ on $X \times Z$ and $Y \times Z$ are respectively Δ_{π_X} and Δ_{π_Y}, which means that we have $z = \pi_X(x) = \pi_Y(y)$ λ-almost surely. In other words, we have identified in the two systems T and S the projections on their common factor R. The two-fold marginal of λ on $X \times Y$ is itself a joining of T and S, which we call the *relatively independent joining* over the common factor R. This joining will be denoted by $\mu \otimes_R \nu$. (Be careful: The projections π_X and π_Y are hidden in this notation, but we have to know them to define this joining.) From (6), we immediately get the formula defining $\mu \otimes_R \nu$:

$$\forall A \in \mathcal{A}\,, \forall B \in \mathcal{B}\,,\ \mu \otimes_R \nu(A \times B) := \int_Z \mathbb{E}_{\Delta_{\pi_X}}[\mathbb{1}_{x \in A}|z]\mathbb{E}_{\Delta_{\pi_Y}}[\mathbb{1}_{y \in B}|z]\,\mathrm{d}\rho(z) . \tag{7}$$

This definition of the relatively independent joining over a common factor can easily be extended to a finite or countable family of systems sharing the same common factor.

Note that $\mu \otimes_R \nu$ coincides with the product measure $\mu \otimes \nu$ if and only if the common factor is the trivial one-point system. We therefore get the following result:

Theorem 5 *If S and T have a non-trivial common factor, then these systems are not disjoint.*

As we already said in the introduction, Rudolph exhibited in [41] a counterexample showing that the converse is not

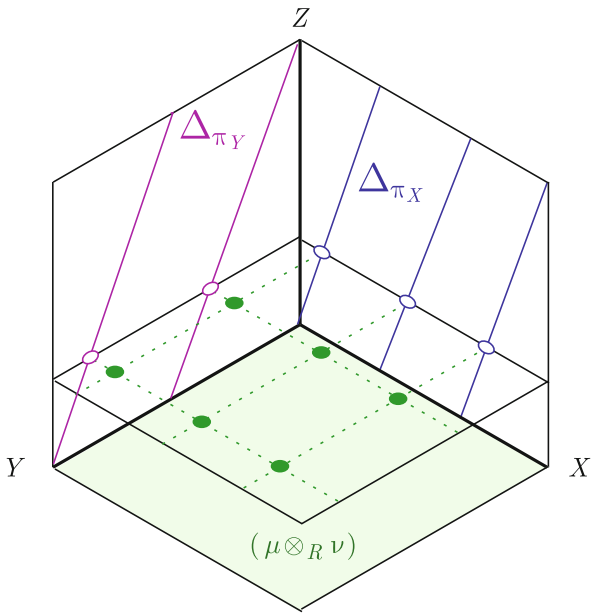

Joinings in Ergodic Theory, Figure 2
The relatively independent joining $\mu \otimes_R \nu$ and its disintegration over Z

true. There exists, however, an important result, which was published in [20,29] allowing us to derive some information on factors from the non-disjointness of two systems.

Theorem 6 *If T and S are not disjoint, then S has a non-trivial common factor with some joining of a countable family of copies of T.*

This result leads to the introduction of a special class of factors when some dynamical system T is given: For any other dynamical system S, call *T-factor* of S any common factor of S with a joining of countably many copies of T. If (Z, C, ρ, R) is a T-factor of S and $\pi : Y \to Z$ is a factor map, we say that the σ-algebra $\pi^{-1}(C)$ is a *T-factor σ-algebra* of S. Another way to state Theorem 6 is then the following: If S and T are not disjoint, then S has a non-trivial T-factor. In fact, an even more precise result can be derived from the proof of Theorem 6: For any joining λ of S and T, for any bounded measurable function f on X, the factor σ-algebra of S generated by the function $\mathbb{E}_\lambda[f(x)|y]$ is a T-factor σ-algebra of S.

With the notion of T-factor, Theorem 6 has been extended in [31] in the following way, showing the existence of a special T-factor σ-algebra of S concentrating anything in S which could lead to a non-trivial joining between T and S.

Theorem 7 *Given two measure-preserving dynamical systems $(X, \mathcal{A}, \mu, T)$ and $(Y, \mathcal{B}, \nu, S)$, there always exists a maximum T-factor σ-algebra of S, denoted by $\mathcal{F}_T$.*

Under any joining λ of T and S, the σ-algebras $\mathcal{A} \otimes \{\emptyset, Y\}$ and $\{\emptyset, X\} \otimes \mathcal{B}$ are independent conditionally to the σ-algebra $\{\emptyset, X\} \otimes \mathcal{F}_T$.

Theorem 6 gives a powerful tool to prove some important disjointness results, such as those stated in Theorem 2. These results involve properties of dynamical systems which are stable under the operations of taking joinings and factors. We will call these properties *stable properties*. This is, for example, the case of the zero-entropy property: We know that any factor of a zero-entropy system still has zero entropy, and that any joining of zero-entropy systems also has zero entropy. In other words, T has zero entropy implies that any T-factor has zero entropy. But the property of S being a K-system is precisely characterized by the fact that any non-trivial factor of S has positive entropy. Hence a K-system S cannot have a non-trivial T-factor if T has zero entropy, and is therefore disjoint from T. The converse is a consequence of Theorem 5: If S is not a K-system, then it possesses a non-trivial zero-entropy factor, and therefore there exists some zero-entropy system from which it is not disjoint.

The same argument also applies to the disjointness of discrete-spectrum systems with weakly mixing systems, since a discrete spectrum is a stable property, and weakly mixing systems are characterized by the fact that they do not have any discrete-spectrum factor.

Markov Intertwinings and Composition of Joinings

There is another way of defining joinings of two measure-preserving dynamical systems involving operators on L^2 spaces, mainly put to light by Ryzhikov (see [47]): Observe that for any joining $\lambda \in J(T, S)$, we can consider the operator $P_\lambda : L^2(X, \mu) \to L^2(Y, \nu)$ defined by

$$P_\lambda(f) := \mathbb{E}_\lambda\left[f(x)|y\right] .$$

It is easily checked that P_λ is a *Markov intertwining* of T and S. Conversely, given any Markov intertwining P of T and S, it can be shown that the measure λ_P defined on $X \times Y$ by

$$\lambda_P(A \times B) := \langle P\mathbb{1}_A, \mathbb{1}_B\rangle_{L^2(Y,\nu)}$$

is a joining of T and S.

This reformulation of the notion of joining is useful when joinings are studied in connection with spectral properties of the transformations (see e. g. [22]). It also provides us with a convenient setting to introduce the *composition* of joinings: If we are given three dynamical systems $(X, \mathcal{A}, \mu, T)$, $(Y, \mathcal{B}, \nu, S)$ and (Z, C, ρ, R), a joining $\lambda \in J(T, S)$ and a joining $\lambda' \in J(S, R)$, the composition of the Markov intertwinings P_λ and $P_{\lambda'}$ is easily seen

to give a third Markov intertwining, which itself corresponds to a joining of T and R denoted by $\lambda \circ \lambda'$. When $R = S = T$, i. e. when we are speaking of *2-fold self-joinings* of a single system T (*cf.* next section), this operation turns $J(T,T) = J^2(T)$ into a semigroup. Ahn and Lemańczyk [1] have shown that the subset $J^2_e(T)$ of ergodic two-fold self-joinings is a sub-semigroup if and only if T is semisimple (see Sect. "Simple Systems").

Self-Joinings

We now turn to the case where the measure-preserving dynamical systems we want to join together are all copies of a single system T. For $k \geq 2$, any joining of k copies of T is called a *k-fold self-joining of T*. We denote by $J^k(T)$ the set of all k-fold self-joinings of T, and by $J^k_e(T)$ the subset of *ergodic* k-fold self-joinings.

Self-Joinings and Commuting Transformations

As soon as T is not the trivial single-point system, T is never disjoint from itself: Since T is obviously isomorphic to itself, we can always find a two-fold self-joining of T which is not the product measure by considering self-joinings supported on graphs of isomorphisms (see Sect. "Joinings and Isomorphism"). The simplest of them is obtained by taking the identity map as an isomorphism, and we get that $J^2(T)$ always contains the *diagonal measure* $\Delta_0 := \Delta_{\mathrm{Id}}$.

In general, an isomorphism of T with itself is an invertible measure-preserving transformation S of $(X, \mathcal{A}, \mu)$ which commutes with T. We call *commutant* of T the set of all such transformations (it is a subgroup of the group of automorphisms of $(X, \mathcal{A}, \mu)$), and denote it by $C(T)$. It always contains, at least, all the powers T^n, $n \in \mathbb{Z}$.

Each element S of $C(T)$ gives rise to a two-fold self-joining Δ_S supported on the graph of S. Such self-joinings are called *off-diagonal self-joinings*. They also belong to $J^k_e(T)$ if T is ergodic.

It follows that properties of the commutant of an ergodic T can be seen in its ergodic joinings. As an example of application, we can cite Ryzhikov's proof of King's *weak closure theorem* for rank-one transformations[1]. Rank-one measure-preserving transformations form a very important class of zero-entropy, ergodic measure-preserving transformations. They have many remarkable properties, among which the fact that their commutant is reduced to the weak limits of powers of T. In other words, if T is rank one, for any $S \in C(T)$ there exists a subsequence of integers (n_k) such that,

$$\forall A \in \mathcal{A}\,,\ \mu\left(T^{-n_k} A \Delta S^{-1} A\right) \xrightarrow[k\to\infty]{} 0\,. \tag{8}$$

King proved this result in 1986 [26], using a very intricate coding argument. Observing that (8) was equivalent to the convergence, in $J^2(T)$, of $\Delta_{T^{n_k}}$ to Δ_S, Ryzhikov showed in [45] that King's theorem could be seen as a consequence of the following general result concerning two-fold self-joinings of rank-one systems:

Theorem 8 *Let T be a rank-one measure-preserving transformation, and $\lambda \in J^2_e(T)$. Then there exist $t \geq 1/2$, a subsequence of integers (n_k) and another two-fold self-joining λ' of T such that*

$$\Delta_{T^{n_k}} \xrightarrow[k\to\infty]{} t\lambda + (1-t)\lambda'\,.$$

Minimal Self-Joinings

For any measure-preserving dynamical system T, the set of two-fold self-joinings of T contains at least the product measure $\mu \otimes \mu$, the off-diagonal joinings Δ_{T^n} for each $n \in \mathbb{Z}$, and any convex combination of these. Rudolph [41] discovered in 1979 that we can find systems for which there are no other two-fold self-joinings than these obvious ones. When this is the case, we say that T has *2-fold-minimal self-joinings*, or for short: $T \in \mathrm{MSJ}(2)$. It can be shown (see e. g. [42]) that, as soon as the underlying probability space is not atomic (which we henceforth assume), two-fold minimal self-joinings implies that T is weakly mixing, and therefore that $\mu \otimes \mu$ and Δ_{T^n}, $n \in \mathbb{Z}$, are *ergodic* two-fold self-joinings of T. That is why two-fold minimal self-joinings are often defined by the following:

$$T \in \mathrm{MSJ}(2) \iff J^2_e(T) = \{\mu \otimes \mu\} \cup \{\Delta_{T^n}, n \in \mathbb{Z}\}\,. \tag{9}$$

Systems with two-fold minimal self-joinings have very interesting properties. First, since for any S in $C(T)$, Δ_S belongs to $J^2_e(T)$, we immediately see that the commutant of T is reduced to the powers of T. In particular, it is impossible to find a square root of T, i. e. a measure-preserving S such that $S \circ S = T$. Second, the existence of a non-trivial factor σ-algebra of T would lead, via the relatively independent self-joining over this factor, to some ergodic two-fold self-joining of T which is not in the list prescribed by (9). Therefore, any factor σ-algebra of a system with two-fold minimal self-joinings must be either the trivial σ-algebra $\{\emptyset, X\}$ or the whole σ-algebra $\mathcal{A}$. This has the remarkable consequence that if ξ is any random

[1] An introduction to finite-rank transformations can be found e. g. in [32]; we also refer the reader to the quite complete survey [12].

variable on the underlying probability space which is not almost-surely constant, then the process $(\xi \circ T^n)_{n\in\mathbb{Z}}$ always generates the whole σ-algebra $\mathcal{A}$. This also implies that T has zero entropy, since positive-entropy systems have many non-trivial factors.

The notion of two-fold minimal self-joinings extends for any integer $k \geq 2$ to *k-fold minimal self-joinings*, which roughly means that there are no other k-fold ergodic self-joinings than the "obvious" ones: Those for which the k coordinates are either independent or just translated by some power of T (see the Glossary for a more precise definition). We denote in this case: $T \in \mathrm{MSJ}(k)$. If T has k-fold minimal self-joinings for all $k \geq 2$, we simply say that T has *minimal self joinings*.

Rudolph's construction of a system with two-fold minimal self-joinings [41] was inspired by a famous work of Ornstein [35], giving the first example of a transformation with no roots. It turned out that Ornstein's example is a mixing rank-one system, and all mixing rank-one systems were later proved by J. King [27] to have *2-fold minimal self-joinings*. This can also be viewed as a consequence of Ryzhikov's Theorem 8. Indeed, in the language of joinings, the mixing property of T translates as follows:

$$T \text{ is mixing} \iff \Delta_{T^n} \xrightarrow[|n|\to\infty]{} \mu \otimes \mu \,. \tag{10}$$

Therefore, if in Theorem 8 we further assume that T is mixing, then either the sequence (n_k) we get in the conclusion is bounded, and then λ is some Δ_{T^n}, or it is unbounded and then $\lambda = \mu \otimes \mu$.

$T \in \mathrm{MSJ}(k)$ obviously implies $T \in \mathrm{MSJ}(k')$ for any $2 \leq k' \leq k$, but the converse is not known. The question whether two-fold minimal self-joinings implies k-fold minimal self-joinings for all k is related to the important open problem of *pairwise independent joinings* (see Sect. "Pairwise-Independent Joinings"). But the latter problem is solved for some special classes of systems, in particular in the category of mixing rank-one transformations. It follows that, if T is mixing and rank one, then T has minimal self-joinings.

In 1980, Del Junco, Rahe and Swanson proved that Chacon's transformation also has minimal self-joinings [9]. This well-known transformation is also a rank-one system, but it is not mixing (it had been introduced by R.V. Chacon in 1969 [4] as the first explicit example of a weakly mixing transformation which is not mixing). For another example of a transformation with two-fold minimal self-joinings, constructed as an exchange map on three intervals, we refer to [7].

The existence of a transformation with minimal self-joinings has been used by Rudolph as a wonderful tool to construct a large variety of striking counterexamples, such as

- A transformation T which has no roots, while T^2 has roots of any order,
- A transformation with a cubic root but no square root,
- Two measure-preserving dynamical systems which are weakly isomorphic (each one is a factor of the other) but not isomorphic…

Let us now sketch the argument showing that we can find two systems with no common factor but which are not disjoint: We start with a system T with minimal self-joinings. Consider the direct product of T with an independent copy T' of itself, and take the *symmetric factor* S of $T \otimes T'$, that is to say the factor we get if we only look at the non-ordered pair of coordinates $\{x, x'\}$ in the Cartesian product. Then S is surely not disjoint from T, since the pair $\{x, x'\}$ is not independent of x. However, if S and T had a non-trivial common factor, then this factor should be isomorphic to T itself (because T has minimal self-joinings). Therefore we could find in the direct product $T \otimes T'$ a third copy $\tilde{T}$ of T, which is measurable with respect to the symmetric factor. In particular, $\tilde{T}$ is invariant by the flip map $(x, x') \mapsto (x', x)$, and this prevents $\tilde{T}$ from being measurable with respect to only one coordinate. Then, since $T \in \mathrm{MSJ}(3)$, the systems T, T' and $\tilde{T}$ have no choice but being independent. But this contradicts the fact that $\tilde{T}$ is measurable with respect to the σ-algebra generated by x and x'. Hence, T and S have no non-trivial common factor.

We can also cite the example given by Glasner and Weiss [21] of a pair of horocycle transformations which have no nontrivial common factor, yet are not disjoint. Their construction relies on the deep work by Ratner [38], which describes the structure of joinings of horocycle flows.

Simple Systems

An important generalization of two-fold minimal self-joinings has been proposed by William A. Veech in 1982 [51]. We say that the measure-preserving dynamical system T is *two-fold simple* if it has no other ergodic two-fold self-joinings than the product measure $\{\mu \otimes \mu\}$ and joinings supported on the graph of a transformation $S \in C(T)$. (The difference with MSJ(2) lies in the fact that $C(T)$ may contain other transformations than the powers of T.) It turns out that simple systems may have non-trivial factors, but the structure of these factors can be explicitly described: They are always associated with some compact subgroup of $C(T)$. More precisely, if K is a com-

pact subgroup of $C(T)$, we can consider the factor σ-algebra

$$\mathcal{F}_K := \{A \in \mathcal{A} : \forall S \in K\,, A = S(A)\}\ ,$$

and the corresponding factor transformation $T_{|\mathcal{F}_K}$ (called a *group factor*). Then Veech proved the following theorem concerning the structure of factors of a two-fold simple system.

Theorem 9 *If the dynamical system T is two-fold simple, and if $\mathcal{F} \subset \mathcal{A}$ is a non-trivial factor σ-algebra of T, then there exists a compact subgroup K of the group $C(T)$ such that $\mathcal{F} = \mathcal{F}_K$.*

There is a natural generalization of Veech's property to the case of k-fold self-joinings, which has been introduced by A. Del Junco and D.J. Rudolph in 1987 [10] (see the precise definition of simple systems in the Glossary). In their work, important results concerning the structure of factors and joinings of simple systems are proved. In particular, they are able to completely describe the structure of the ergodic joinings between a given simple system and any ergodic system (see also [18,49]). Recall that, for any $r \geq 1$, the *symmetric factor* of $T^{\otimes r}$ is the system we get if we observe the r coordinates of the point in X^r and forget their order. This is a special case of group factor, associated with the subgroup of $C(T^{\otimes r})$ consisting of all permutations of the coordinates. We denote this symmetric factor by $T^{\langle r\rangle}$.

Theorem 10 *Let T be a simple system and S an ergodic system. Assume that λ is an ergodic joining of T and S which is different from the product measure. Then there exists a compact subgroup K of $C(T)$ and an integer $r \geq 1$ such that*

- *$(T_{|\mathcal{F}_K})^{\langle r\rangle}$ is a factor of S,*
- *λ is the projection on $X \times Y$ of the relatively independent joining of $T^{\otimes r}$ and S over their common factor $(T_{|\mathcal{F}_K})^{\langle r\rangle}$.*

If we further assume that the second system is also simple, then in the conclusion we can take $r = 1$. In other words, ergodic joinings of simple systems S and T are either the product measure or relatively independent joinings over a common group factor. This leads to the following corollary:

Theorem 11 *Simple systems without non-trivial common factor are disjoint.*

As for minimal self-joining, it is not known in general whether two-fold simplicity implies k-fold simplicity for all k. This question is studied in [19], where sufficient spectral conditions are given for this implication to hold. It is also proved that any three-fold simple weakly mixing transformation is simple of all order.

Relative Properties with Respect to a Factor

In fact, Veech also introduced a weaker, "relativized", version of the two-fold simplicity. If $\mathcal{F} \subset \mathcal{A}$ is a non-trivial factor σ-algebra of T, let us denote by $J^2(T, \mathcal{F})$ the two-fold self-joinings of T which are "constructed over $\mathcal{F}$", which means that their restriction to the product σ-algebra $\mathcal{F} \otimes \mathcal{F}$ coincides with the diagonal measure. (The relatively-independent joining over $\mathcal{F}$ is the canonical example of such a joining.) For the conclusion of Theorem 9 to hold, it is enough to assume only that the ergodic elements of $J^2(T, \mathcal{F})$ be supported on the graph of a transformation $S \in C(T)$. This is an important situation where the study of $J^2(T, \mathcal{F})$ gives strong information on the way $\mathcal{F}$ is embedded in the whole system T, or, in other words, on the relative properties of T with respect to the factor $T|_{\mathcal{F}}$. A simple example of such a relative property is the *relative weak mixing with respect to $\mathcal{F}$*, which is characterized by the ergodicity of the relatively-independent joining over $\mathcal{F}$ (recall that weak-mixing is itself characterized by the ergodicity of the direct product $T \otimes T$).

For more details on this subject, we refer the reader to [30]. We also wish to mention the generalization of simplicity called *semisimplicity* proposed by Del Junco, Lemańczyk and Mentzen in [8], which is precisely characterized by the fact that, for any $\lambda \in J^2_e(T)$, the system $(T \otimes T)_\lambda$ is a relatively weakly mixing extension of T.

Some Applications and Future Directions

Joinings Proofs of Ornstein's and Krieger's Theorems

We have already seen that joinings could be used to prove isomorphisms between systems. This fact found a nice application in the proofs of two major theorems in ergodic theory: Ornstein's isomorphism theorem [34], stating that two Bernoulli shifts with the same entropy are isomorphic, and Krierger's finite generator theorem [28], which says that any dynamical system with finite entropy is isomorphic to the shift transformation on a finite-valued stationary process. The idea of this joining approach to the proofs of Krieger's and Ornstein's theorems was originally due to Burton and Rothstein, who circulated a preliminary report on the subject which was never published [3]. The first published and fully detailed exposition of these proofs can be found in Rudolph's book [42] (see also in Glasner's book [18]).

In fact, Ornstein's theorem goes far more beyond the isomorphism of two given Bernoulli shifts: It also gives

a powerful tool for showing that a specific dynamical system is isomorphic to a Bernoulli shift. In particular, Ornstein introduced the property for an ergodic stationary process to be *finitely determined*. We shall not give here the precise definition of this property (for a complete exposition of Ornstein's theory, we refer the reader to [36]), but simply point out that Bernoulli shifts and mixing Markov chains are examples of finitely determined processes. Rudolph's argument to show Ornstein's theorem via joinings makes use of Theorem 4, and of the topology of $J(T,S)$.

Theorem 12 (Ornstein's Isomorphism Theorem) *Let T and S be two ergodic dynamical systems with the same entropy, and both generated by finitely determined stationary processes. Then the set of joinings of T and S which are supported on graphs of isomorphisms forms a dense G_δ in $J_e(T,S)$.*

Krieger's theorem is not as easily stated in terms of joinings, because it does not refer to the isomorphism of two specific systems, but rather to the isomorphism of one given system with some other system which has to be found. We have therefore to introduce a larger set of joinings: Given an integer n, we denote by Y_n the set of double-sided sequences taking values in $\{1,\dots,n\}$. We consider on Y_n the shift transformation S, but we do not determine yet the invariant measure. Now, for a specific measure-preserving dynamical system T, consider the set $J(n,T)$ of all possible joinings of T with some system (Y_n,ν,S), when ν ranges over all possible shift-invariant probability measures on Y_n. $J(n,T)$ can also be equipped with a topology which turns it into a compact convex metric space, and as soon as T is ergodic, the set $J_e(n,T)$ of *ergodic* elements of $J(n,T)$ is not empty. In this setting, Krieger's theorem can be stated as follows:

Theorem 13 (Krieger's Finite Generator Theorem) *Let T be an ergodic dynamical system with entropy $h(T) < \log_2 n$. Then the set of $\lambda \in J(n,T)$ which are supported on graphs of isomorphisms between T and some system (Y_n,ν,S) forms a dense G_δ in $\overline{J_e(n,T)}$.*

Since any system of the form (Y_n,ν,S) obviously has an n-valued generating process, we obtain as a corollary that T itself is generated by an n-valued process.

Joinings and Pointwise Convergence

The study of joinings is also involved in questions concerning pointwise convergence of (non-conventional) ergodic averages. As an example, we present here the relationships between disjointness and the following well-known open problem: Given two commuting measure-preserving transformations S and T acting on the same probability space $(X,\mathcal{A},\mu)$, is it true that for any f and g in $L^2(\mu)$, the sequence

$$\left(\frac{1}{n}\sum_{k=0}^{n-1} f(T^k x)g(S^k x)\right)_{n>0} \tag{11}$$

converges μ-almost surely?

It turns out that disjointness of T and S is a sufficient condition for this almost-sure convergence to hold. Indeed, let us first consider the case where T and S are defined on a priori different spaces $(X,\mathcal{A},\mu)$ and $(Y,\mathcal{B},\nu)$ respectively, and consider the ergodic average in the product

$$\frac{1}{n}\sum_{k=0}^{n-1} f(T^k x)g(S^k y)\,, \tag{12}$$

which can be viewed as the integral of the function $f\otimes g$ with respect to the empirical distribution

$$\delta_n(x,y) := \frac{1}{n}\sum_{k=0}^{n-1}\delta_{(T^k x, S^k y)}\,.$$

We can always assume that T and S are continuous transformations of compact metric spaces (indeed, any measure-preserving dynamical system is isomorphic to such a transformation on a compact metric space; see e. g. [15]). Then the set of probability measures on $X\times Y$ equipped with the topology of weak convergence is metric compact. Now, here is the crucial point where joinings appear: If T and S are ergodic, we can easily find subsets $X_0\subset X$ and $Y_0\subset Y$ with $\mu(X_0)=\nu(Y_0)=1$, such that for all $(x,y)\in X_0\times Y_0$, any cluster point of the sequence $(\delta_n(x,y))_{n>0}$ is automatically a joining of T and S. (We just have to pick x and y among the "good points" for the ergodic theorem in their respective spaces.) When T and S are disjoint, there is therefore only one possible cluster point to the sequence $\delta_n(x,y)$ which is $\mu\otimes\nu$. This ensures that, for continuous f and g, (12) converges to the product of the integrals of f and g as soon as (x,y) is picked in $X_0\times Y_0$. The subspace of continuous functions being dense in L^2, the classical ergodic maximal inequality (see [17]) ensures that, for any f and g in $L^2(\mu)$, (12) converges for any (x,y) in a rectangle of full measure $X_0\times Y_0$.

Coming back to the original question where the spaces on which T and S act are identified, we observe that with probability one, x belongs both to X_0 and Y_0, and therefore the sequence (11) converges.

The existence of a rectangle of full measure in which the sequence of empirical distributions $(\delta_n(x,y))_{n>0}$ always converges to some joining has been studied in [31] as

a natural generalization of the notion of disjointness. This property was called *weak disjointness* of S and T, and it is indeed strictly weaker than disjointness, since there are examples of transformations which are weakly disjoint from themselves.

There are other situations in which joinings can be used in the study of everywhere convergence, among which we can cite Rudolph's joinings proof of Bourgain's return time theorem [43].

Joinings and Rohlin's Multifold Mixing Question

We have already seen that the property of T being mixing could be expressed in terms of two-fold self-joinings of T (see (10)). Rohlin proposed in 1949 [39] a generalization of this property, called *multifold mixing*: The measure-preserving transformation T is said to be *k-fold mixing* if $\forall A_1, A_2, \ldots, A_k \in \mathcal{A}$,

$$\lim_{n_2,n_3,\ldots,n_k\to\infty} \mu(A_1 \cap T^{-n_2}A_2 \cap \cdots \cap T^{-(n_2+\cdots+n_k)}A_k) = \prod_{i=1}^{k} \mu(A_i)\,.$$

Again, this definition can easily be translated into the language of joinings: T is k-fold mixing when the sequence $(\Delta_{T^{n_2},\ldots,T^{n_2+\cdots+n_k}})$ converges in $J^k(T)$ to $\mu^{\otimes k}$ as $n_2, \ldots, n_k$ go to infinity, where $(\Delta_{T^{n_2},\ldots,T^{n_2+\cdots+n_k}})$ is the obvious generalization of Δ_{T^n} to the case of k-fold self-joinings. The classical notion of mixing corresponds in this setting to two-fold mixing. (We must point out that Rohlin's original definition of k-fold mixing involved $k+1$ sets, thus the classical mixing property was called *1-fold mixing*. However it seems that the convention we adopt here is now used by most authors, and we find it more coherent when translated in the language of multifold self-joinings.)

Obviously, *3-fold mixing* is stronger than *2-fold mixing*, and Rohlin asked in his article whether the converse is true. This question is still open today, even though many important works have dealt with it and supplied partial answers. Most of these works directly involve self-joinings via the argument exposed in the following section.

Pairwise-Independent Joinings Let T be a two-fold mixing dynamical system. If T is not three-fold mixing, $(\Delta_{T^n,T^{n+m}})$ does not converge to the product measure as n and m go to ∞. By compactness of $J^3(T)$, we can find subsequences (n_k) and (m_k) such that $(\Delta_{T^{n_k},T^{n_k+m_k}})$ converges to a cluster point $\lambda \neq \mu \otimes \mu \otimes \mu$. However, by two-fold mixing, the three coordinates must be pairwise independent under λ. We therefore get a three-fold self-joining λ with the unusual property that λ has pairwise independent coordinates, but λ is not the product measure.

In fact, systems with this kind of pairwise-independent but non-independent three-fold self-joining are easy to find (see e. g. [6]), but the examples we know so far are either periodic transformations (which cannot be counterexamples to Rohlin's question since they are not mixing!), or transformations with positive entropy. But using an argument provided by Thouvenot, we can prove that, if there exists a two-fold mixing T which is not three-fold mixing, then we can find such a T in the category of zero-entropy dynamical systems (see e. g. [5]). Therefore, a negative answer to the following question would solve Rohlin's multifold mixing problem:

Question 14 Does there exist a zero-entropy, weakly mixing dynamical system T with a self-joining $\lambda \in J^3(T)$ for which the coordinates are pairwise independent but which is different from $\mu \otimes \mu \otimes \mu$?

(non) existence of such pairwise-independent joinings is also related to the question of whether MSJ(2) implies MSJ(3), or whether two-fold simplicity implies three-fold simplicity. Indeed, any counter-example to one of these implication would necessarily be of zero entropy, and would possess a pairwise-independent three-fold self-joining which is not the product measure.

Question 14 has been answered by B. Host and V. Ryzhikov for some special classes of zero-entropy dynamical systems.

Host's and Ryzhikov's Theorems The following theorem, proved in 1991 by B. Host [23] (see also [18,33]), establishes a spectacular connection between the spectral properties of a finite family of dynamical systems and the non-existence of a pairwise-independent, non-independent joining:

Theorem 15 (Host's Theorem on Singular Spectrum) *Let $(X_i, \mathcal{A}_i, \mu_i, T_i)_{1\le i\le r}$ be a finite family of measure-preserving dynamical systems with purely singular spectrum. Then any pairwise-independent joining $\lambda \in J(T_1, \ldots, T_r)$ is the product measure $\mu_1 \otimes \cdots \otimes \mu_r$.*

Corollary 16 *If a dynamical system with singular spectrum is two-fold mixing, then it is k-fold mixing for any $k \ge 2$.*

The multifold-mixing problem for rank-one measure-preserving systems was solved in 1984 by S. Kalikow [25], using arguments which do not involve the theory of joinings. In 1993, V. Ryzhikov [46] extended Kalikow's result to finite-rank systems, by giving a negative answer to Question 14 in the category of finite-rank mixing systems:

Theorem 17 (Ryzhikov's Theorem for Finite Rank Systems) *Let T be a finite-rank mixing transformation, and $k \geq 2$. Then the only pairwise-independent k-fold self-joining of T is the product measure.*

Corollary 18 *If a finite-rank transformation is two-fold mixing, then it is k-fold mixing for any $k \geq 2$.*

Future Directions

A lot of important open questions in ergodic theory involve joinings, and we already have cited several of them: Joinings are a natural tool when we want to deal with some problems of pointwise convergence involving several transformations (see Sect. "Joinings and Pointwise Convergence"). Their use is also fundamental in the study of Rohlin's question on multifold mixing. As far as this latter problem is concerned, we may mention a recent approach to Question 14: Start with a transformation for which some special pairwise-independent self-joining exists, and see what this assumption entails. In particular, we can ask under which conditions there exists a pairwise-independent three-fold self-joining of T under which the third coordinate is a function of the two others. It has already been proven in [24] that if this function is sufficiently regular (continuous for some topology), then T is periodic or has positive entropy. And there is strong evidence leading to the conjecture that, when T is weakly mixing, such a situation can only arise when T is a Bernoulli shift of entropy $\log n$ for some integer $n \geq 2$. A question in the same spirit was raised by Ryzhikov, who asked in [44] under which conditions we can find a factor of the direct product $T \times T$ which is independent of both coordinates.

There is also a lot of work to do with joinings in order to understand the structure of factors of some dynamical systems, and how different classes of systems are related. An example of such a work is given in the class of Gaussian dynamical systems, i. e. dynamical systems constructed from the shift on a stationary Gaussian process: For some of them (which are called *GAG*, from the French *Gaussien à Autocouplages Gaussiens*), it can be proven that any ergodic self-joining is itself a Gaussian system (see [29,50]), and this gives a complete description of the structure of their factors. This kind of analysis is expected to be applicable to other classes of dynamical systems. In particular, Gaussian joinings find a nice generalization in the notion of *infinitely divisible joinings*, studied by Roy in [40]). These ID joinings concern a wider class of dynamical systems of probabilistic origin, among which we can also find Poisson suspensions. The counterpart of Gaussian joinings in this latter class are *Poisson joinings*, which have been introduced by Derriennic, Frączek, Lemańczyk and Parreau in [11]. As far as Poisson suspensions are concerned, the analog of the GAG property in the Gaussian class can also be considered, and a family of Poisson suspension for which the only ergodic self-joinings are Poisson joinings has been given recently by Parreau and Roy [37]. In [11], a general joining property is described: T satisfies the *ELF property* (from the French: *Ergodicité des Limites Faibles*) if any joining which can be obtained as a limit of off-diagonal joinings $\Delta_{T^{n_k}}$ is automatically ergodic. It turns out that this property is satisfied by any system arising from an infinitely divisible stationary process (see [11,40]). It is proven in [11] that ELF property implies disjointness with any system which is two-fold simple and weakly mixing but not mixing. ELF property is expected to give a useful tool to prove disjointness between dynamical systems of probabilistic origin and other classes of systems (see e. g. [13] in the case of $\mathbb{R}$-action for disjointness between ELF systems and a class of special flows over irrational rotations).

Many other questions involving joinings have not been mentioned here. We should at least cite *filtering problems*, which were one of the motivations presented by Furstenberg for the introduction of the disjointness property in [14]. Suppose we are given two real-valued stationary processes (X_n) and (Y_n), with their joint distribution also stationary. We can interpret (X_n) as a signal, perturbed by a noise (Y_n), and the question posed by Furstenberg is: Under which condition can we recover the original signal (X_n) from the observation of $(X_n + Y_n)$? Furstenberg proved that it is always possible if the two processes (X_n) and (Y_n) are integrable, and if the two measure-preserving dynamical systems constructed as the shift of the two processes are disjoint. Furstenberg also observed that the integrability assumption can be removed if a stronger disjointness property is satisfied: A perfect filtering exists if the system T generated by (X_n) is *doubly disjoint* from the system S generated by (Y_n), in the sense that T is disjoint from any ergodic self-joining of S. Several generalizations have been studied (see [2,16]), but the question of whether the integrability assumption of the processes can be removed is still open.

Bibliography

1. Ahn Y-H, Lemańczyk M (2003) An algebraic property of joinings. Proc Amer Math Soc 131(6):1711–1716 (electronic)
2. Bułatek W, Lemańczyk M, Lesigne E (2005) On the filtering problem for stationary random $\mathbb{Z}^2$-fields. IEEE Trans Inform Theory 51(10):3586–3593
3. Burton R, Rothstein A (1977) Isomorphism theorems in ergodic theory. Technical report, Oregon State University
4. Chacon RV (1969) Weakly mixing transformations which are not strongly mixing. Proc Amer Math Soc 22:559–562

5. de la Rue T (2006) 2-fold and 3-fold mixing: why 3-dot-type counterexamples are impossible in one dimension. Bull Braz Math Soc (NS) 37(4):503–521
6. de la Rue T (2006) An introduction to joinings in ergodic theory. Discret Contin Dyn Syst 15(1):121–142
7. del Junco A (1983) A family of counterexamples in ergodic theory. Isr J Math 44(2):160–188
8. del Junco A, Lemańczyk M, Mentzen MK (1995) Semisimplicity, joinings and group extensions. Studia Math 112(2):141–164
9. del Junco A, Rahe M, Swanson L (1980) Chacon's automorphism has minimal self-joinings. J Analyse Math 37:276–284
10. del Junco A, Rudolph DJ (1987) On ergodic actions whose self-joinings are graphs. Ergod Theory Dynam Syst 7(4):531–557
11. Derriennic Y, Frączek K, Lemańczyk M, Parreau F (2008) Ergodic automorphisms whose weak closure of off-diagonal measures consists of ergodic self-joinings. Colloq Math 110:81–115
12. Ferenczi S (1997) Systems of finite rank. Colloq Math 73(1): 35–65
13. Frączek K, Lemańczyk M (2004) A class of special flows over irrational rotations which is disjoint from mixing flows. Ergod Theory Dynam Syst 24(4):1083–1095
14. Furstenberg H (1967) Disjointness in ergodic theory, minimal sets, and a problem in Diophantine approximation. Math Syst Theory 1:1–49
15. Furstenberg H (1981) Recurrence in ergodic theory and combinatorial number theory. In: M.B. Porter Lectures. Princeton University Press, Princeton
16. Furstenberg H, Peres Y, Weiss B (1995) Perfect filtering and double disjointness. Ann Inst H Poincaré Probab Stat 31(3):453–465
17. Garsia AM (1970) Topics in almost everywhere convergence. In: Lectures in Advanced Mathematics, vol 4. Markham Publishing Co, Chicago, IL
18. Glasner E (2003) Ergodic theory via joinings. In: Mathematical Surveys and Monographs, vol 101. American Mathematical Society, Providence
19. Glasner E, Host B, Rudolph DJ (1992) Simple systems and their higher order self-joinings. Isr J Math 78(1):131–142
20. Glasner E, Thouvenot J-P, Weiss B (2000) Entropy theory without a past. Ergod Theory Dynam Syst 20(5):1355–1370
21. Glasner S, Weiss B (1983) Minimal transformations with no common factor need not be disjoint. Isr J Math 45(1):1–8
22. Goodson GR (2000) Joining properties of ergodic dynamical systems having simple spectrum. Sankhyā Ser A 62(3):307–317, Ergodic theory and harmonic analysis (Mumbai, 1999)
23. Host B (1991) Mixing of all orders and pairwise independent joinings of systems with singular spectrum. Isr J Math 76(3):289–298
24. Janvresse É, de la Rue T (2007) On a class of pairwise-independent joinings. Ergod Theory Dynam Syst (to appear)
25. Kalikow SA (1984) Twofold mixing implies threefold mixing for rank one transformations. Ergod Theory Dynam Syst 4(2): 237–259
26. King J (1986) The commutant is the weak closure of the powers, for rank-1 transformations. Ergod Theory Dynam Syst 6(3):363–384
27. King J (1988) Joining-rank and the structure of finite rank mixing transformations. J Anal Math 51:182–227
28. Krieger W (1970) On entropy and generators of measure-preserving transformations. Trans Amer Math Soc 149:453–464
29. Lemańczyk M, Parreau F, Thouvenot J-P (2000) Gaussian automorphisms whose ergodic self-joinings are Gaussian. Fund Math 164(3):253–293
30. Lemańczyk M, Thouvenot J-P, Weiss B (2002) Relative discrete spectrum and joinings. Monatsh Math 137(1):57–75
31. Lesigne E, Rittaud B, and de la Rue T (2003) Weak disjointness of measure-preserving dynamical systems. Ergod Theory Dynam Syst 23(4):1173–1198
32. Nadkarni MG (1998) Basic ergodic theory. In: Birkhäuser Advanced Texts: Basler Lehrbücher, 2nd edn. Birkhäuser, Basel
33. Nadkarni MG (1998) Spectral theory of dynamical systems. In: Birkhäuser Advanced Texts: Basler Lehrbücher. Birkhäuser, Basel
34. Ornstein DS (1970) Bernoulli shifts with the same entropy are isomorphic. Adv Math 4:337–352
35. Ornstein DS (1972) On the root problem in ergodic theory. In: Proceedings of the Sixth Berkeley Symposium on Mathematical Statistics and Probability, Univ. California, Berkeley, 1970/1971, vol II: Probability theory. Univ California Press, Berkeley, pp 347–356
36. Ornstein DS (1974) Ergodic theory, randomness, and dynamical systems. In: James K Whittemore Lectures in Mathematics given at Yale University, Yale Mathematical Monographs, vol 5. Yale University Press, New Haven
37. Parreau F, Roy E (2007) Poisson joinings of Poisson suspension. Preprint
38. Ratner M (1983) Horocycle flows, joinings and rigidity of products. Ann of Math 118(2):277–313
39. Rohlin VA (1949) On endomorphisms of compact commutative groups. Izvestiya Akad Nauk SSSR Ser Mat 13:329–340
40. Roy E (2007) Poisson suspensions and infinite ergodic theory. Ergod Theory Dynam Syst(to appear)
41. Rudolph DJ (1979) An example of a measure preserving map with minimal self-joinings, and applications. J Anal Math 35:97–122
42. Rudolph DJ (1990) The title is Fundamentals of Measurable Dynamics: Ergodic Theory on Lebesgue Spaces. Oxford University Press, New York
43. Rudolph DJ (1994) A joinings proof of Bourgain's return time theorem. Ergod Theory Dynam Syst 14(1):197–203
44. Ryzhikov VV (1992) Stochastic wreath products and joinings of dynamical systems. Mat Zametki 52(3):130–140, 160
45. Ryzhikov VV (1992) Mixing, rank and minimal self-joining of actions with invariant measure. Mat Sb 183(3):133–160
46. Ryzhikov VV (1993) Joinings and multiple mixing of the actions of finite rank. Funktsional Anal Prilozhen 27(2):63–78, 96
47. Ryzhikov VV (1993) Joinings, wreath products, factors and mixing properties of dynamical systems. Izv Ross Akad Nauk Ser Mat 57(1):102–128
48. Thorisson H (2000) Coupling, stationarity, and regeneration. In: Probability and its Applications (New York). Springer, New York
49. Thouvenot J-P (1995) Some properties and applications of joinings in ergodic theory. In: Ergodic theory and its connections with harmonic analysis, Alexandria, 1993. London Math Soc Lecture Note Ser, vol 205. Cambridge Univ Press, Cambridge, pp 207–235
50. Thouvenot J-P (1987) The metrical structure of some Gaussian processes. In: Proceedings of the conference on ergodic theory and related topics, II, Georgenthal, 1986. Teubner-Texte Math, vol 94. Teubner, Leipzig, pp 195–198
51. Veech WA (1982) A criterion for a process to be prime. Monatsh Math 94(4):335–341